

**Multifractal Analysis and Modeling of the
Large-Scale Distribution of
Galactic Luminosity**

by

Pablo Garrido

**A thesis submitted to the Faculty of Graduate Studies and
Research in partial fulfillment of the requirements for the degree of
Master of Science**

**Department of Physics
McGill University
Montréal
Canada**

June 1994

@Pablo Garrido 1994

Name

PABLO GARRIDO

Dissertation Abstracts International is arranged by broad, general subject categories. Please select the one subject which most nearly describes the content of your dissertation. Enter the corresponding four-digit code in the spaces provided.

ASTRONOMY AND ASTROPHYSICS

SUBJECT TERM

0606

SUBJECT CODE

U·M·I

Subject Categories

THE HUMANITIES AND SOCIAL SCIENCES

COMMUNICATIONS AND THE ARTS

Architecture	0729
Art History	0377
Cinema	0900
Dance	0378
Fine Arts	0357
Information Science	0723
Journalism	0391
Library Science	0399
Mass Communications	0708
Music	0413
Speech Communication	0459
Theater	0465

EDUCATION

General	0515
Administration	0514
Adult and Continuing	0516
Agricultural	0517
Art	0273
Bilingual and Multicultural	0282
Business	0688
Community College	0275
Curriculum and Instruction	0727
Early Childhood	0518
Elementary	0524
Finance	0277
Guidance and Counseling	0519
Health	0680
Higher	0745
History of	0520
Home Economics	0278
Industrial	0521
Language and Literature	0279
Mathematics	0280
Music	0522
Philosophy of	0998
Physical	0523

Psychology	0525
Reading	0535
Religious	0527
Sciences	0714
Secondary	0533
Social Sciences	0534
Sociology of	0340
Special	0529
Teacher Training	0530
Technology	0710
Tests and Measurements	0288
Vocational	0747

LANGUAGE, LITERATURE AND LINGUISTICS

Language	
General	0679
Ancient	0289
Linguistics	0290
Modern	0291
Literature	
General	0401
Classical	0294
Comparative	0295
Medieval	0297
Modern	0298
African	0316
American	0591
Asian	0305
Canadian (English)	0352
Canadian (French)	0355
English	0593
Germanic	0311
Latin American	0312
Middle Eastern	0315
Romance	0313
Slavic and East European	0314

PHILOSOPHY, RELIGION AND THEOLOGY

Philosophy	0422
Religion	
General	0318
Biblical Studies	0321
Clergy	0319
History of	0320
Philosophy of	0322
Theology	0469

SOCIAL SCIENCES

American Studies	0323
Anthropology	
Archaeology	0324
Cultural	0326
Physical	0327
Business Administration	
General	0310
Accounting	0272
Banking	0770
Management	0454
Marketing	0338
Canadian Studies	0385
Economics	
General	0501
Agricultural	0503
Commerce Business	0505
Finance	0508
History	0509
Labor	0510
Theory	0511
Folklore	0358
Geography	0366
Gerontology	0351
History	
General	0578

Ancient	0579
Medieval	0581
Modern	0582
Black	0328
African	0331
Asia, Australia and Oceania	0332
Canadian	0334
European	0335
Latin American	0336
Middle Eastern	0333
United States	0337
History of Science	0585
Law	0398
Political Science	
General	0615
International Law and Relations	0616
Public Administration	0617
Recreation	0814
Social Work	0452
Sociology	
General	0626
Criminology and Penology	0627
Demography	0938
Ethnic and Racial Studies	0631
Individual and Family Studies	0628
Industrial and Labor Relations	0629
Public and Social Welfare	0630
Social Structure and Development	0700
Theory and Methods	0344
Transportation	0709
Urban and Regional Planning	0999
Women's Studies	0453

THE SCIENCES AND ENGINEERING

BIOLOGICAL SCIENCES

Agriculture	
General	0473
Agronomy	0285
Animal Culture and Nutrition	0475
Animal Pathology	0476
Food Science and Technology	0359
Forestry and Wildlife	0478
Plant Culture	0479
Plant Pathology	0480
Plant Physiology	0817
Range Management	0777
Wood Technology	0746
Biology	
General	0306
Anatomy	0287
Biostatistics	0308
Botany	0309
Cell	0379
Ecology	0329
Entomology	0353
Genetics	0369
Limnology	0793
Microbiology	0410
Molecular	0307
Neuroscience	0317
Oceanography	0416
Physiology	0433
Radiation	0821
Veterinary Science	0778
Zoology	0472
Biophysics	
General	0786
Medical	0760
EARTH SCIENCES	
Biogeochemistry	0425
Geochemistry	0996

Geodesy	0370
Geology	0372
Geophysics	0373
Hydrology	0388
Mineralogy	0411
Paleobotany	0345
Paleoecology	0426
Paleontology	0418
Paleozoology	0985
Palynology	0427
Physical Geography	0368
Physical Oceanography	0415

HEALTH AND ENVIRONMENTAL SCIENCES

Environmental Sciences	0768
Health Sciences	
General	0566
Audiology	0300
Chemotherapy	0992
Dentistry	0567
Education	0350
Hospital Management	0769
Human Development	0758
Immunology	0982
Medicine and Surgery	0564
Mental Health	0347
Nursing	0569
Nutrition	0570
Obstetrics and Gynecology	0380
Occupational Health and Therapy	0354
Ophthalmology	0381
Pathology	0571
Pharmacology	0419
Pharmacy	0572
Physical Therapy	0382
Public Health	0573
Radiology	0574
Recreation	0575

Speech Pathology	0460
Toxicology	0383
Home Economics	0386

PHYSICAL SCIENCES

Pure Sciences	
Chemistry	
General	0485
Agricultural	0749
Analytical	0486
Biochemistry	0487
Inorganic	0488
Nuclear	0738
Organic	0490
Pharmaceutical	0491
Physical	0494
Polymer	0495
Radiation	0754
Mathematics	0405
Physics	
General	0605
Acoustics	0986
Astronomy and Astrophysics	0606
Atmospheric Science	0608
Atomic	0748
Electronics and Electricity	0607
Elementary Particles and High Energy	0798
Fluid and Plasma	0759
Molecular	0609
Nuclear	0610
Optics	0752
Radiation	0756
Solid State	0611
Statistics	0463
Applied Sciences	
Applied Mechanics	0346
Computer Science	0984

Engineering	
General	0537
Aerospace	0538
Agricultural	0539
Automotive	0540
Biomedical	0541
Chemical	0542
Civil	0543
Electronics and Electrical	0544
Heat and Thermodynamics	0348
Hydraulic	0545
Industrial	0546
Marine	0547
Materials Science	0794
Mechanical	0548
Metallurgy	0743
Mining	0551
Nuclear	0552
Packaging	0549
Petroleum	0765
Sanitary and Municipal System Science	0554
System Science	0790
Geotechnology	0428
Operations Research	0796
Plastics Technology	0795
Textile Technology	0994

PSYCHOLOGY

General	0621
Behavioral	0384
Clinical	0622
Developmental	0620
Experimental	0623
Industrial	0624
Personality	0625
Physiological	0989
Psychobiology	0349
Psychometrics	0632
Social	0451



*A mi familia; y en especial a quienes me dieron mucho más que la vida:
Raquel y Guillermo.*

Abstract

Studies on the statistical properties of the large scale structure of the universe have often separated the problem into a spatial point distribution of galaxies and a functional variation of their luminosity independent of position. We consequently attempt to bridge these two approaches by defining a family of generalized luminosity fields which depends on both spatial resolution and luminosity intensity. From analysis of 3, 2, and 1-dimensional catalogues, we find that in 3d the galaxy luminosity field exhibits two signatures of multifractal behavior: multiscaling and divergent statistical moments. Furthermore, we find evidence suggesting that the statistics governing this multifractal behaviour are determined by the parameters α (the degree of multifractality of the field) and $C_{1,1}$ (the codimension of the mean luminosity) which we estimate as 1.2 ± 0.4 and 1.28 ± 0.06 respectively. We consequently suggest that the non-linear mechanisms responsible for the formation of galaxies may be of multifractal origin. As many of the analyses were performed on projected fields a theoretical framework for multifractal projections is also developed.

Résumé

Les études statistiques des structures de grande échelle de l'univers ont souvent considéré que séparément la distribution spatiale ponctuelle des galaxies et l'analyse fonctionnelle de leur luminosité sans regard de leur position. Nous essayons donc de concilier les deux approches en définissant une famille de champs de luminosité généralisée qui dépend à la fois de la résolution spatiale et de l'intensité lumineuse. D'après l'analyse des répertoires à trois, deux et une dimension, nous trouvons que le champ tri-dimensionnel de luminosité des galaxies porte deux signatures de multifractalité : l'invariance d'échelle multiple et des moments statistiques divergents. De plus, certains indices permettent de croire que les statistiques qui gouvernent ce comportement multifractal sont déterminées par les paramètres α (le degré de multifractalité du champ) et $C_{1,1}$ (la codimension de la luminosité moyenne) que nous avons estimé à $1,2 \pm 0,4$ et $1,28 \pm 0,06$ respectivement. Conséquemment, nous suggérons que les mécanismes non-linéaires responsables de la formation des galaxies pourraient être d'origine multifractale. Puisque plusieurs des analyses ont été effectuées sur la projection des champs, un cadre théorique pour la projection des multifractales a été élaboré.

Table of Contents.

Abstract.	i
Résumé.	ii
Table of Contents.	iii
Acknowledgments.	v
Contributions to Original Knowledge.	vi
Chapter One: Introduction.	1
1.1 Motivation and Previous Studies.	1
1.1.1 The spatial distribution of Galaxies.	1
1.1.2 Studies on the Luminosity Distribution.	6
1.2 Generalized Luminosity Fields.	7
1.2.1 Definition of the generalized luminosity fields.	7
1.2.2 The relation between $L_{\eta,\lambda}$ and $\ell_{\eta,\lambda}$.	11
1.3 The Data.	14
1.4 Summary of the Thesis.	17
Chapter Two: Multiscaling of the Luminosity Fields.	18
2.1 Fractals as Scale-invariant Sets.	18
2.1.1 Intersection of Fractal Sets.	19
2.1.2 Projection of Fractal Sets.	21
2.2 Multifractals as Scale-Invariant Fields.	23
2.2.1 The Scaling of Moments: Definition of $K(q, \eta)$.	25
2.3 Results from Multiscaling Analysis.	27
2.3.1 Results for $K(q, \eta)$.	27
2.3.2 Comments on the scaling ranges.	29
2.3.3 Results for $c(\gamma, \eta)$.	34
2.3.4 $C_{1,\eta}$: The codimension of the mean of the field.	38
2.4 Universal Multifractals.	41
2.4.1 Estimating α : the DTM Technique.	41

2.4.2 Multifractal simulations of the observed field $\ell_{1,\lambda}$.	46
2.4.3 Comments on the results.	47
Chapter Three: Multifractal Phase Transitions and Self-organized Criticality	49
3.1 Motivation.	49
3.2 Dressed Statistics: Definition of $q_{D,\eta}$.	49
3.2.1 Estimation of the universal parameter H .	52
3.3 Some Consequences of the Observed Value of $q_{D,1}$.	54
3.4 Implications on the Luminosity Function $\Phi(L_\lambda)$.	54
3.4.1 Experimental tests on the form of $I(L_\lambda)$.	54
3.5 The Dressing Dimension D_{dress} .	57
3.6 Estimation of α using D_{dress} .	59
Chapter Four: Conclusions.	61
4.1 General Comments.	61
4.2 Multifractal Picture of the Large-Scale Distribution of Galactic Luminosity.	62
4.3 Concluding Remarks on the Physical Implications of Multifractality.	65
4.3.1 The range of multiscaling.	65
4.3.2 Origins of a multifractal cascade.	65
Appendix One: On Multifractal Notation.	67
Appendix Two: On the Projection of Multifractals.	68
II.1 The Effect of Projections on $K(q)$.	68
II.1.1 The case of the galactic luminosity field $\ell_{1,\lambda}$.	71
II.2 Generalization to the $\eta \neq 1$ Case.	73
II.3 Comments on the Application of the DTM Technique to Integrated Fields.	74
Bibliography.	77

Acknowledgments.

I wish to express my deepest gratitude to my supervisor S. Lovejoy. Mainly for having given me the opportunity of enrolling into this scientific adventure and also for having shared with me his research instincts. If any scientific intuition I have developed during these years of research, has been through the useful (and at times exhausting) discussions that we sustained.

The scientific expertise of D. Schertzer and D. Lavallée was also extremely appreciated, especially at times when the thin veil that divides truth from illusion seemed to play gambling games. Special thanks are addressed to C. Hooge for all the technical advices concerning the computer network.

It would be certainly unfair to not mention the academic support received from my colleagues at McGill's G.A.N.G. : S. Pecknold, G. Brösamlen, N. Desaulniers-Soucy, C. Larnder, G. Lewis, J.F. Malouin, P.Silas and F. Bégin. To all of them, I address my gratitude and wish them enlightenment and success.

The intellectual and/or emotional encouragement of my friends Lautaro (fiel a su tierra), Kiko (libre como su risa), Daniel (the Dutch Kiwi), Peter (electric as a Hungarian ion), and Gerd (the German "cachaco") is also deeply thanked.

The write-up of this thesis started back in my homeland of South America, under the vigil of the Southern Cross. While there, I enjoyed the warmth and love of my family. Mauri, Memo, Queni, Moni, Gina y Nacho: these 80 pages of work are for you.

During the last stages of the write-up I benefited from the hospitality of Doña Rosa and her family. To them my deepest gratitude.

Y para terminar con broche de oro, I wish to publicly thank mi compañera Joyce (compañera de sueños y realidades) for her love, comprehension and encouragement. Obrigado viu.

Contributions to Original Knowledge.

In this thesis, we present for the first time the concept of a family of generalized luminosity fields representing (among others) the galactic density, luminosity and mass fields.

The method of estimating the correlation dimension D_c , presented in section 2.1, has been for the first time applied to the catalogue CfA2²⁶ and to the Merged Catalogue of Galaxies⁵⁴.

The multifractal analyses presented in section 2.3 are a generalization of previous studies (done on the specific cases of the galactic density and mass) to a whole family of fields characterized by the exponent η . The methods outlined in this section, of estimating the statistical functions $K(q, \eta)$ and $c(\gamma, \eta)$ are for the first time applied to astronomical research.

This thesis is the first study on the universal character (in a multifractal sense) of the large-scale distribution of galactic luminosity. In particular, the parameters $C_{1,1}$, α and H which describe such universal character have been estimated for the first time.

This thesis represents the first treatment of the power-law behaviour at the high end of the luminosity function as a first order multifractal phase transition. The estimates of the quantities $q_{D,\eta}$ and D_{dress} are also original.

The formalism discussed in appendix 2 on the spatial projection of multifractal fields has been developed in collaboration with S. Lovejoy and D. Schertzer. This formalism, although represents a preliminary study, has been for the first time presented in this thesis.

Chapter One

Introduction.

1.1 Motivation and Previous Studies.

Since the birth of modern cosmology, statistical studies on the large-scale distribution of luminous objects in the universe have either treated the problem as a point distribution in space, or as a functional variation in the luminosity independent of the spatial distribution. However, neither approach by itself is sufficient to completely describe the observed universe. In this chapter we shall present an overview of the main achievements and disadvantages of each approach. We shall then argue that multifractals provide a natural framework to combine both the spatial and the luminous properties of celestial objects and will consequently define a family of generalized luminosity fields. These fields will be the primary subject of study of this thesis.

1.1.1 The spatial distribution of galaxies.

The most widely accepted view of the spatial distribution of galaxies arose in the 70's following Peebles' work on the two-point correlation function $\xi(r)$. This function is defined in terms of the point density $\rho(\vec{r})$ of a set of N galaxies embedded in a volume V within which statistical homogeneity and isotropy are assumed to exist:

$$\xi(r) \equiv \frac{\langle \rho(\vec{r}_1) \rho(\vec{r}_1 + \vec{r}) \rangle}{\langle \rho \rangle^2} - 1 \quad (1.1)$$

where $\langle \rho \rangle = N/V$ is the spatially-averaged density of the sample and \vec{r}_1 is the position of a galaxy in the set. We note that $\xi(r)=0$ for a uniform random process, $\xi(r)>0$ if the

positions of galaxies are correlated and $\xi(r) < 0$ if the galaxies' positions are anticorrelated.

Peebles and his collaborators (see for instance refs. 1-5) found that $\xi(r)$ scales as a power-law

$$\xi(r) \propto \left(\frac{r_0}{r}\right)^C \quad (1.2)$$

where $r_0 \approx 5 - 10 h^{-1}$ Mpc (h is in units of $100 \text{ km sec}^{-1} \text{ Mpc}^{-1}$), and* $C \approx 1.77$. An important point about the expression in 1.2 is the value of the so-called "correlation length"## r_0 . We note that for distances comparable to r_0 , $\xi(r)$ approaches unity, which indicates that r_0 corresponds to the inner scale of the scaling relation 1.2.

A power-law behavior of $\xi(r)$ at scales smaller than r_0 indicates a fractal distribution in this range of scales (see for example refs. 6-8). This fractal interpretation had been previously suggested by Mandelbrot in 1975⁹. In 1983, Grassberger and Procaccia¹⁰ defined the correlation dimension D_c as the limiting behavior of the correlation integral $C_1(r)$ defined as

$$C_1(r) = \int_0^r 4\pi s^2 (1 + \xi(s)) ds \quad (1.3)$$

so that

$$\lim_{r \rightarrow 0} C_1(r) = r^{D_c} \quad (1.4)$$

$C_1(r)$ measures the probability of finding a second object inside a sphere of radius r , centered on an object of the set. By differentiating both sides of 1.3, and using 1.4 as the asymptotic form of $C_1(r)$ we obtain that

$$\begin{aligned} 1 + \xi(r) &\propto \left(\frac{1}{4\pi r^2}\right) \frac{d}{dr} C_1(r) \\ &\propto \left(\frac{1}{4\pi r^2}\right) r^{D_c-1} \\ 1 + \xi(r) &\propto r^{D_c-3} \end{aligned} \quad (1.5)$$

These researchers actually denoted "C" as "γ". In this thesis however, "C" denotes codimensions and "γ" orders of singularities

Note however, that this is not a true correlation length, since this would imply exponential decorrelations at $r=r_0$. Therefore, the fact that $\xi(r)$ approaches unity does not necessarily imply a transition towards homogeneity, but is dependent on the resolution of the catalogues

By comparing 1.5 and 1.2, it can be deduced that $3 - D_c = C \approx 1.77$. Consequently, the exponent C can be interpreted as the "correlation codimension"[#] of the fractal distribution of galaxies with dimension D_c . This correlation dimension D_c was estimated as $D_c \approx 1.23$. As it will be seen in chapter two, D_c is a lower bound for the actual fractal (box-counting) dimension of the set. The value of 1.23 implies that the clustering of galaxies is far from space filling or homogeneous ($D=3$), and is more compatible with filamentary structures ($D=1$).

Based on Peebles' work (and later by various authors¹¹⁻¹³) on the correlation functions, the picture of the universe that became widely accepted was that at scales smaller than about 10 Mpc, the distribution of galaxies is highly clustered and forms a fractal set with dimension of about 1.23. At larger scales, galaxies seem to be uniformly distributed in agreement with the idea of a homogeneous and isotropic universe. This picture was based on the fact that the quantity r_o represents the upper limit for spatial correlations. However, as discussed below, more recent analyses (see for instance reference 8) have severely challenged this physical interpretation of r_o on the grounds that for scaling relations such as 2.1, the quantity r_o is non-relevant and simply represents the inner scaling limit of the sample studied.

In recent years various numerical models based on this standard picture have been introduced¹⁴⁻¹⁸. Some authors have accepted the scaling break at ~ 10 Mpc as real (rather than as an artifact of the data set and analysis methods), and attempted to produce "broken" scaling models in order to reproduce the effect (see for instance Castagnoli and Provenzale¹⁵ and Calzetti *et al*¹⁶). However, even for these models the simulations of the galaxy distribution which have been produced often lack the large-scale clustering observed in real data samples. This fact has been attributed, by some researchers^{8,19}, to apparent inconsistencies found in the standard analysis.

- Inconsistencies in the standard analysis.

Despite the general acceptance of the large-scale homogeneity assumption, a few researchers have criticized its validity. The two main arguments are against the value of the correlation length:

1.- If the universe was constructed as a hierarchy of structures up to the largest scales (as it was first proposed by Fournier d'Albe²⁰ in 1907 and later by Charlier²¹ in 1922), then a value for smaller scales of the mean-space density $\langle \rho \rangle$ (as defined in equation 1.1) would

In chapter two it will be shown that for any fractal set of dimension D_f , its "codimension" C is defined as $C \equiv D - D_f$ (where D is the dimension of the embedding space).

become ill-defined. In such case an estimate of the function $\xi(r)$ could become strictly sample-dependent, and hence any analysis performed using this function would induce spurious results especially on the value of the correlation length^{8,22-24,63}. Furthermore, if the distribution of luminous matter in the universe turns out to be multifractal, then over the scaling range the densities would be singular measures whose statistical properties will be dependent in strong ways on the scales over which they are averaged. In such case, the "correlation length" actually corresponds to the internal scale of the scaling regime of the data. Although in principle, this internal scale could correspond to the internal scale of the physics we will argue that it is more likely to reflect the intrinsic resolution of the catalogue, in particular this scale may be associated with the finite number of galaxies in the catalogues.

2.- Recently published 3-dimensional catalogues^{25,26} show large inhomogeneous structures at scales much larger than 10 Mpc. Figure 1.1a shows a 'slice of the universe' 135° wide and $150 h^{-1}$ Mpc deep compiled by de Lapparent *et al*²⁷. Observations show that nearly 90% of all galaxies are located along giant filamentary structures, clusters, and superclusters. It can be seen that in between these structures voids of up to $60 h^{-1}$ Mpc are found^{28,29}. Clearly, a claim that galaxies are correlated only up to a distance of about 10 Mpc seems to be an artifact of the catalogues' statistical limitations and of the data analysis techniques.

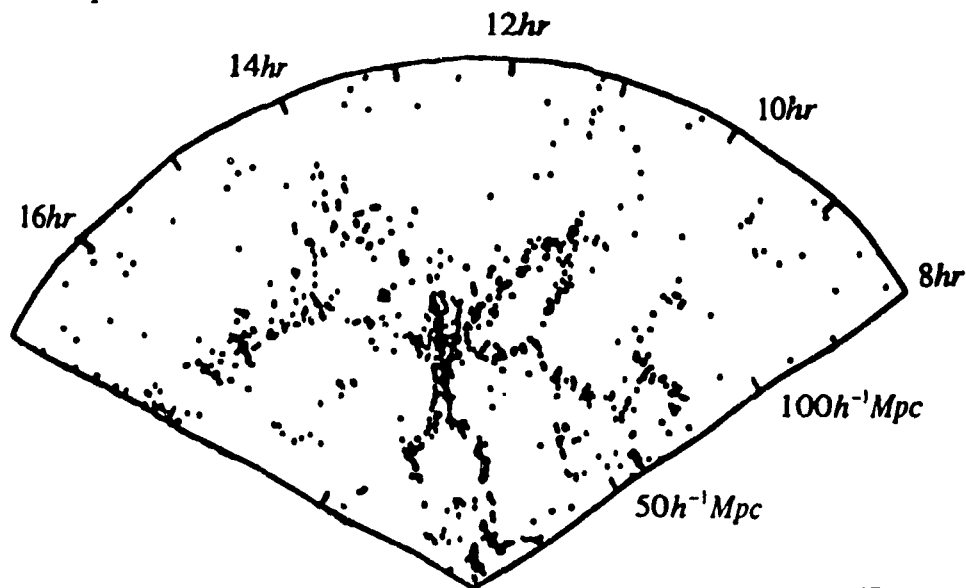


Figure 1.1a. "Slice of the Universe" as compiled by de Lapparent *et al*²⁷. The figure displays 1068 galaxies with apparent magnitude $m \leq 15.5$ located in the region $8hr \leq \alpha \leq 17hr$ and $26^\circ.5 \leq \delta \leq 32^\circ.5$. The sample's depth is $150 h^{-1}$ Mpc (h is in units of $100 \text{ km sec}^{-1} \text{ Mpc}^{-1}$). The large voids observed show the existence of inhomogeneous structures at scales much greater than the "correlation length" r_0 . (Figure from de Lapparent *et al*²⁷).

We have tested the extent of the scaling region in the galaxy distribution using a straightforward method: we estimated the correlation dimension D_c (defined in equation 1.4), from the 1068 galaxies showed in figure 1.1a. To do so, for each galaxy, we counted the number $N(r)$ of neighbours within a distance r from it (in order to avoid edge-effects, we have only considered those galaxies located at a distance larger than r from the edge of the sample). For a scaling fractal set, the average value of $N(r)$ should be given by

$$N(r) \propto r^{D_c} \quad (1.6)$$

Hence, the extent of the linear behavior on a plot of $\text{Log}_{10}(N(r))$ versus $\text{Log}_{10}(r)$, indicates the extent of the scaling region of the set. The result of our analysis is presented in figure 1.1b. The scaling region extends from a few to about 50 Mpc (the radius of the largest circle embedded in the sample). This scaling range is similar to that found by Weng *et al*³⁸ and by Coleman and Pietronero⁸, who used a method of analysis based on an integrated form of the correlation function $\xi(r)$. The break on the scaling observed in figure 1.1b for short distances is a natural cut-off due to the fact that only few galaxies are less than 1 Mpc apart from each other#. Shown for comparison in this figure, is the expected slope for a homogeneous ($D_c=2$) set. It is clear that the distribution of galaxies does not reach homogeneity in this range of scales.

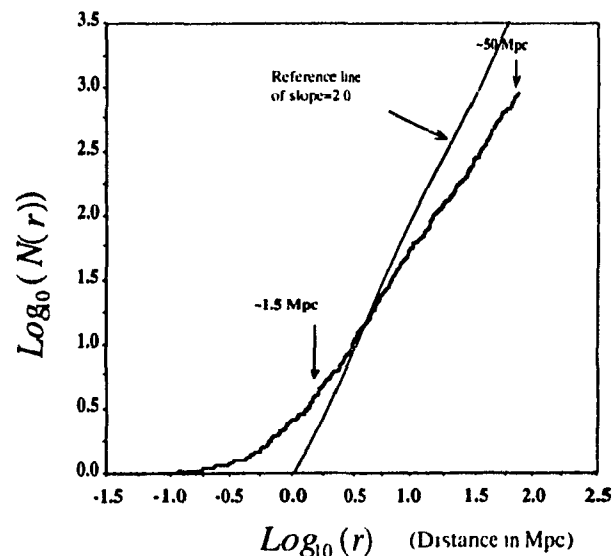


Figure 1.1b. Scaling analysis of a "Slice of the Universe" (as compiled by de Lapparent *et al*²⁷ and described as sample CfA2 in section 1.3). The linear scaling range extends from a few up to about $50 h^{-1}$ Mpc, the size of the largest circle embedded in the sample.

Note that our galaxy's diameter is just a few kpc.

1.1.2 Studies on the Luminosity distribution.

Although there is still debate on the range, consensus exists among researchers on the scaling power-law form of the correlation function. This result is expected since the fundamental processes responsible for the formation of the universe are scaling (as it will be explained in section 1.2) However, a complete statistical description of these processes must go beyond the treatment of galaxies as mathematical point objects and take into account other properties such as their mass and luminosity. Furthermore, the large majority of the research done on the distribution of luminosity ignores its spatial dependence (the only exception being the study done on the multifractal distribution of absolute luminosity^{8,48}). The main functional tool in the standard analyses of luminosity distributions has been the luminosity function $\Phi(L)$. This function is defined in terms of the probability dP that a galaxy with luminosity L in the range L to $L+dL$ is located inside a randomly chosen volume dV :

$$dP = \Phi(L)dLdV \quad (1.7)$$

Integrated forms of this function were fitted to empirical data by Zwicky³⁰ in 1957, Kiang³¹ in 1961 and Abell³² in 1965. Later in 1976, Schechter³³ fitted $\Phi(L)$ (as defined by 1.7) based on the observed luminosity of bright nearby galaxies. Schechter's fit of $\Phi(L)$ was so successful, that since then it has become a standard analytic tool in astronomy (see for example references 34 and 35). Unfortunately, no consensus exists among researchers on the physical process responsible for the mathematical form of this function. Later in chapter three we will propose that the dynamical process responsible for this form is scale-invariant yielding multifractals and multifractal first order phase transitions, related to a non-classical form of stochastic Self Organized Criticality³⁶.

A different analysis^{37,38} done on the luminosity distribution of galaxies revealed the existence of "luminosity segregation"; that is, an increased clustering among brighter galaxies. In terms of the fractal formalism, this research showed that the fractal dimension of a set of galaxies decreased with an increase in the minimum limiting luminosity. In chapter two we will see that if the galactic luminosity is seen as a multifractal field, this result causes no surprise; for in non-linear processes that result in multifractal fields, extreme events (such as highly bright galaxies) are much sparser and less common than "weaker" events (faint galaxies).

1.2 Generalized Luminosity Fields.

In the last few years, it has become fairly clear that non-linear dynamical systems which have no characteristic length-scale produce multifractal fields³⁹. Moreover, since the dynamics of the large scale structure of the universe are scaling (such as gravitational and electro-dynamical interactions) and since scale-invariance is a fundamental symmetry principle⁴⁰, it is then expected that unless strong scale-breaking mechanisms exist the resulting fields (of mass, luminosity and density for instance) should be multifractal.

Multifractal fields possess some well-defined properties and features. The most important is that they show multiscaling; that is, the different moments of the fields also scale in a non-trivial manner. This will be the subject of chapter two. A second generic feature of multifractal fields comes as a consequence of the existence in nature of rare and extreme events such as large storms in the atmosphere⁴¹, violent earthquakes⁴² and in our case, of ultra-bright and massive galaxies. Such extreme events tend to dominate the probability distributions of the fields, leading to the observation of divergent statistical moments associated with first order multifractal phase transitions and related to self-organized criticality³⁶. Such multifractal phase transitions will be the subject of chapter three.

1.2.1 Definition of the generalized luminosities $L_{\eta,\lambda}$ and $\ell_{\eta,\lambda}$.

In order to test the multifractal character of the universe at large scales, we define a family of generalized luminosity fields. These fields are constructed as follows (see figure 1.2a for a schematic representation of the construction of these fields): we first denote the standard information about a galaxy's position and luminosity as $\ell_{\Lambda}(\tilde{\Omega})$ and $L_{\Lambda}(r, \tilde{\Omega})$ (for relative and absolute luminosity respectively[#]). The capital Greek letter Λ indicates raw data at maximum available spatial resolution and the parameters r and $\tilde{\Omega}$ represent respectively the galaxy's radial and angular position in spherical coordinates.

Next, consider a region of space A of size S . In order to define a field, this region is subdivided into smaller regions B_{λ} of size $s < S$ (the quantity λ is the scale-ratio defined as $\lambda \equiv S/s > 1$). The values of all the events $\ell_{\Lambda}(\tilde{\Omega})$ located within each B_{λ} are raised to a power η and then summed up. Finally, this sum is normalized over the entire region A (see figure 1.2a) and the resulting quantity is defined as the "Generalized (apparent) Luminosity Field" $\ell_{\eta,\lambda}$ at resolution λ :

[#] Note that (as it is standard in astronomy) throughout this thesis ℓ denotes apparent whereas L denotes absolute luminosity.

$$\ell_{\eta,\lambda}(\bar{\Omega}_i) \equiv \frac{\int_{B_\lambda(\bar{\Omega}_i)} (\ell_\lambda(\bar{\Omega}))^\eta d\bar{\Omega}}{\left\langle \left(\int_{B_\lambda(\bar{\Omega}_i)} \ell_\lambda(\bar{\Omega}) d\bar{\Omega} \right)^\eta \right\rangle} \quad (1.8)$$

where $B_\lambda(\bar{\Omega}_i)$ is the angular region at resolution λ located at an angular position $\bar{\Omega}_i$, within the field (the subscript i runs between 1 and λ^D , D being the dimension of the sample), and the exponent η is the index that represents the member of the luminosity family under study. The brackets “ $\langle \rangle$ ” indicate ensemble average at resolution λ over the entire region A , so that the denominator in 1.8 ensures the normalization of the field (ie. $\langle \ell_{\eta,\lambda}(\bar{\Omega}_i) \rangle = 1$). Note that the corresponding definition of the generalized absolute luminosity $L_{\eta,\lambda}$ is identical to equation 1.8, but with $\ell_\lambda(\bar{\Omega})$ replaced by $L_\lambda(r,\bar{\Omega})$.[#]

The systematic study of normalized η powers of a multifractal field (as given by equation 1.8) was first proposed by Lavallée⁶⁴. However, the application of such study to an astronomical field has been done for the first time in this thesis.

- Some important members of the family of luminosity fields.

From the definition in equation 1.8, it can be noticed that $\ell_{0,\lambda}$ represents the density field of galaxies at scale-ratio λ equivalent to the quantity $\rho(\bar{r})$ (used in equation 1.1) for the $\lambda \rightarrow \Lambda$ case. This field has been studied by various authors^{7,16,43-47} finding good evidence for multiscaling, some of them up to angular distances greater than 30° (in agreement with the large-scale inhomogeneities observed in figure 1.1a).

$\ell_{1,\lambda}$ represents the apparent luminosity field at scale λ ; that is, the (normalized) total amount of light received from all galaxies located within an angular region B_λ of extent s .

Members of $L_{\eta,\lambda}$ indexed by $0.8 < \eta < 1.25$ (depending on the semi-empirical method used to relate absolute luminosity to mass) represent the corresponding field of mass distribution. Coleman and Pietronero^{8,48}, using an integrated form of the correlation function $\xi(r)$, have recently analyzed the $L_{1,\lambda}$ field finding good support for multifractality up to distances comparable with the size of the catalogues (~ 50 Mpc).

By varying η it is possible to study the statistical features of the whole family of fields as a function of scale (or resolution). The reason for this is that as η is increased

[#] In order to simplify the notation in the rest of the thesis, the generalized luminosity fields will be written as $\ell_{\eta,\lambda}$, so that their spatial dependence will be implicit

emphasis is placed on the extreme values of the field, whereas the opposite occurs for $\eta < 1$. This effect is shown in Figure 1.2b with the $\ell_{\eta,80}$ field for $\eta = 0, 1, 2$ and 3. The data corresponds to 6820 galaxies located in a square of 80° by 80° , centered on the north galactic pole. This sample is denoted MCG80x80 and will be described in detail in section 1.3. Here, the value of λ is 80 corresponding to a cell size of $1''$.

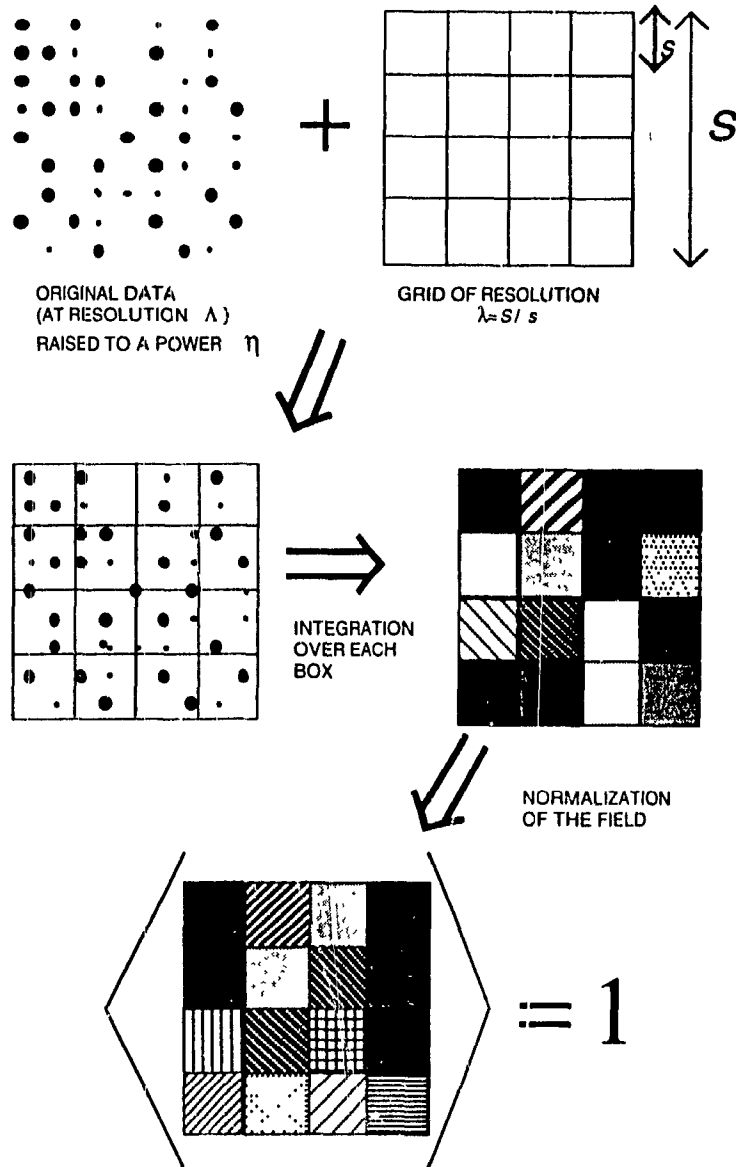


Figure 1.2a. Construction of a 'Generalized Luminosity field': a grid of resolution λ ($\lambda=4$ in this figure) is superimposed onto the original luminosity data (already raised to a power η) and the values of all luminosities within each field-box are summed up. These integrated luminosities (from each field-box) are then multiplied by a normalization constant, so that the average value of the field is made equal to 1.

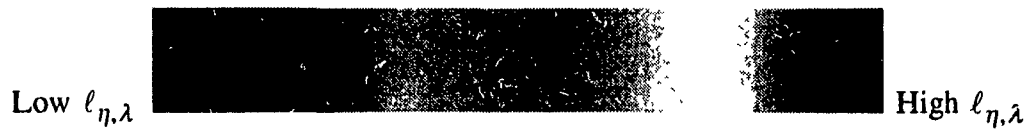
 $\eta = 0.0$  $\eta = 1.0$  $\eta = 2.0$  $\eta = 3.0$ 

Fig 1.2b Example of four fields of $\ell_{\eta,\lambda}$. The values of η are 0, 1, 2, and 3. λ is 80 for all pictures. Each square represents a region of $80^\circ \times 80^\circ$ centered on the north galactic pole. The pixel size is 1° . There are 6820 galaxies in each picture. It can be noticed that as η increases, the extreme values of the field are amplified.

1.2.2 The relation between $L_{\eta,\lambda}$ and $\ell_{\eta,\lambda}$.

The field $\ell_{\eta,\lambda}$ is an angular projection (along the radial direction) of the corresponding field $L_{\eta,\lambda}$. The fact that relative and absolute luminosities are generally related by an angular projection has often stopped researchers from combining results of both analyses. In the case of the angular projection of fractal sets, some results from analyses on simulations have already been given by Dogterom and Pietronero²⁴. These results are qualitative and indicate that large-scale homogeneity observed in projected fractal sets is compatible with large-scale inhomogeneity in the actual 3-dimensional distribution. Moreover, for regular cartesian projections the statistical properties of both projected and unprojected fractal sets can generally be related by a set of simple projection rules (see for instance Falconer⁴⁹), some of which will be discussed in sections 2.1.1 and 2.1.2. We will now propose that the statistical properties of the multifractal fields $L_{\eta,\lambda}$ and $\ell_{\eta,\lambda}$, can also be related due to the specific relation between $L_{\Lambda}(r, \tilde{\Omega})$ and $\ell_{\Lambda}(\tilde{\Omega})$.

The projection of a fractal set can be understood as the “shadow” that the set produces on a plane perpendicular to the direction of integration (see figure 2.2a for a pictorial representation). In the case of multifractal fields, the projection is the integral along one of the spatial coordinates. Since in turbulence the integral of a multifractal density is a flux, both terms: “flux” and “multifractal projection” will be equivalently used throughout this thesis.

Consider first the simpler problem of a regular cartesian projection of a multifractal field. Specifically consider a unit-square with axes along the x and y direction respectively. Suppose that a grid of box size s ($s < 1$) is superimposed onto the square, and then a value $T_{\Lambda}(x, y)$ is assigned to each box. Let us further suppose that the distribution of intensities of the $T_{\Lambda}(x, y)$'s is governed by multifractal statistics. Then a projection $T_{pr}(x)$ along the y axis is defined as the integral

$$T_{pr}(x) \equiv \int_0^1 T_{\Lambda}(x, y) dy \quad (1.9)$$

The left-hand-side of equation 1.9 is independent of the projected coordinate y , which ensures that for multifractals the statistical properties of both $T_{\Lambda}(x, y)$ and $T_{pr}(x)$ are related by a set of projection rules discussed in detail in appendix two.

Let us now consider the specific case of the luminosity fields. For astronomers, the apparent luminosity $\ell_{\Lambda}(\tilde{\Omega})$ is a measure of how bright a celestial object appears to the

observers on the earth. It is not equal to the absolute luminosity $L_\Lambda(r, \bar{\Omega})$, which is intrinsic to the object, due to the distance r that light must travel from its source to us. In particular, radiative transfer theory predicts that the observed luminosity decreases with the inverse square of the distance to the galaxy. In the case of the luminosity fields defined in section 1.2.1, and ignoring the unimportant normalization factor, the quantity $\ell_\Lambda(\bar{\Omega})$ is given by

$$\ell_\Lambda(\bar{\Omega}) = \int_{V_c} \frac{L_\Lambda(r, \bar{\Omega})}{r^2} dV \quad (1.10)$$

where V_c is the volume of the cone whose vertex is at the earth and whose base is the angular region B_Λ where a galaxy at a distance r is located. Noticing that dV is an element of volume equal to $r^2 dr d\bar{\Omega}$ in spherical coordinates ($d\bar{\Omega}$ is the corresponding element of solid angle) we can rewrite 1.10 as

$$\begin{aligned} \ell_\Lambda(\bar{\Omega}) &= \int_{B_\Lambda} \left(\int_0^1 \frac{L_\Lambda(r, \bar{\Omega})}{r^2} r^2 dr \right) d\bar{\Omega} \\ \ell_\Lambda(\bar{\Omega}) &= \int_{B_\Lambda} L_\Lambda(\bar{\Omega}) d\bar{\Omega} \end{aligned} \quad (1.11)$$

The right-hand-side of 1.11 is no longer an explicit function of the projected coordinate r and equations 1.9 and 1.11 are hence analogous in their form. Furthermore, this analogy indicates that as in the case of regular cartesian projections, the statistical properties of the fields $\ell_{\eta,\lambda}$ (derived from $\ell_\Lambda(\bar{\Omega})$) will be related to the statistical properties of the fields $L_{\eta,\lambda}$ (derived from $L_\Lambda(r, \bar{\Omega})$). Hence by combining the results from analyses on both fields, we can maximize the amount of information acquired about the universe's actual structure. A detailed discussion of cartesian projection relationships for multifractal fields will be presented in appendix two.

A further advantage of the use of $\ell_{\eta,\lambda}$ is that since all catalogues of galaxies' position and luminosity are limited by a minimum detectable apparent magnitude, a field constructed using $\ell_\Lambda(\bar{\Omega})$ has a constant minimum threshold. On the other hand, the minimum threshold of a catalogue of absolute luminosity is distance-dependent (see figure 1.3 and equation 1.13 in the next section). Since spurious results may arise from analyses done on fields having non-constant thresholds, researchers using $L_\Lambda(r, \bar{\Omega})$ on their analyses must resort to either constructing sub-samples with constant threshold (the

so-called "volume-limited samples"), or to invoking functions such as the luminosity function $\Phi(L)$ to predict the luminosity of the unobserved galaxies. Unfortunately, neither solution is completely satisfactory since the former severely decreases the number of galaxies available for analysis⁵⁰ (which is already small in a statistical sense), and the latter is based on the empirical assumption that the numerical fits of $\Phi(L)$ are applicable and correct everywhere in space, neglecting any possible statistical spatial correlation.

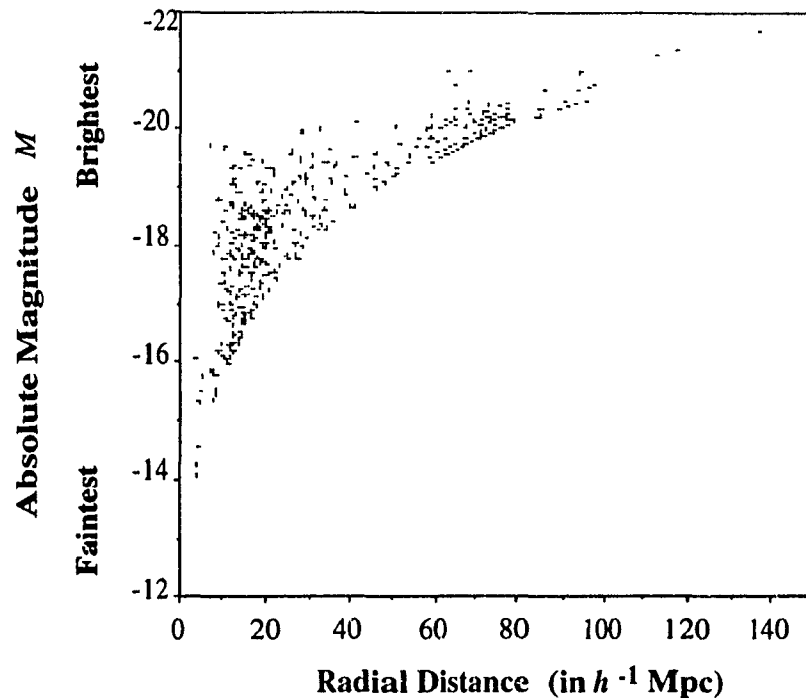


Figure 1.3. Radial distribution of the 1682 galaxies from the sample z40 (described in the next section). The abscissa shows the absolute magnitude M of each galaxy. Observations of luminous objects on the sky are limited by a minimum apparent magnitude, which in terms of absolute magnitudes, is observed as a logarithmic function of the radial distance r . This produces the strong distance-dependence of the minimum threshold observed in this sample. We have used h in units of $100 \text{ km s}^{-1} \text{ Mpc}^{-1}$. (Data from Huchra *et al* ²⁵)

1.3 The data.

In their original forms, catalogs contain information on the apparent magnitude m of the galaxies. The values of the corresponding apparent luminosities ℓ are obtained using⁵¹

$$\ell = 10^{\{(m'-m)/2.5\}} \quad (1.12)$$

where m' is the limiting magnitude of the catalog. The values of the absolute magnitudes M are obtained using the information on the radial distance r to the galaxies⁵¹:

$$M = m - 25 - \text{Log}(r) \quad (1.13)$$

where r is in Mpc. In our analysis all distances are derived using a Hubble constant $H_0 = 100 \text{ km s}^{-1} \text{ Mpc}^{-1}$ and expansion velocities corrected for virgocentric flow, according to^{38,52}

$$V_{corr} = V_m (\sin \delta_i \sin \delta_v + \cos \delta_i \cos \delta_v \cos(\alpha_i - \alpha_v)) \quad (1.14)$$

where V_{corr} is the redshift correction for a galaxy located at right ascension α_i and declination δ_i . V_m is the infall velocity of the Virgo center located at coordinates α_v and δ_v . We used $V_m = 300 \text{ km s}^{-1}$.

Four data samples were used to test the multifractal character of the distribution of generalized luminosities. Three of them are sub-samples of available redshift surveys from the Harvard-Smithsonian Center for Astrophysics (CfA). These samples will be denoted CfA2, CfA2proj and z40. The fourth sample (called MCG80x80) comes from the Merged Catalogue of Galaxies. This catalog contains all galaxies in Zwicky's catalogue⁵³ and was compiled by Kogoshvili⁵⁴ in 1986. The specifications about each sample are:

a) z40: This sub-sample of the CfA1 catalogue²⁵ forms a cone bounded by (in galactocentric coordinates) $b'' \geq 40^\circ$ and $\delta \geq 0^\circ$, and centered on the north galactic pole. Its limiting apparent magnitude is 14.5 and contains 1682 galaxies. This sample contains 3-dimensional information (in spherical coordinates) on the galaxies' position and luminosity. A radial distribution of the galaxies contained in this sample is presented in figure 1.3.

b) CfA2²⁶: This sample contains 1091 galaxies with apparent magnitude less than or equal to 15.5 located within a 6° by 135° strip passing through the Coma cluster. The sample is 150 Mpc deep and is bounded by the angular positions $8h \leq \alpha \leq 17h$ and

$26^{\circ}.5 \leq \delta \leq 32^{\circ}.5$ (where α denotes right ascension and δ is the declination). In the context of this thesis, this sample will be treated as the intersection between a 2-dimensional plane and the actual 3-d distribution (see figure 1.5). This "slice of the universe" contains information on luminosity and position in radial and angular coordinates as depicted in figure 1.1a.

c) CfA2proj: This sample is a projection along constant right ascension α of the CfA2 sample. It contains information only on the galaxies' angular position and luminosity and it is therefore treated as a 1-dimensional sample. Consequently, the luminosity fields constructed from it, correspond to 1-dimensional fluxes of the original 3d distribution. This sample can also be regarded as the intersection between a 1-dimensional strip and a 2-D projection of the actual 3-D distribution. Some examples of the field $L_{1,\lambda}$ as obtained from this sample are shown in figure 2.3 (next chapter) for various values of the scale-ratio λ .

d) MCG80x80 : This sample is a square $80^{\circ} \times 80^{\circ}$ centered on the north galactic pole. Its limiting apparent magnitude is 15.5 and contains information on the luminosity and angular position of 6820 galaxies. Since it can be regarded as a 2-dimensional projection of the actual 3-d distribution, this sample contains no information on radial distance. Consequently, the luminosity fields constructed from it can be regarded as 2-dimensional fluxes of the original distribution in 3d. Figure 1.4 shows the position of this sample on the northern (galactic) hemisphere. The sample was constructed as follows: from the original data file⁵⁴ the angular position of each galaxy (in α and δ) was obtained and then projected onto a plane using a standard equal-area Lambert projection⁵⁵ which retains the density of points of the original distribution. A cartesian grid with origin at the north galactic pole was then superimposed onto this plane. Each axis was labeled from -90° to $+90^{\circ}$ and only those galaxies contained between -40° and $+40^{\circ}$ (for both axes) were included in the final sample. Examples of $\ell_{\eta,\lambda}$ fields produced from MCG80x80 can be observed in figure 1.2b.

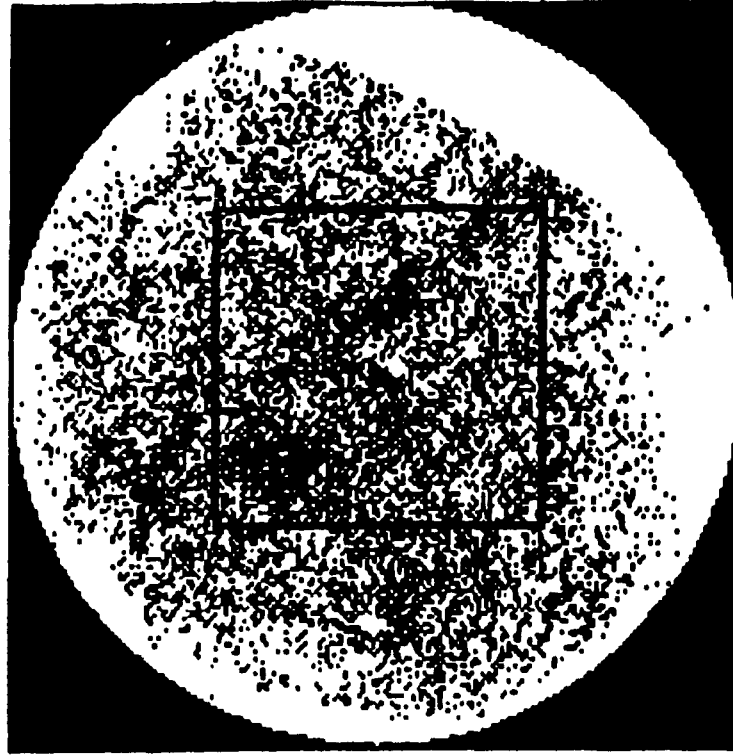


Figure 1.4 Location of the MCG80x80 sample in the northern galactic hemisphere. Each pixel represents an angular box $1^\circ \times 1^\circ$. This figure was produced using data from the Merged Catalogue of Galaxies compiled by Kogoshvili in 1986⁵⁴. This catalogue contains information on the position and apparent magnitude of 20,513 galaxies located in the north galactic hemisphere.

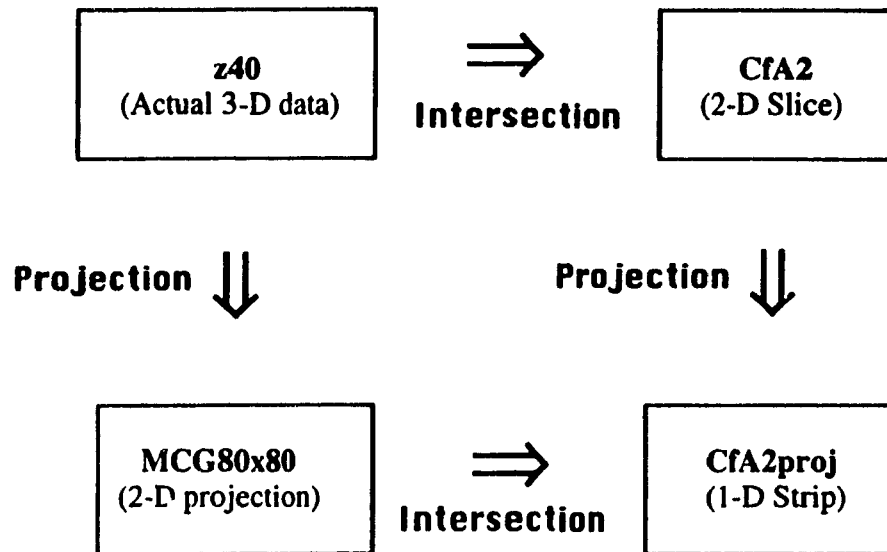


Figure 1.5. Relation among the four catalogues used in this thesis. The sample z40 has 3d information on the actual distribution. The sample CfA2 can be regarded as a 2d intersection of the set z40. CfA2proj is a radial projection along constant angles of CfA2. Finally, the sample MCG80x80 can be understood as a 2d angular projection of the original 3d universe (see the discussion in the text for more details on the various samples).

1.4 Summary of the Thesis.

Chapter two begins by presenting the formalism of fractal projections and intersections. It then explains the theory behind multiscaling and presents the results of the analysis done on the data. The last section of this chapter discusses the theory of “universal multifractals”. Predictions from this theory are then verified using the generalized luminosity fields.

Chapter three concentrates on multifractal phase transitions. Starting from theory, we apply this formalism to the data sets and study the consequences of this phenomenon on the luminosity function $\Phi(L)$.

The last chapter of this thesis is devoted to the conclusions and the physical implications of this research. We examine the advantages and disadvantages of the use of the generalized luminosity fields, and give a hint on a new picture of the large-scale structure of the universe.

This thesis contains two appendices. Appendix one discusses multifractal notation. Due to the importance of projected fields in this thesis, appendix two is entirely devoted to the question of the projection of multifractals. It begins with theoretical considerations and ends with some tests performed on simulations.

Chapter Two

Multiscaling of the Luminosity Fields.

2.1 Fractals as Scale-Invariant Sets.

In nature one often finds phenomena which respect some type of symmetry principle. In physics, these principles are reflected by the equations describing such phenomena and usually the two descriptions are considered equivalent. For example in mechanics, conservation of angular momentum is observed as rotational invariance and energy conservation produces time independent equations. Equations that retain their form under the isotropic transformation $x \rightarrow x / \lambda$ (where λ is some scalar) are said to be scale invariant#. Scale-invariance is a symmetry principle characteristic of non-linear equations and in recent years has become clear that the resulting fields reveal multifractal features³⁹. In mathematical terms scale-invariance is usually represented by power laws. This property is known as scaling and gives us a transformation rule among physical processes acting at different scales. Consequently, the existence of scaling in a physical system implies that what happens at very small scales can be simply related to what is observed at larger scales, and vice versa.

The simplest examples of scale invariance are fractal sets. A proper definition of a fractal set is a mathematical object whose fractal (Hausdorff) dimension D_f is strictly larger than its topological dimension D_T . As an example, D_T for a fractal set of points is zero whereas $0 < D_f \leq D$, D being the dimension of the embedding space.

Consider a D -dimensional space A with size S subdivided into boxes of size $s < S$. Let us define $\lambda \equiv S / s$ ($\lambda > 1$ always). Then the total number N_{tot} of boxes in A is proportional to λ^D (λ for a line, λ^2 for a surface and λ^3 for a volume). Furthermore, suppose that a fractal set F of dimension D_f has N_λ boxes embedded in A . The scaling rules for a fractal set predict that $N_\lambda \propto \lambda^{D_f}$. Consequently, the probability Pr that the n^{th}

Rigorously speaking, this definition corresponds to self-similar scale invariance, a special case of scale invariance in which all spatial coordinates are isotropically re-scaled. For anisotropic scaling, see refs 68 and 69.

box will belong to F is given by the ratio

$$\Pr(n \in F) \propto \frac{N_\lambda}{N_{tot}} = \frac{\lambda^{D_f}}{\lambda^D}$$

$$\Pr(n \in F) \propto \lambda^{-C} \quad (2.1)$$

where $C \equiv D - D_f$ is called the "codimension" of the fractal set.

2.1.1 Intersection of Fractal Sets.

Consider 2 objects with dimensions D_1 and D_2 respectively, both of them embedded in a space of dimension D . Then, the dimension D_I of the intersection of both objects is given by (see for instance ref. 49)

$$D_I = \max[0, (D_1 + D_2) - D] \quad (2.2)$$

or in terms of codimensions: $C_I = \min[D, C_1 + C_2]$ (2.3)

where $C_I = D - D_I$. The intersection relations 2.2 and 2.3 predict, for instance, that the intersection between two planes ($D_1 = D_2 = 2$) in a 3d-space will be a line ($D_I = 1$). Equations 2.2 and 2.3 are not constrained to continuous objects; points sets (such as fractal sets) also obey them^{49,56}. A few examples of intersections are presented in figure 2.1a:

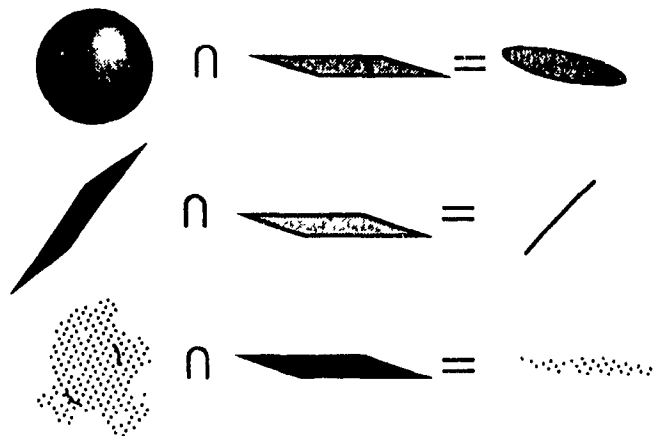


Figure 2.1a. Examples of intersecting objects. In 3-d, the intersection between a sphere ($D_1=3$) and a plane ($D_2=2$) is a plane ($D_I=2$), whereas between two planes ($D_1=D_2=2$) the intersection is a line ($D_I=1$). For a fractal set of dimension D_f the dimension of the intersecting set will depend on D_f . In this figure intersections are represented by the mathematical symbol \cap .

The correlation dimension D_c (defined in equation 1.4) is often very close to the actual fractal (or box-counting) dimension of a set (it is actually a lower bound estimate of it). In chapter one a direct method of estimating D_c was developed and then applied to the CfA2 sample (see figure 1.1b). Figure 2.1b now shows the estimates of D_c as obtained from the MCG80x80 and CfA2proj data samples. The scaling regions for both samples are well defined and reach up to about 40° (the size of the largest angular box totally embedded within the sample) in agreement with previous studies done by Atmanspacher *et al*⁴⁴.

The obtained values of D_c are 1.85 ± 0.04 and 0.85 ± 0.03 respectively for MCG80x80 and CfA2proj, implying a correlation codimension C_c of 1.15 in 3d. Since the 1-dimensional data set CfA2proj can be regarded as the intersection between a 1d-strip and a 2d set such as MCG80x80 (see figure 1.5), we have that in this case $D_1=1$, $D_2=1.85$ (the observed dimension of the set in MCG80x80), and $D=2$. Equations 2.2 and 2.3 predict then that $D_I=0.85$ and $C_I=0.15$ in perfect agreement with the observed values from CfA2proj, as seen below in figure 2.1b:

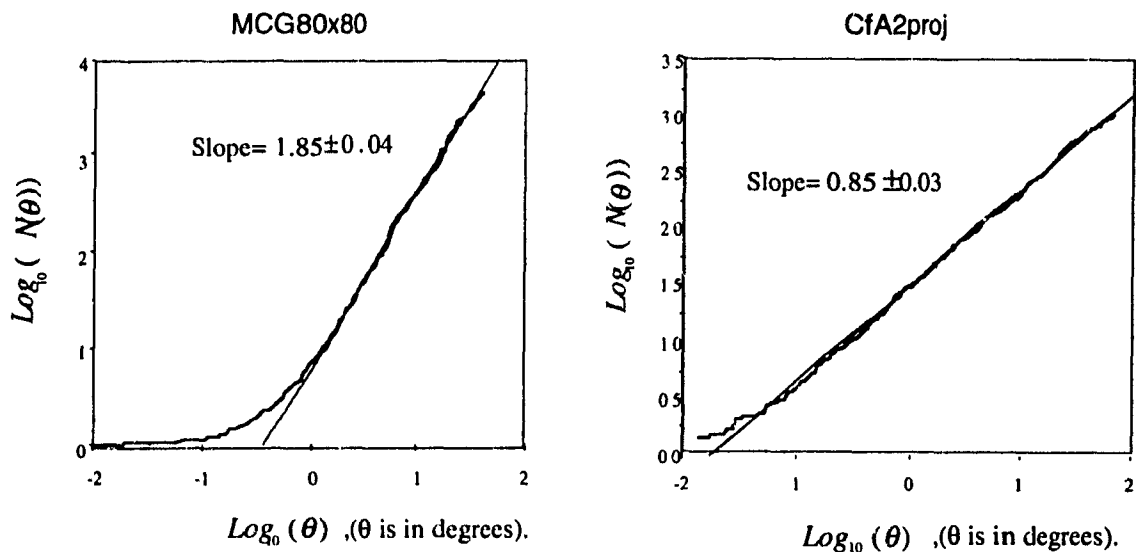


Figure 2.1b . Correlation dimension analysis for the samples MCG80x80 and CfA2proj. The values of the corresponding D_c 's are obtained from the slopes of the linear region on these figures. The observed values are 1.85 ± 0.04 and 0.85 ± 0.03 respectively for MCG80x80 and CfA2proj, in agreement with the intersection relation 2.2. In this figure the quantity θ characterizes the angular box-size (in degrees) used in the analysis of these samples.

2.1.2 Projection of Fractal Sets.

An equation similar to 2.2 predicts the observed dimension D_p of the projection (or shadow) of an object with dimension D_f (embedded in a D -dimensional space), orthogonally projected onto a space of dimension D' :

$$D_p = \min(D', D_f) \quad (2.4)$$

or in terms of codimensions

$$C_p = \max(C_f - C, 0) \quad (2.5)$$

where $C_f = D - D_f$ and $C = D - D'$ (see reference 49 for a discussion). As an example of equation 2.4, a cube ($D_f=3$) produces a square ($D_p=2$) when projected onto a plane ($D'=2$), whereas a line ($D_f=1$) retains its dimensionality after the projection. Some examples of projections are shown below in figure 2.2a.

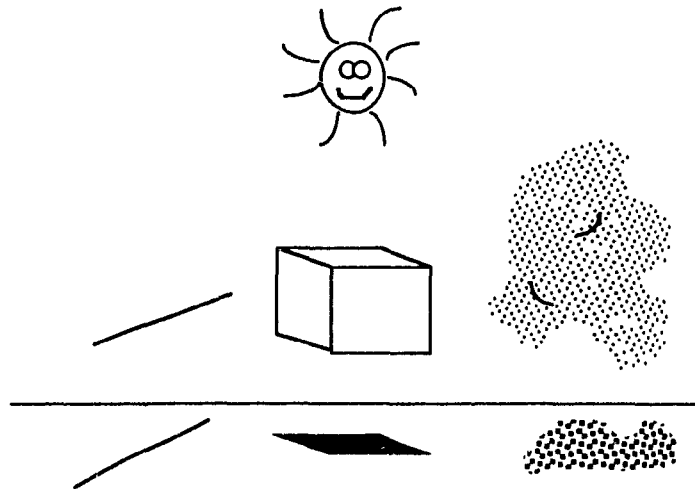


Figure 2.2a. Examples of the projection of objects: the shadow (or projection) of a cube ($D_f=3$) on a plane ($D'=2$) is a plane ($D_p=2$), whereas a line retains its dimensionality ($D_f=1$) after the projection ($D_p=1$). For a fractal set the value of D_p will depend on D_f .

In our analysis of the generalized luminosities, the 2-dimensional data set MCG80x80 can be regarded as a 2-d projection of the 3-dimensional catalogue z40 (see figure 1.5). Consequently, since in the last section D_c was found to be smaller than two for the MCG80x80 sample, equation 2.4 predicts that both samples should show the same value of D_c . This is shown in figure 2.2b where we present the results of the correlation analysis of the z40 sample. The scaling (linear) range seems to reach up to about 60 Mpc. Between about 1 and 7 Mpc the curve shows a well defined slope implying a value of D_c

of 1.80 ± 0.05 and a corresponding codimension of 1.20 (in 3-d). These values are in agreement with those previously estimated from the MCG80x80 sample (see figure 2.1b). Beyond about 7 Mpc a change in the slope is observed. Unfortunately, due to the low number of galaxies in this sample it is hard to conclude whether this change in the slope reflects an underlying physical phenomenon, or is just an artifact of the poor statistics. It is hoped that in the near future, the publication of more complete catalogues will allow us to perform a statistically more robust study.

Another interesting point to be noticed from figures 2.1b and 2.2b is the fact that the obtained estimates of D_c are in disagreement with the previous estimates found from correlation function analysis, where D_c was estimated as being 1.23 (see section 1.1.1). However, our estimates are in perfect agreement with more recent estimates obtained in a more direct manner by Atmanspacher *et al*⁴⁴ using Zwicky's catalogue⁵³ (similar to our MCG80x80 sample) and Wen *et al*³⁸ using the CfA1 catalogue²⁵ (from which our sample z40 was constructed). This discrepancy may arise from the fact that the former estimates of D_c were often derived from analyses on the angular version of $\xi(r)$ (denoted as $\omega(\theta)$) and relating these results to those of $\xi(r)$ via Limber's equation⁷⁰. However, this equation assumes that spatial homogeneity is reached within the sample's limits, which is not the case of the samples analysed here (as shown in figures 1.1a,b). Our analysis on the other hand, is free from such assumptions and it is hence expected to provide more reliable results.

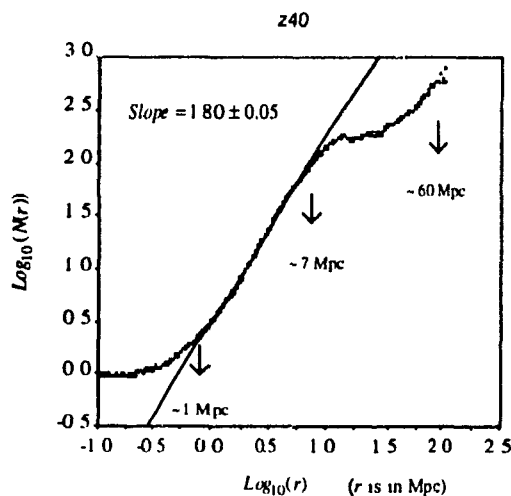


Figure 2.2b. Correlation dimension analysis for the 3-d sample z40. The value of the slope of the linear region implies $D_c = 1.80 \pm 0.05$. This value is in agreement with the value found from the analysis of the MCG80x80 sample (see figure 2.1b) as predicted by equation 2.4. Although a change in the slope is observed at about 7 Mpc, the scaling (linear) region of this sample reaches up to about 60 Mpc (the radius of the largest circle totally contained within the sample).

2.2 Multifractals as Scale-Invariant Fields.

Usually in nature one deals with fields rather than geometric sets. Very few physical phenomena can be reduced to geometric sets of points. On the contrary, most display strong variability on their intensities. Furthermore, the observed intensity of a field depends strongly on the resolution of the measurement as shown in figure 2.3. Here we show the non-normalized fields $L_{i,\lambda}$ of absolute luminosity obtained from the 1091 galaxies in the CfA2proj sample. It can be seen that as the resolution λ decreases from $\lambda=\Lambda$ to $\lambda=5$ (ie. as the luminosities are averaged over increasingly larger angles), the luminosity variation also decreases severely as a result of the averaging process. In this figure the absolute luminosity L_Λ at maximum resolution was estimated using $L_\Lambda=r^2\ell_\Lambda$, where ℓ_Λ and r are the known values of the apparent luminosity and radial distance to the galaxy (in Mpc).

In order to account for the dependence of the measurement on the resolution λ (as observed in figure 2.3), we will write the observed value of the field $\ell_{\eta,\lambda}$ (at resolution λ) as λ^γ . The exponent γ is called the "order of singularity" and is large for strong events and is negative for weak ones^{41,57,66}.

For multifractal fields, a single dimension (or codimension) is not sufficient to characterize all the scaling properties of the distribution. In particular, the codimension of the set of boxes with luminosities $\ell_{\eta,\lambda}$ greater than a value λ^γ will depend on γ . Furthermore, for multifractal fields it is expected that the codimension of a field will decrease with decreasing γ . Since, as we shall show, the large-scale galactic luminosity is indeed a multifractal field, the so-called "luminosity segregation" (reported by various authors^{37,38} and explained in section 1.1.2) can be then easily understood as the natural result of the variation on γ of the galaxy distributions under study.

When dealing with multifractal fields it is convenient to generalize the previous definition of the codimension C of a fractal set to a "codimension function" $c(\gamma, \eta)$ that represents the whole family of exponents characterizing the statistical properties of the field. A relation analogous to equation 2.1 is then obtained for the probability Pr of a certain value $\ell_{\eta,\lambda}$ within the field, of being greater than a given value λ^γ :

$$\text{Pr}(\ell_{\eta,\lambda} \geq \lambda^\gamma) \propto \lambda^{-c(\gamma,\eta)} \quad (2.6)$$

Equation 2.6 is one of the fundamental properties of multifractals and corresponds to the generic outcome of cascade type of processes responsible for the formation of most multifractal fields⁴⁰. The proportionality symbol in equation 2.6 reflects the fact that there are slowly varying prefactors on the right-hand-side of this equation. These prefactors,

however, may be ignored since our interest focuses on the exponential part which will be the dominant behaviour for large λ .

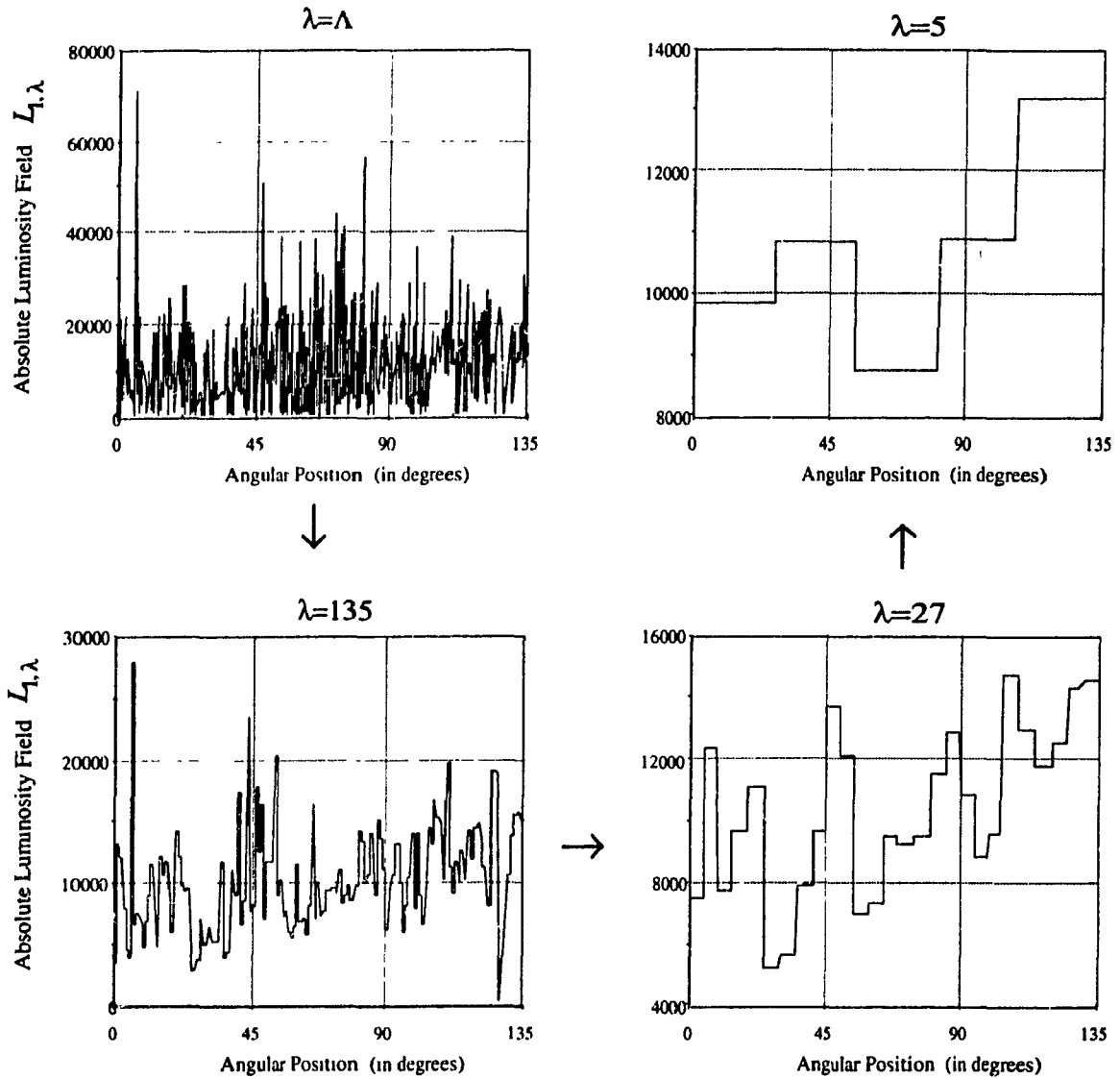


Figure 2.3. Luminosity variability as a function of the resolution λ for the field $L_{1,\lambda}$ as obtained from the 1091 galaxies of the sample CfA2proj. The figures have been produced by averaging the luminosity over increasing angular scales. As the resolution decreases from the original raw-data ($\lambda = \Lambda$) down to a resolution of 27° ($\lambda = 5$), both the variability and the intermittence of the field are observed to decrease severely. In order to facilitate the intercomparison among the figures, the luminosity fields were not normalized.

2.2.1 The Scaling of Moments: Definition of the $K(q, \eta)$ Function# .

A statistically equivalent approach to the question of characterizing the scaling properties of a multifractal is to study the behavior of the different moments of the distribution. Consider the ensemble average of the q^{th} moment of a field $\ell_{\eta, \lambda}$, defined as⁵⁶

$$\langle (\ell_{\eta, \lambda})^q \rangle \equiv \int (\ell_{\eta, \lambda})^q d\text{Pr}(\ell_{\eta, \lambda} \geq \lambda^\gamma) \quad (2.7)$$

Substituting the value of $\ell_{\eta, \lambda}$ by λ^γ and using equation 2.6, we can approximate

$$\langle (\ell_{\eta, \lambda})^q \rangle \propto \int \lambda^{\gamma q - c(\gamma, \eta)} d\gamma \quad (2.8)$$

For large λ , this integral can be evaluated using a saddle point approximation and invoking the Legendre transform of $c(\gamma, \eta)$ which maximizes the value of the exponent in 2.8 (see Parisi and Frisch⁵⁷). This function will be denoted as $K(q, \eta)$ and is defined as

$$K(q, \eta) \equiv \max_{\gamma} (\gamma q - c(\gamma, \eta)) \quad (2.9)$$

Equation 2.8 can then be written as

$$\langle (\ell_{\eta, \lambda})^q \rangle = \lambda^{K(q, \eta)} \quad (2.10)$$

Equation 2.10 is the mathematical definition of multiscaling and is another fundamental property of multifractal fields. For a monofractal $K(q, \eta)$ is linear in q , whereas for multifractals, $K(q, \eta)$ is nonlinear. In general, $K(0, \eta) = 0$ (since $\langle x^0 \rangle = 1$ for any $x \neq 0$) and for a conservative field equation 2.10 predicts that $K(1, \eta) = 0$. Moreover, since $K(q, \eta)$ mathematically corresponds to the second Laplacian characteristic function of the field⁵⁶ it follows that it must be convex. Furthermore, since $c(\gamma, \eta)$ is the Legendre transform of $K(q, \eta)$, it must also be convex. The theoretical forms of both functions $K(q, \eta)$ and $c(\gamma, \eta)$ are shown in figure 2.4 for several values of the exponent η . The plots correspond to estimates obtained from a series of computer-made simulations with

Note that the explicit inclusion of the variable η in $K(q, \eta)$ and $c(\gamma, \eta)$ is specific to the study of the generalized luminosity fields, and most literature on the subject considers only the functions $c(\gamma)$ and $K(q)$ (with η implicitly assumed to be 1) The relations between the latter functions and the functions $f(\alpha)$ and $\tau(q)$ (of common use on strange attractor theory) are discussed in appendix one

known multifractal properties[#]. For high η values the largest singularities of the field are amplified hence extending the γ -range of the $c(\gamma, \eta)$ function. Consequently for increasing η the convexity of $c(\gamma, \eta)$ decreases whereas for $K(q, \eta)$ it increases.

$K(q, \eta)$ and $c(\gamma, \eta)$ are two equivalent forms of fully describing the statistical properties of a multifractal distribution, and throughout this thesis will be the main analytical tools employed. However, when dealing with real data, before attempting to estimate $K(q, \eta)$ or $c(\gamma, \eta)$ we must first verify that the multiscaling relations 2.6 and 2.10 are respected over a broad range of scales. This is an essential pre-requisite (which is not always taken seriously enough) to being confident that the estimates obtained are a robust representation of the statistical properties of the large-scale distribution of luminosity.

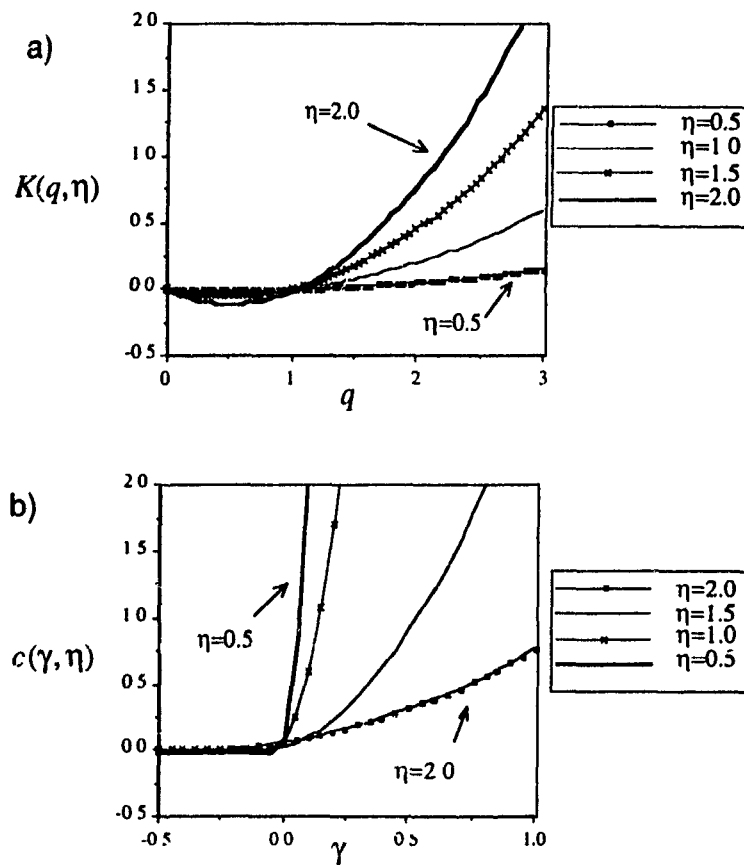


Figure 2.4 . Theoretical forms for the functions: a) $K(q, \eta)$ and b) $c(\gamma, \eta)$ for $\eta=0.5, 1.0, 1.5$ and 2.0 . The curves have been obtained from simulated 2-d multifractal fields of known statistical parameters $\alpha=2.0$ and $C_{1,1}=0.1$ (see section 2.4 for a discussion on these parameters).

[#] For a detailed discussion on the simulation of multifractal fields see references 58 and 41.

2.3 Results from multiscaling analysis.

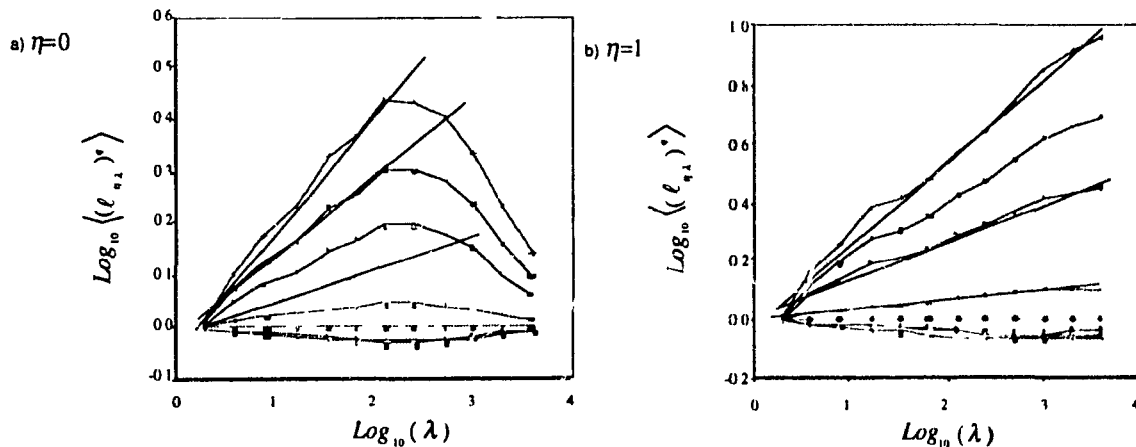
2.3.1 Results for $K(q, \eta)$.

As mentioned in the last section, before estimating the actual form of $K(q, \eta)$ from the data samples, we must check that the scaling regions are well defined. This is shown for the 1091 galaxies of the sample CfA2proj in figure 2.5 which presents the plot of $\text{Log}_{10} \left\langle (\ell_{\eta, \lambda})^q \right\rangle$ versus $\text{Log}_{10}(\lambda)$ for $\eta=0, 1, 2, 3$. The ensemble averages have been calculated over the number \tilde{N}_λ of non-empty boxes at resolution λ using the formula:

$$\left\langle (\ell_{\eta, \lambda})^q \right\rangle = \frac{1}{\tilde{N}_\lambda} \sum_{i=1}^{\tilde{N}_\lambda} (\ell_{\eta, \lambda})_i^q \quad (2.11)$$

where the quantity $(\ell_{\eta, \lambda})_i^q$ represents the field value (raised to a power q) of the i^{th} box in the field. According to equation 2.10, for a multifractal the plots in figure 2.5 should give straight lines. In general this seems to be the case, although (as expected for a finite sample) only for a limited range of scales. The most restricted scaling range is observed for $\eta=0$. In this case the scaling region extends from $\lambda \approx 4$ to $\lambda \approx 128$, implying angular scaling between 1° and about 35° (recall that the maximum extent of this sample is 135°). For higher η 's, the scaling region extends from 35° down to about 0.13° ($\lambda \approx 1024$).

For all values of the exponent η in figure 2.5, fluctuations from linearity are also observed within the scaling regions. This result is not surprising taken into account the statistically low number of events used in this analysis (recall that the total number of galaxies in this catalogue is 1091). Consequently, although multiscaling seems to be observed in all fields studied, the poor statistics derived from the available catalogues are expected to introduce significant uncertainties on the estimates of the function $K(q, \eta)$.



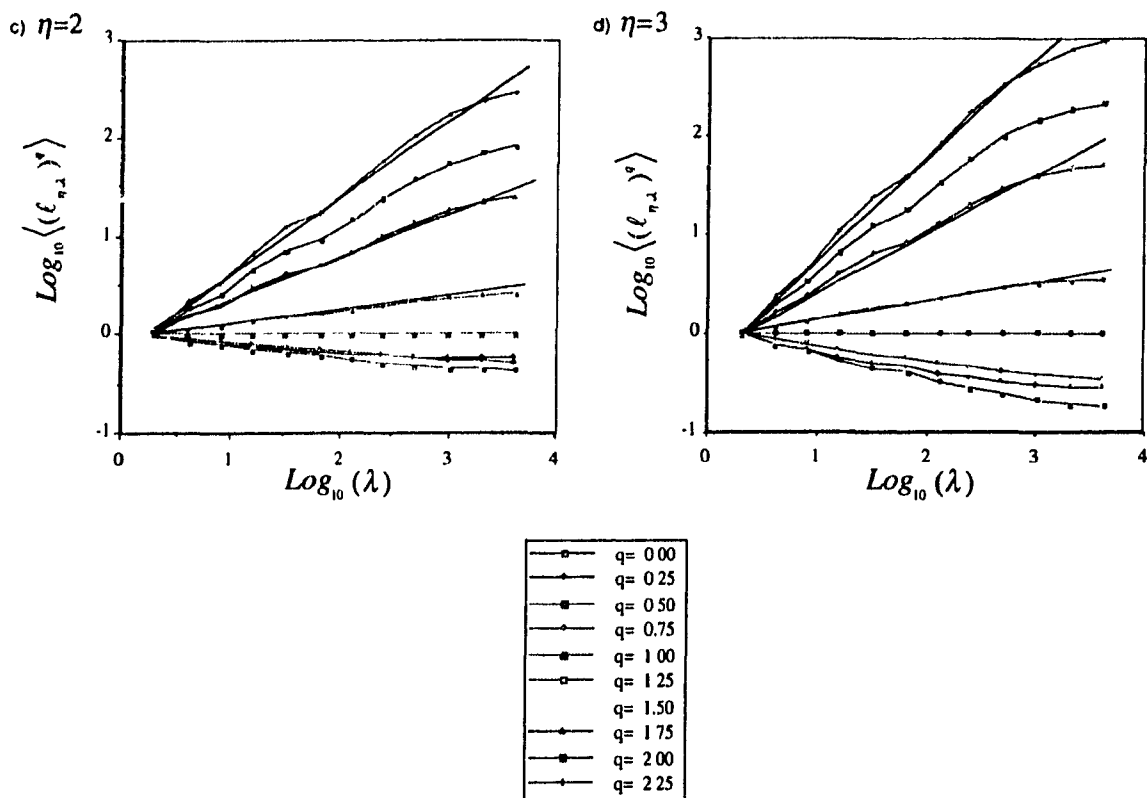


Figure 2.5 . Multiscaling of four $\ell_{\eta, \lambda}$ fields as predicted by equation 2.10. The values of η are 0, 1, 2 and 3. The analysis shown corresponds to the 1091 galaxies from the CfA2pro; sample. Angular scaling regions are clearly observed in all of the fields.

For a given η , the value of $K(q, \eta)$ is obtained for each q from the value of the respective slope in figure 2.5. These slopes have been estimated using a linear regression over the linear scaling region of the curves. The estimated values of $K(q, \eta)$ are shown in figure 2.6 for $\eta=0; 0.5; 1; 1.5; 2$ and 3. Error bars were estimated from the standard deviation of the slope fits, and in order to preserve the clarity of the figure, they are just shown for $\eta=1.5$ and 3.0. The curves are far from linear showing strong convexity (a good signature of multifractality) for all fields $\ell_{\eta, \lambda}$. These results are a generalization of the results found by various authors^{7,16,43-47} on the multifractal features of the point-density field (the $\eta=0$ case). Furthermore, these results suggest that the physical processes responsible for the spatial distribution of luminous objects in the universe are of multifractal character.

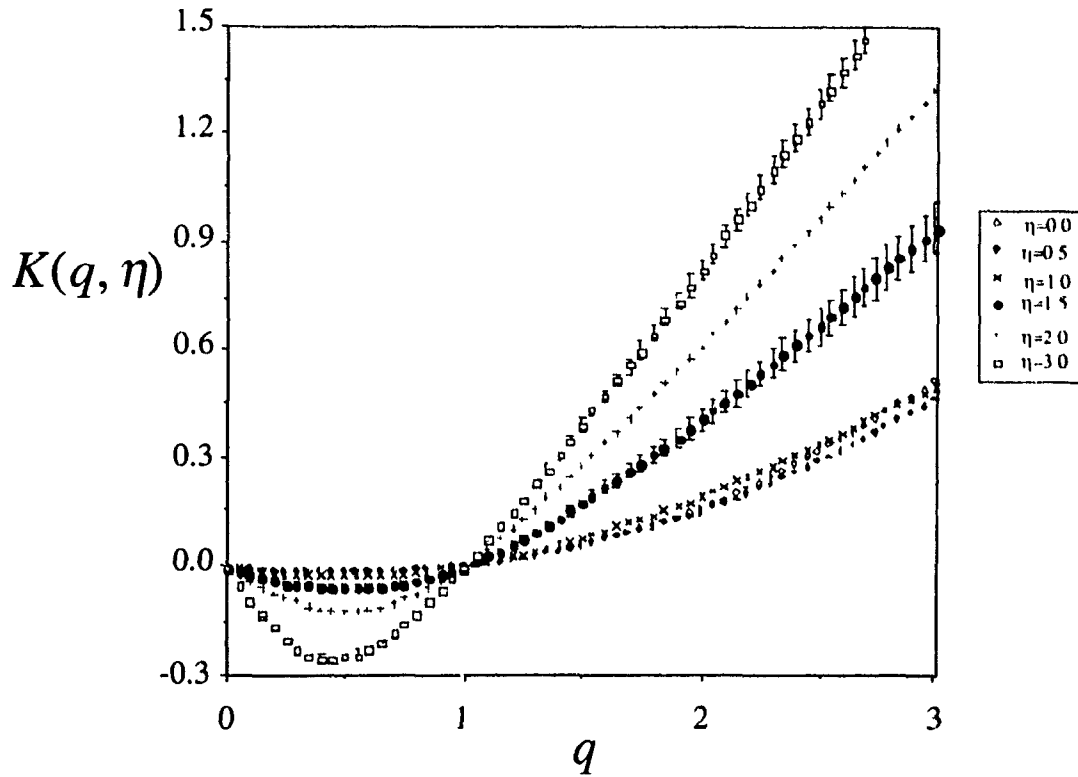


Figure 2.6. $K(q, \eta)$ for the multiscaling curves of figure 2.5. In this figure we have also shown the results corresponding to $\eta=0.5$ and $\eta=1.5$. The number density field ($\eta=0$), the apparent luminosity field ($\eta=1$) and all of the other η -fields show strong convexity, as expected from multifractality.

2.3.2 Comments on the Scaling Ranges.

Figures 2.7a and b show the multiscaling for the function $K(q, 1)$ as estimated from the 1091 galaxies in the sample CfA2 and from its radial projection the sample CfA2proj. It can be noticed that the scaling region for CfA2proj is much more extensive than for CfA2. Since the only difference between these two samples is an integral along the radial direction, it must be concluded that the decreased scaling region of CfA2 is either an artifact of the angular integration, or that is due to a much smaller average number of galaxies per box (since there is only a finite number of galaxies, a break is expected to occur at scales corresponding to densities close to 1 galaxy per box). In figure 2.7c we have plotted the multiscaling corresponding to a version of CfA2 but integrated along constant radii (not along constant angles as in the case of CfA2proj). We note an increase in the scaling region almost identical to figure 2.7b. Also, the corresponding $K(q, 1)$ curves are very similar for these two integrated fields as shown in figure 2.8. Since the latter integration is not an

angular integration we are left to conclude that the break is only due to the insufficient number of galaxies per box. In particular we note that for a field integrated by D dimensions, the average number of galaxies per box increases by λ^D .

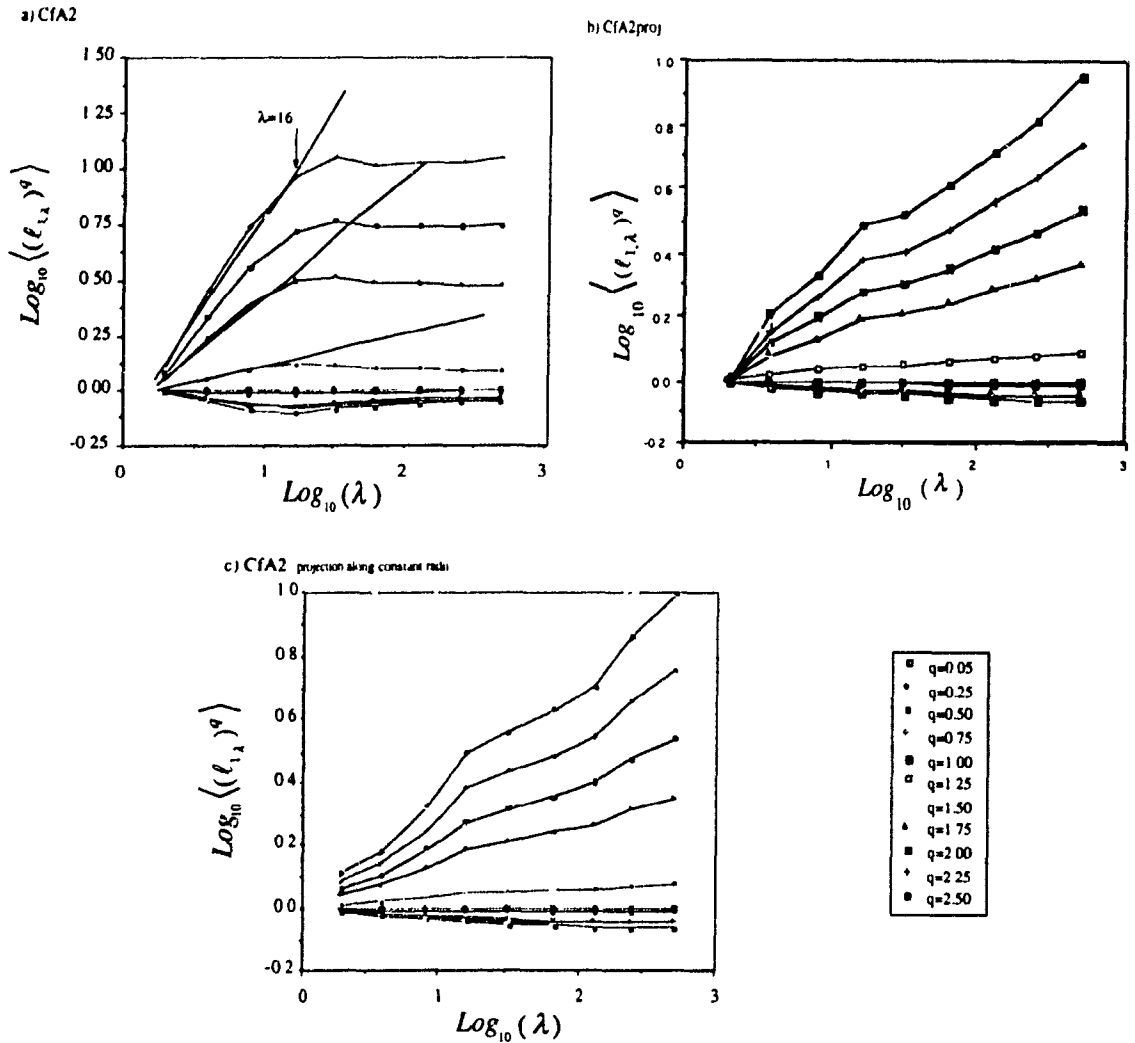


Figure 2.7 Multiscaling of $K(q,1)$ for various samples. a) CFA2. b) CFA2proj. c) A version of CFA2 integrated along constant radii (not constant angles as in the case of CFA2proj). The similarity between the scaling ranges of figures b and c suggests that the improvement on the scaling regions is independent of angular fluxes or integrations.

The agreement of the statistical functions (as evidenced by figures 2.7b,c and 2.8) of both fluxes (along constant angles and along constant radii) suggests that standard cartesian integrations can be used as a first order approximation of the actual angular integrals. This will be our assumption in the remaining of this thesis,

The improved scaling regions observed in the projected fields make us more confident on the statistical parameters estimated from them. Consequently, in the remainder of this thesis emphasis will be placed upon the results from analyses on the integrated samples CfA2proj and MCG80x80. Since these two samples are related via an intersection (see figure 1.5) the knowledge of the statistical properties of (multi)fractal intersections will be fundamental in comparing the results of the analyses from both samples.

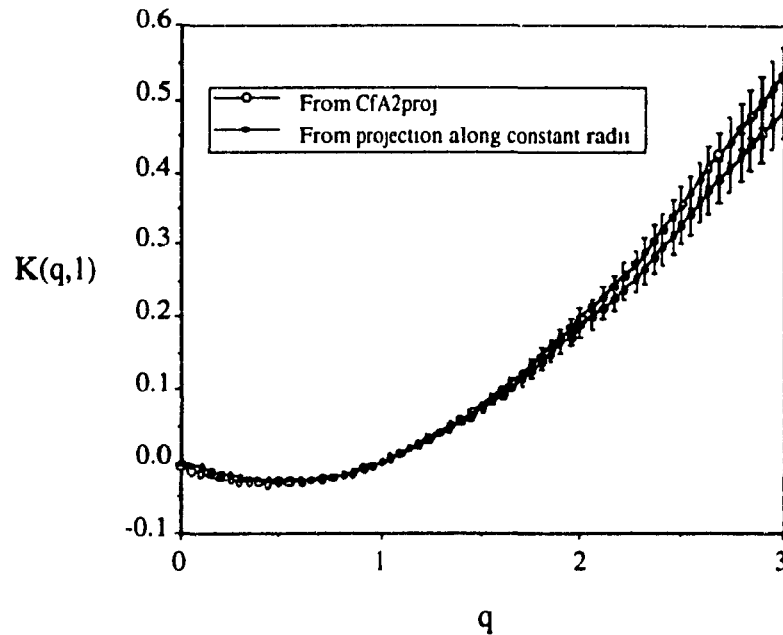


Figure 2.8. $K(q,1)$ curves estimated from two integrated sub-samples of the sample CfA2: one along constant angles (this is the standard CfA2proj sample), and the other along constant radii. Both curves agree implying that cartesian projections are in this case a good first order approximation of the actual angular integrals. These curves were obtained from linear regressions on the slopes of the linear region of the curves shown in figures 2.7b and 2.7c

A further example of the importance of having sufficient galaxies per box can be observed when the MCG80x80 sample is divided into 6° strips, and each strip is treated as a 1 dimensional slice of the sky[#]. Figures 2.9a to 2.9d show the multiscaling of four of the thirteen resulting strips. It can be noticed that both the scaling range and the values of the slopes (for a constant q) vary strongly. This (as it will be explained in chapter three) is a consequence of the critical behaviour of the luminosity fields associated to first order multifractal phase transitions.

[#] This is an approximation to the fact that each strip is 6° by 80° long

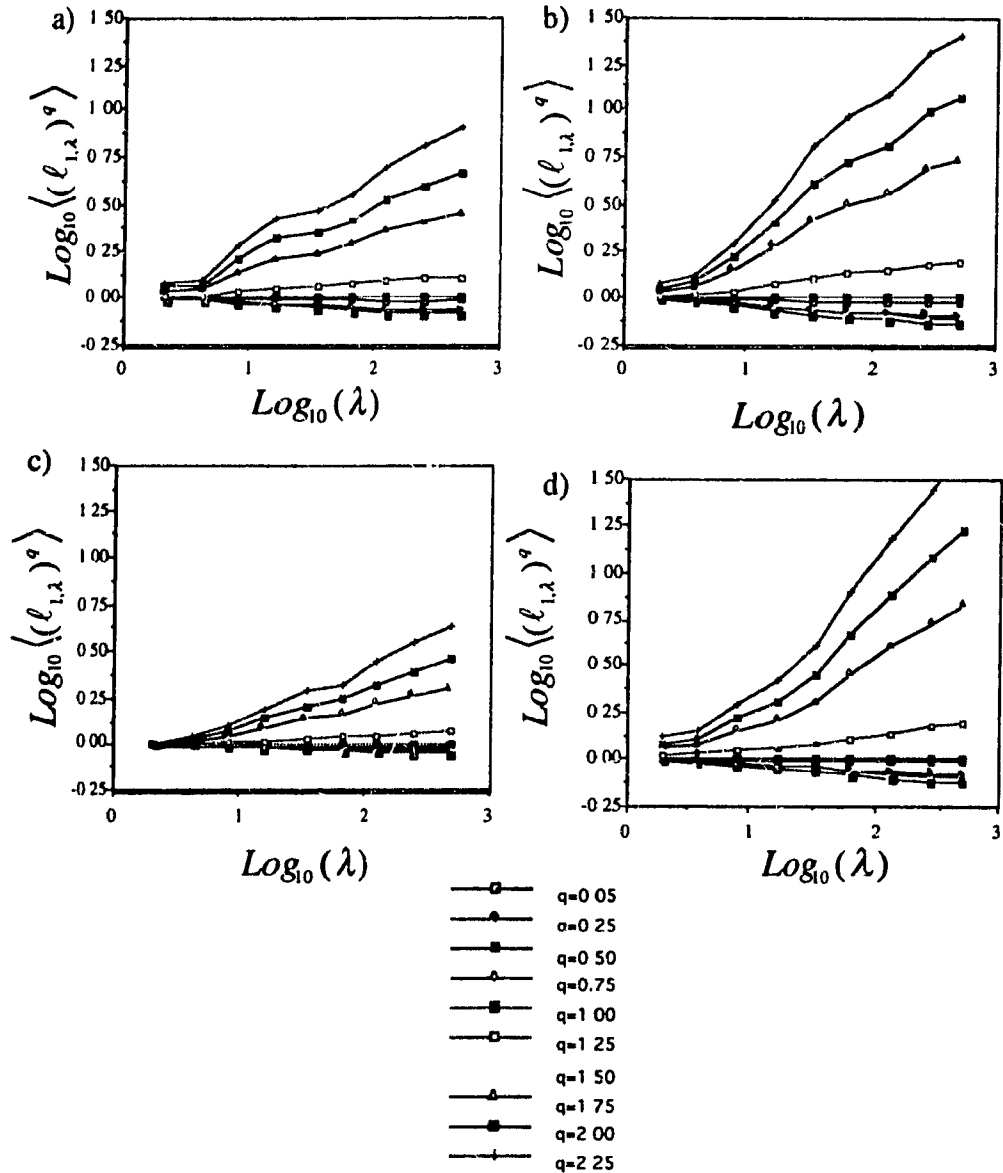


Figure 2.9. Multiscaling corresponding to four of the thirteen 1-dimensional flux-strips produced by slicing the MCG80x80 sample into 6° strips. It can be observed that both the scaling range and the value of the slopes (for a given q) vary significantly from strip to strip. This will be explained in chapter three as the result of the critical behaviour of the luminosity fields (section 3.3).

In statistical terms, each of these thirteen flux-strips is equivalent to the sample CfA2proj (see figure 1.5) and they are hence expected to show scaling ranges broader than the corresponding ranges of the whole MCG80x80 sample. This effect can be better observed in figure 2.10 where we see that the multiscaling of the ensemble average of the thirteen 1d strips (shown in figure 2.10a) shows an increased scaling range when compared to the scaling of the original 2-dimensional MCG80x80 sample (see figure 2.10b).

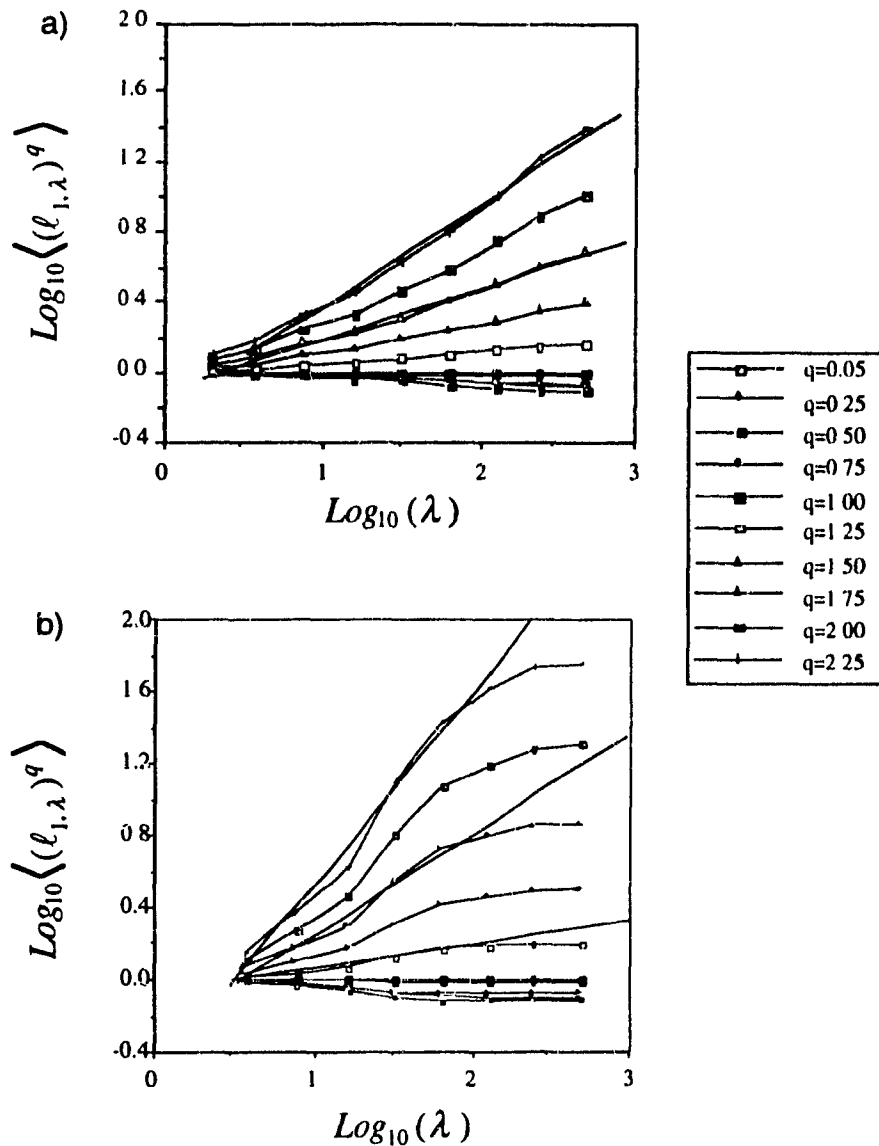
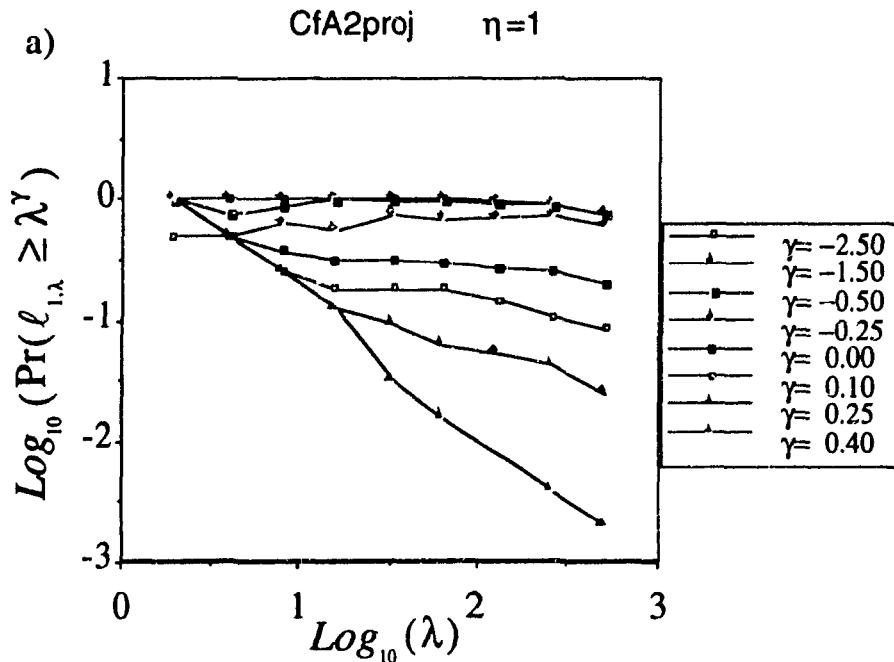


Figure 2.10. Multiscaling of the apparent luminosity field $\ell_{1,\lambda}$ as obtained from a) the ensemble average of the thirteen 1-dimensional flux-strips obtained from the sample MCG80x80; and b) the original 2-dimensional MCG80x80 catalogue. The scaling region is significantly broader for the case of the averaged multiscaling curves. It is argued that this effect is a consequence of the increased box-density of galaxies in the 1-dimensional samples.

In this section we have shown that in order to obtain statistically robust scaling ranges, it is necessary that the corresponding fields be constructed from a sufficiently high number of galaxies per field-box. Since this number is generally higher in integrated fields, in the remaining of this thesis the estimates of the statistical functions $K(q, \eta)$ and $c(\gamma, \eta)$ will be obtained from analyses performed on the integrated samples CfA2proj and MCG80x80.

2.3.3 Results for $c(\gamma, \eta)$.

When studying probability distributions, the definition of multiscaling that applies is given by equation 2.6. In this case the probabilities are estimated (at a given resolution λ) from the ratio of the number N_γ of structures with orders of singularity greater than a given γ , to the total number N_λ of boxes at scale λ . Figures 2.11a and 2.11b show the multiscaling corresponding to the function $c(\gamma, 1)$ as estimated from the CfA2proj and CfA2 samples. Once again, more extensive scaling regions are observed for the radially integrated field in agreement with the conclusions of the last section. However, the curves in these graphs are less straight than the corresponding analyses using $K(q, \eta)$. This is consistent with the fact that $c(\gamma, \eta)$ is highly sensitive to normalization due to the slowly varying prefactors neglected on the right hand side of equation 2.6#. Furthermore, the situation is worsened by the fact that, because of a statistical “dressing” of the field, the sample mean may actually be a poor estimate of the actual ensemble mean (as it will be discussed in section 3.3). In our analysis, we have normalized the field so that at every scale λ the average luminosity is given by $\langle \ell_{\eta, \lambda} \rangle = 1$.



Notice that since $K(q, \eta)$ is defined from a strict equality (see equation 2.10) the estimation of this function is free from normalization problems.

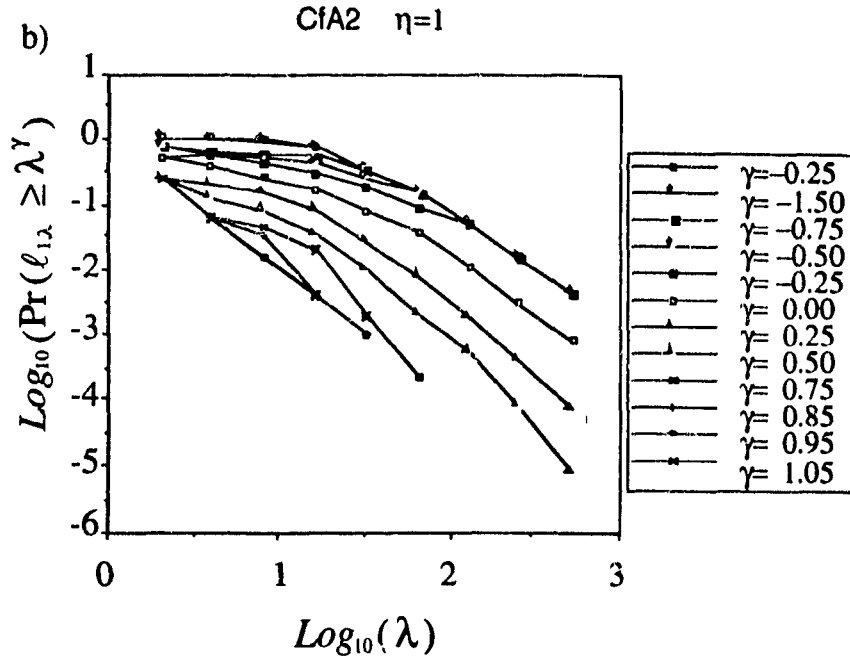


Figure 2.11. Multiscaling for the field $\ell_{1,\lambda}$ as obtained from a) the CfA2proj sample, and b) the CfA2 sample. Although the scaling for the radially integrated field seems to be better defined, the curves shown in these figures are less straight than the corresponding multiscaling curves obtained from the moment scaling analysis (section 2.3.1). It is argued that this is probably due to the normalization of the fields which affects primarily the estimates of the probabilities.

The normalization problem produces scaling regions with greater uncertainty than those from the moment analysis, which are not affected by this problem. Nevertheless, some information can still be extracted and figure 2.12 shows the multiscaling of $c(\gamma, \eta)$ for $\eta=0.5$ and 2.0 (using CfA2proj). The scaling regions are not always very well defined, but roughly linear curves are observed to extend up to $\lambda=512$. In particular, the scaling curves are noticed to become less straight for increasing γ . This is due the existence of very few structures in the field having high order singularities, which in turn leads to poor statistics.

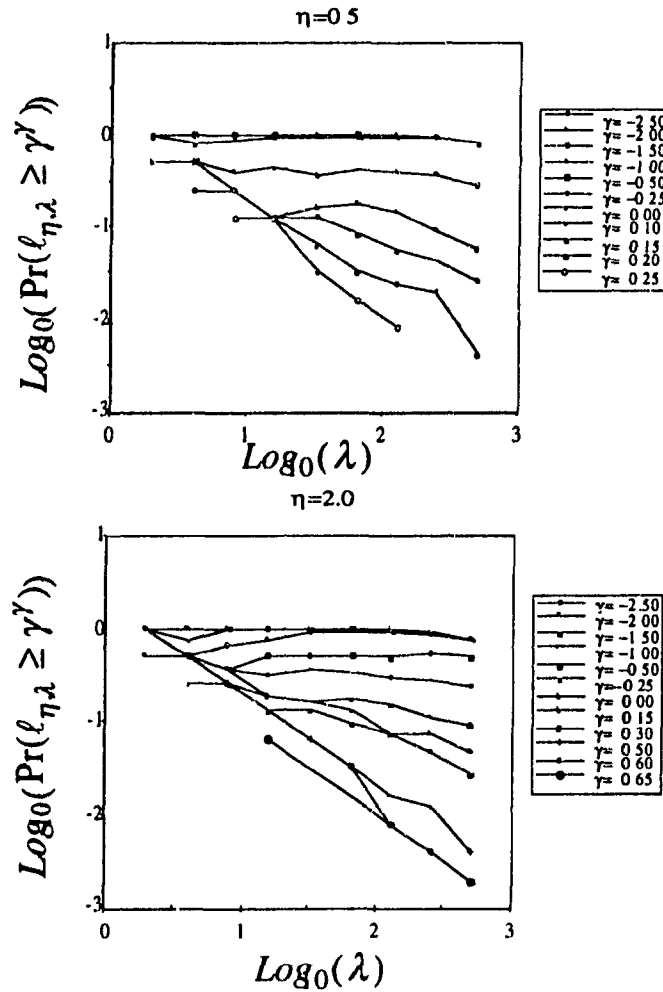


Figure 2.12. Multiscaling for $\eta=0.5$ and $\eta=2.0$ as estimated from the sample CfA2proj. The scaling curves are observed to be less straight than those observed in the analysis of statistical moments.

The lack of good scaling observed in these fields means that the estimates of the corresponding functions $c(\gamma, \eta)$ will not be very accurate. Consequently; due to the relevance in this thesis of the luminosity distribution, the remaining of this section shall concentrate exclusively on the case $\eta=1$. From the slopes of the scaling curves in figure 2.11a (as estimated from a linear regression over the range $2 \leq \lambda \leq 512$) we have estimated the codimension function $c(\gamma, 1)$ corresponding to the apparent luminosity field of the sample CfA2proj. This estimate is shown in figure 2.13. It is observed that there exists a certain order of singularity[#] γ (~ -0.5 in this case), below which $c(\gamma, 1)$ converges to a value

[#] This order of singularity (denoted as $\gamma_{q1,p}$ in appendix 2) corresponds to the minimum order of singularity observable in a projected field. In appendix 2, the value of $\gamma_{q1,p} \sim -0.5$ is actually predicted from purely theoretical considerations.

of about 0.10, the codimension of the lowest singularity. This implies that the dimension of the fractal point set (where all galaxies are treated as mathematical points) is about $1 - 0.10 = 0.90$ for the CfA2proj sample. This value is consistent with estimate from the \mathcal{D}_L (~ 0.85) analysis already shown in section 2.1.1.

A second interesting point about the curve on figure 2.13 is that the high- γ end of $c(\gamma, 1)$ seems to be linear with a slope close to 1.35. In chapter three we will argue that this is indeed the case and that the physical process responsible for this behavior is a first order multifractal phase transition related to a non-classical form of self-organized criticality.

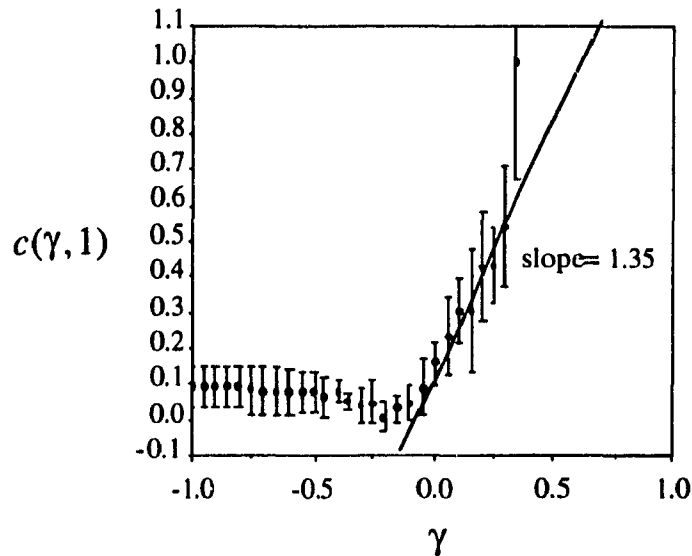


Figure 2.13. Codimension $c(\gamma, 1)$ of the apparent luminosity field as estimated from the CfA2proj sample (the corresponding multiscaling curves are shown in figure 2.11a). The linear behavior for the high- γ end of this curve will be interpreted in chapter three as the signature of a multifractal phase transition, associated to a self-organized critical phenomenon.

In this section we have learned that normalization and statistical noise problems inhibit the existence of well defined scaling regions (as estimated from probability distributions) and consequently that the estimates of the codimension function $c(\gamma, \eta)$ are statistically less robust than the corresponding estimates of $K(q, \eta)$ obtained from the moment-scaling analysis (shown in section 2.3.1). Nevertheless, in the specific case of the apparent luminosity field, the obtained curve of $c(\gamma, 1)$ still contains valuable information on some multifractal properties of the distribution. In particular, in this section we have found some evidence for the existence of a critical behaviour associated with first-order multifractal phase transitions (see figure 2.13). This subject will be developed in detail in the next chapter.

2.3.4 $C_{1,\eta}$: The Codimension of the Mean of the Field.

In section 2.2.1 it was explained that for a conservative field $K(q, \eta)$ is zero for $q=1$. In such a case, equation 2.9 implies that there exists a certain γ (denoted as γ_1) such that, when $q=1$, $\gamma_1 = c(\gamma_1, \eta)$. This fixed point on $c(\gamma, \eta)$ will be denoted as $C_{1,\eta}$ and will correspond to the codimension of the mean of the field $\ell_{\eta,\lambda}$. Since $K(q, \eta)$ and $c(\gamma, \eta)$ are Legendre transforms of each other the following inverse relations apply⁵⁷:

$$q = \frac{\partial}{\partial \gamma} c(\gamma, \eta) \qquad \gamma = \frac{\partial}{\partial q} K(q, \eta) \qquad (2.12)$$

hence for any given q (or γ) there exists a corresponding exponent γ (or q). Equation 2.12 gives us a simple method of estimating $C_{1,\eta}$:

$$C_{1,\eta} = \left(\frac{\partial}{\partial q} K(q, \eta) \right)_{q=1} \qquad (2.13)$$

In its original form, the value of $C_{1,\eta}$ was defined by Schertzer *et al*⁶² in terms of the function $K(q, \eta)$ as obtained from the ensemble average over the whole field#. However, as pointed out in section 2.3.1, the ensemble average of the fields $\ell_{\eta,\lambda}$ were computed over the number \tilde{N}_λ of non-zero boxes in the field at resolution λ (ie, over the fractal set). \tilde{N}_λ can be approximated as $\lambda^{D_{box}}$ (where D_{box} is the box-counting or fractal dimension of the set) and is not necessarily equal to the total number of boxes in the field (given by λ^D , where D is the dimension of the embedding space). Hence, it is expected that the functions $K(q, \eta)$ estimated from each of these methods will differ from each other. In fact, the difference amounts to a linear factor $C_{box}(q-1)$, such that:

$$K(q, \eta)_{whole-field} = K(q, \eta)_{fractal} + C_{box}(q-1) \qquad (2.14)$$

where $C_{box} \equiv D - D_{box}$ is defined as the box-counting codimension. The correlation codimension C_c is an upper bound estimate of C_{box} (both quantities are in general quite similar, and for monofractals they are identical). In section 2.1.1 C_c was estimated in 3d as 1.15 and consequently we estimate $C_{box} \approx 1.15$. Substituting equation 2.14 into 2.13, and denoting $K(q, \eta)_{fractal}$ as $K(q, \eta)$ (as it has been done throughout the thesis) we obtain that the codimension of the mean singularity of the 3 dimensional distribution is given by:

These authors actually defined $C_{1,\eta}$ only for the $\eta=1$ case.

$$C_{1,\eta} = \left(\frac{\partial}{\partial q} K(q, \eta) \right)_{q=1} + C_{\text{bias}} \quad (2.15)$$

In figures 2.14a and 2.14b, the functions $K(q,1)$ and $K'(q,1)$ [#] (corresponding to the apparent luminosity field $\ell_{1,\lambda}$) estimated from the sample CfA2proj are shown. The scaling region extends from $\approx 0.1^\circ$ to $\approx 35^\circ$ (this was shown in figure 2.5b). From the value of $K'(q,1)$ at $q=1$ and using equation 2.15 we estimated $C_{1,1} = 1.25 \pm 0.05$. In chapter 3 it will be argued that the large uncertainty involved on this estimate of $C_{1,1}$ is due to divergence of high statistical moments of the field, related to the linear behaviour previously observed for $c(\gamma,1)$ in figure 2.13.

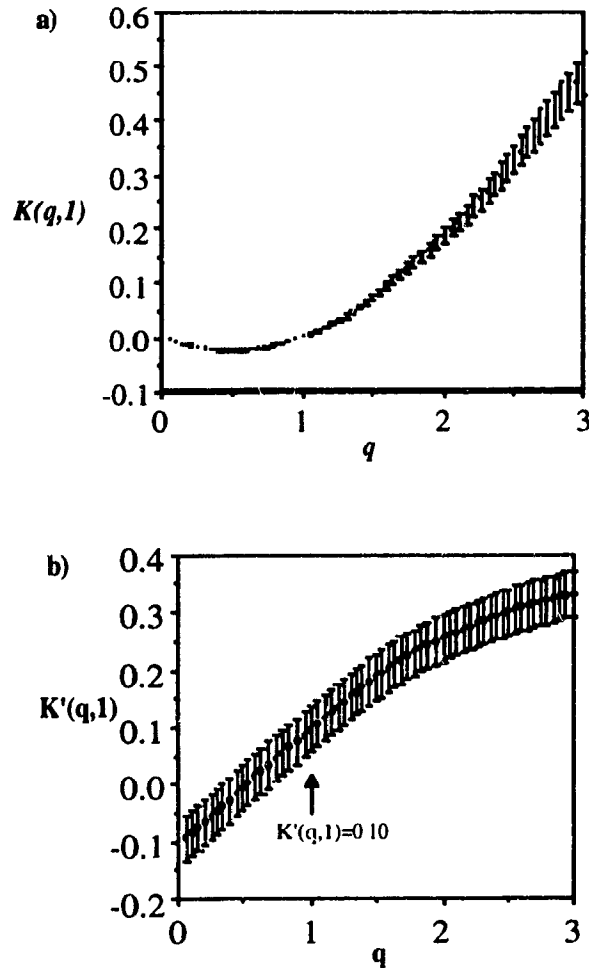


Figure 2.14. a) $K(q,1)$ and b) $K'(q,1)$ as deduced from the CfA2proj sample. From the value of $K'(q,1)$ at $q=1$, we have estimated the codimension $C_{1,1}$ of the mean of the apparent luminosity field to be 1.25 ± 0.05 .

[#] Note that primes (') will never denote differentiation with respect to η in this thesis.

The observed value of $C_{1,1}$ is fairly close to the codimension of the minimum singularity C_c . This raises suspicions about the estimate of $C_{1,1}$, for if such value were correct it would imply that the singularities corresponding to the mean luminosity of the universe are (fortunately for us) just above the minimum singularity responsible for the limiting apparent luminosity observed from the earth. This suggests that the luminosity estimates will be in general quite sensitive to the minimum detectable magnitude. On the other hand, the observed value of $C_{1,1} \sim 1.25-1.30$ appears consistently from the analysis of other samples (as shown in the next figure for the ensemble average of thirteen 6° strips obtained from the MCG80x80 sample).

In the next chapter our analysis will reveal that in fact the estimates of $C_{1,1}$ should be taken cautiously because of a statistical dressing mechanism which contaminates such estimates. Nevertheless, the value of $C_{1,1} \sim 1.28$ may be taken as a rough approximation and will in fact be used in the next section to model simulations of the generalized luminosity fields.

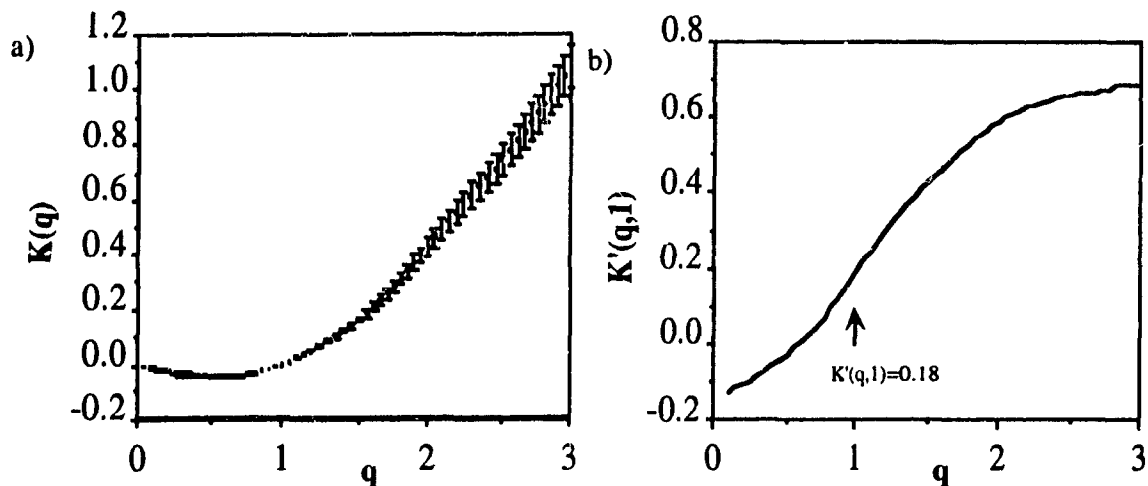


Figure 2.15. a) $K(q,1)$ function and b) its corresponding derivative as estimated from the ensemble average of thirteen 1-dimensional strips obtained from the MCG80x80 sample. From the value of $K'(q,1)$ at $q=1$ we estimated $C_{1,1} = 1.33 \pm 0.05$ in agreement with estimates from CfA2proj (see figure 2.14). The corresponding multiscaling curves were already shown in figure 2.10a.

2.4 Universal Multifractals.

When many multifractal cascade processes interact and "mix" over a finite range of scales, the resulting fields usually attain a stable attractive behaviour which can be expected to fall into specific universality classes. In such case, the functions $c(\gamma, \eta)$ and $K(q, \eta)$ which describe the statistical properties of the resulting fields, can be fully characterized by three parameters. In fact, as in standard probability theory a Gaussian curve can be completely characterized by its mean and its variance, similarly for the case of these "universal multifractals" the statistical properties of the multifractal distribution can be completely described by the quantities $C_{1,\eta}$, α , and H :

$C_{1,\eta}$ corresponds to the codimension of the mean of the distribution, already defined in equation 2.15.

α is called the "index of multifractality" and it can vary between zero (for a monofractal set) and two for a log-normal multifractal field. The value of α is related to the curvature of the function $c(\gamma, \eta)$ at $\gamma=C_{1,\eta}$.

The parameters α and $C_{1,\eta}$ totally determine the form of both functions $K(q, \eta)$ and $c(\gamma, \eta)$. Estimates of these two parameters have been found by various authors for multifractal fields such as seismic moments⁴², turbulent velocity fields⁵⁹, cloud liquid-water content⁶⁰, landscape topography⁶¹, and hadron jets⁶³.

The third universal parameter H is a measure of the non-stationarity of the process and it is consequently equal to zero for all conservative fields. In section 3.2 it will be estimated that $H=0$ in the case of the generalized luminosity fields. In such a case for universal multifractals we obtain that[#]

$$K(q, \eta) = \eta^\alpha K(q, 1) \quad (2.16)$$

Equation 2.16 implies that if the fields correspond to universal multifractals, then the quantity α (corresponding to the index of multifractality of the original 3d distribution) may be estimated from the slope of a plot of $\text{Log}_{10}(K(q, \eta))$ versus $\text{Log}_{10}(\eta)$.

2.4.1 Estimating α : the Double Trace Moment technique (DTM).

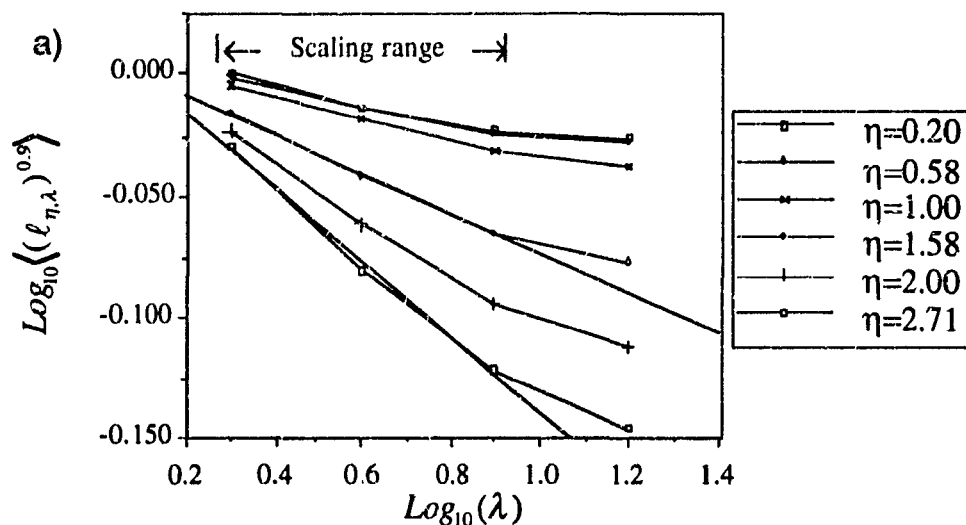
We have attempted to use the above described procedure (denoted in the literature as DTM⁶⁴, which stands for Double Trace Moment) to estimate α for the fields $\ell_{\eta,\lambda}$. The values of the function $K(q, \eta)$ are found from the slopes of plots of $\text{Log}_{10}(\langle \ell_{\eta,\lambda}^q \rangle)$ versus

[#] A complete treatment of the theory of Universal multifractals may be found in reference 62.

$\text{Log}_{10}(\lambda)$ (as predicted by equation 2.10) in the same manner as previously done for the standard moment-scaling analysis (section 2.3.1). The difference with the DTM technique is that here we fix the value of q and then plot $\text{Log}_{10}\langle(\ell_{\eta,\lambda})^q\rangle$ for various values of η whereas in the standard moment-scaling technique the converse was done.

Universality is expected to be observed only within a certain range of q 's. In particular, finite observing dimension leads to the divergence of high order statistical moments, hence even for large enough samples universality can only be observed up to a critical value of q , denoted as $q_{D,1}$. In the next chapter we will estimate that $q_{D,1} = 1.33 \pm 0.05$. Also, the integration (along the radial direction) of the projected samples MCG80x80 and CfA2proj imposes a minimum q (denoted as q_1 in appendix 2) below which universality may no longer be observed. In appendix 2, q_1 will be estimated as 0.6 ± 0.1 . Consequently, when performing a DTM analysis on the fields $\ell_{\eta,\lambda}$, the allowed values of q must be contained within the range $0.6 \leq q \leq 1.33$. This narrow range of allowed q 's is expected to weaken the estimates of some of the statistical parameters that describe the multifractal distribution of luminosity.

Figure 2.16a shows the multiscaling for the fields $\ell_{\eta,\lambda}$ as obtained from the sample CfA2. The multiscaling is shown for $q=0.9$. As previously shown in figure 2.7a, the scaling range of this sample is very short and restricted to $2 \leq \lambda \leq 8$. Using this range, the values of $K(0.9, \eta)$ were estimated from the corresponding slopes and are shown in figure 2.16b as a function of $\text{Log}_{10}(\eta)$. Clearly, this restricted scaling range is not expected to yield very robust estimates of the function $K(q, \eta)$, but at least allows us to make a rough estimate of what the true multifractality index α (obtained from the slope of the linear region in figure 2.16b) should be in 3d, without the complications introduced by the projection of the fields.



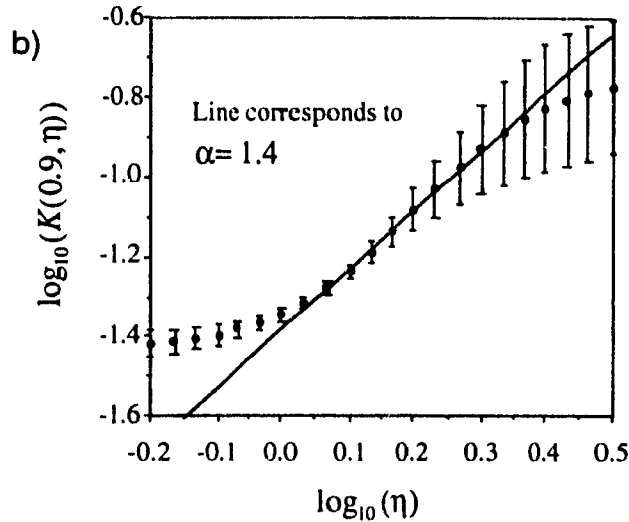


Figure 2.16. a) Multiscaling and b) DTM analysis for the fields $\ell_{\eta,\lambda}$ as obtained from the sample CfA2. The linear region in figure 2.16b is evidence of the universal character of the $\ell_{\eta,\lambda}$ fields. However, the short multiscaling region observed in fig. 2.16a ($2 \leq \lambda \leq 8$) allows only for a "rough" estimate of the multifractality index α in 3d. From the slope of the linear region in figure 2.16b we have estimated $\alpha \sim 1.4$ (according to equation 2.16). We have used $q = 0.9$.

The linear region observed in figure 2.16b is (according to equation 2.16) evidence for the presence of universal behaviour in the three dimensional luminosity fields. Unfortunately, as already mentioned, because of the short range of scales used for the estimation of $K(0.9, \eta)$, the estimate of α obtained in this analysis must only be taken as a first approximation to the actual value. In section 3.6, a more indirect argument, using the projected samples, will be used to estimate $\alpha = 1.2 \pm 0.4$. This value is compatible with the value obtained from figure 2.16b.

The departure from linearity observed in figure 2.16b for low η 's, is due to the fact that as η approaches zero the luminosity intensities are severely diminished and statistical noise dominates the distribution; thus killing the universal behaviour.

In section 2.3.2 we saw that broader scaling regions are generally observed in samples which are radial integrations of the actual three dimensional distributions. Figure 2.17 shows the multiscaling of the fields $\ell_{\eta,\lambda}$ as obtained from the 1091 galaxies of the CfA2proj sample. The multiscaling is shown for $q = 0.9$ and $q = 1.2$. In both cases the scaling ranges are clearly defined from $\lambda = 2$ up to the largest scale $\lambda = 512$ implying scaling between $\sim 0.26^\circ$ and $\sim 67^\circ$ (recall that the total angular extent of this sample is 135°).

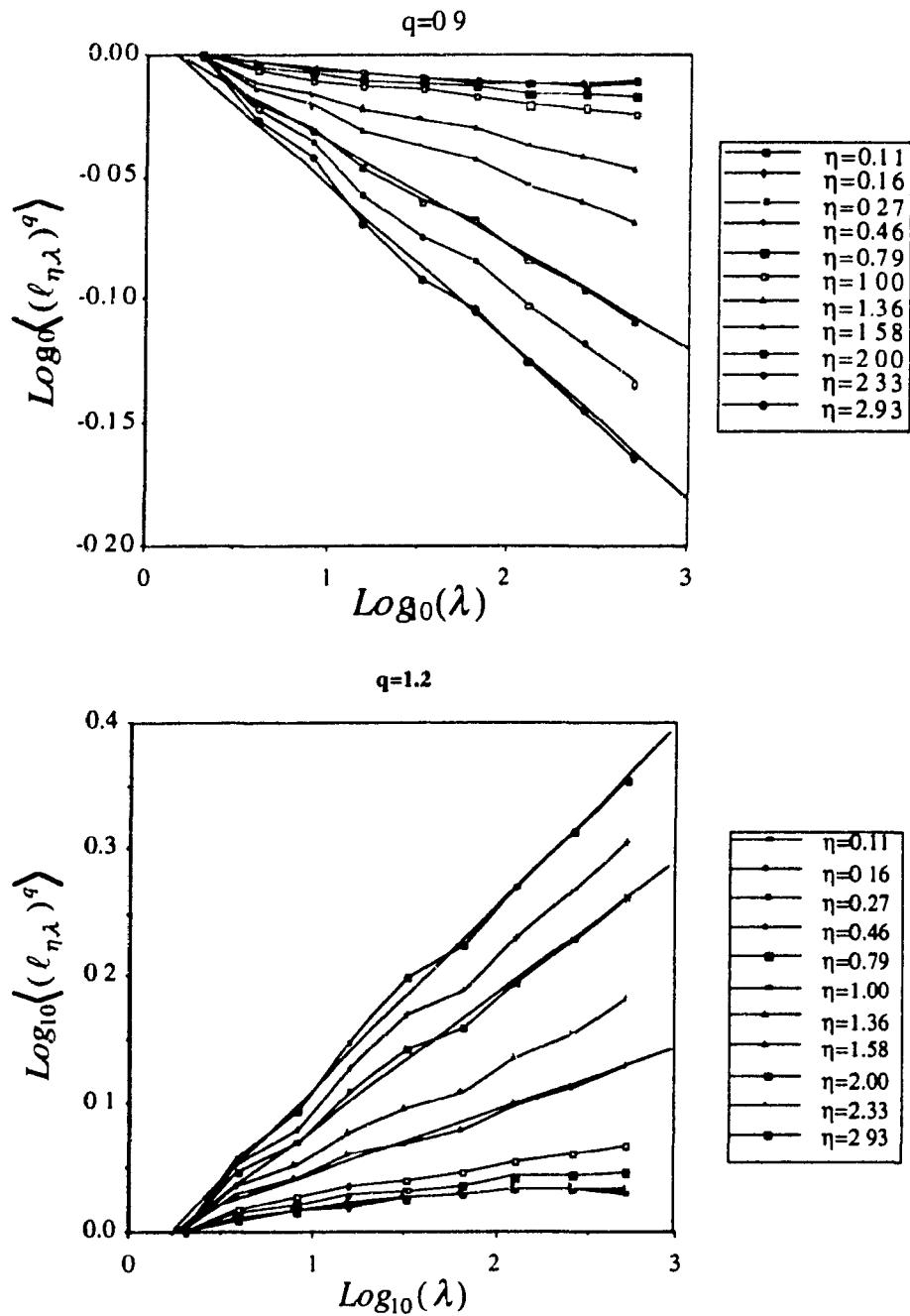


Figure 2.17. Multiscaling for the $\ell_{\eta,\lambda}$ fields as estimated from the sample CfA2proj. Shown are the curves corresponding to $q = 0.9$ and $q = 1.2$. Both figures show linear curves in agreement with equation 2.10. For each set of values q and η , the quantity $K(q,\eta)$ is obtained from the corresponding slope μ of these figures. The resulting functions $K(q,\eta)$ are plotted in the next figure as a function of the variable η (not q as in the standard moment analysis).

Figure 2.18 shows a plot of $\text{Log}_{10}(K(q, \eta))$ versus $\text{Log}_{10}(\eta)$ for $q=0.9$ and $q=1.2$. Both curves display roughly parallel linear regions implying a slope $\alpha_p=2.00\pm 0.06$ independent of q (the subscript "p" refers to the α of the "projected" field). However, this estimate must be cautiously interpreted. In appendix two (section II.3) we show empirical and theoretical evidence that suggests that for integrated (or projected) multifractal fields the value of the observed index α_p is 2, independent of the true value of α for the original distribution in 3d. Therefore, the observed value of α_p should be understood as a signature of the spatial integration of a multifractal field, and does not reflect the intrinsic value of α corresponding to the actual 3d distribution (see appendix 2, section II.3, for a short discussion on the subject).

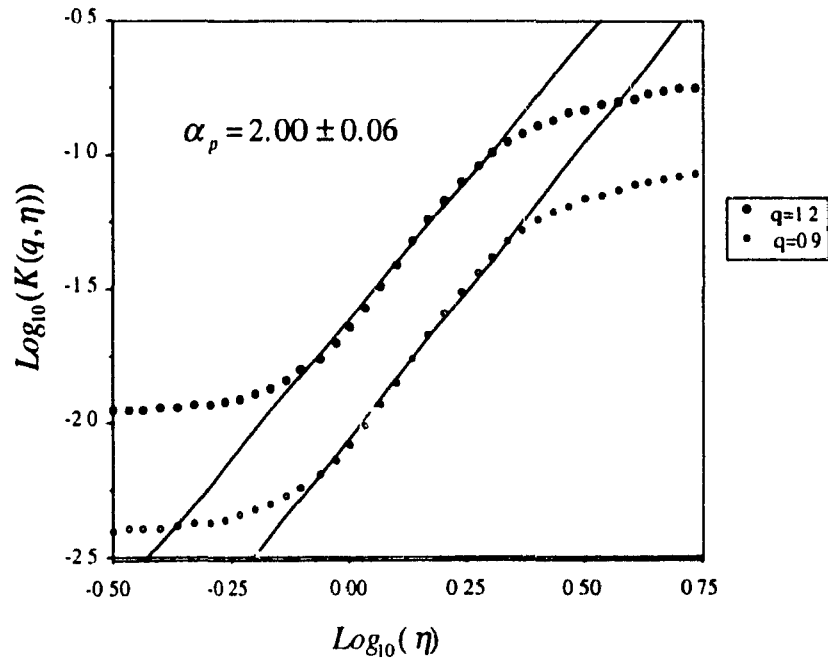


Figure 2.18. DTM analysis for the fields $\ell_{\eta, \lambda}$ obtained from the sample CfA2proj. The slope of the linear region is roughly the same for both curves implying that the projected luminosity distribution can be described by an index of multifractality $\alpha_p=2.0$, different from that corresponding to the actual 3d distribution. It is argued that this difference arises as an artifact of the projection of the luminosity fields. The breakdown of the linear behaviour is due to the spatial integration of the fields (for low η 's) and to the divergence of statistical moments due to a dressing mechanism (for large η 's) as it will be shown in the next chapter.

Although the linear regions in figure 2.18 seem to be well defined they are relatively short (in terms of the range of η 's). In fact, both curves are observed to depart from

linearity for both high and low η 's. In the case of the high η end, the bending of the curves is caused by a dressing mechanism that induces a critical behaviour in the high statistical moments of the fields (as it will be explained in the next chapter). For low values of η the break is due to the fact that when projecting (or integrating) a multifractal field, the information on the lower orders of singularity of the field is lost (as discussed in appendix two). In section II.2 (appendix two) we use the obtained values of α and $C_{1,1}$ to predict that the break on the universal behaviour should occur (for $q=1.2$) at $\text{Log}_{10}(\eta) \approx -0.13$. This predicted value agrees with the minimum value of $\text{Log}_{10}(\eta)$ observed to display universality in figure 2.18.

2.4.2 Multifractal simulations of the observed luminosity field $\ell_{1,\lambda}$.

In order to verify the validity of our estimates, we have compared the observed form of $K(q, \eta)$ (as obtained from the radially integrated sample MCG80x80) to that corresponding to simulated universal multifractal fields. We have produced five two-dimensional simulations[#] of universal multifractal fields with $\Lambda=256$, all having the same statistical parameters $\alpha=1.4$ and $C_{1,1}=1.28$ (corresponding to the universal parameters estimated for the field $\ell_{1,\lambda}$). One such simulation is shown at the end of this chapter in figure 2.20. Each of these simulated fields has been projected from 2 to 1 dimension, and to each of them we have imposed a minimum threshold so that events with an intensity less than such threshold are set equal to zero. This threshold has been selected so that the box-counting codimension C_{box} of the thresholded fields be equal to 0.15 (the same as the C_{box} observed in the samples CfA2proj and MCG80x80). We have further compared the statistical function $K(q, 1)$ as obtained from the thresholded simulations to that observed from the sample MCG80x80. In figure 2.19 we show the $K(q, 1)$ curve for the ensemble average of thirteen 6° strips from the MCG80x80 sample (already shown in figure 2.15a). Also shown is the corresponding $K(q, 1)$ from the simulated fields. It is observed that both curves agree fairly well for low values of q implying that in this range, the observed statistics of the luminosity distribution are well characterized by the above mentioned values of α and $C_{1,1}$. The curves start diverging near $q \sim 1.33$. In the next chapter it will be shown that this value has important physical connotations since it arises as a result of the "dressing" of the luminosity fields. This "dressing" mechanism is related to a Self-Organized-Critical phenomenon and dominates the behaviour of $K(q, 1)$ for high values of q (see discussion in section 3.2).

[#] For a detailed discussion on the simulations of multifractal fields, see references 58 and 41.

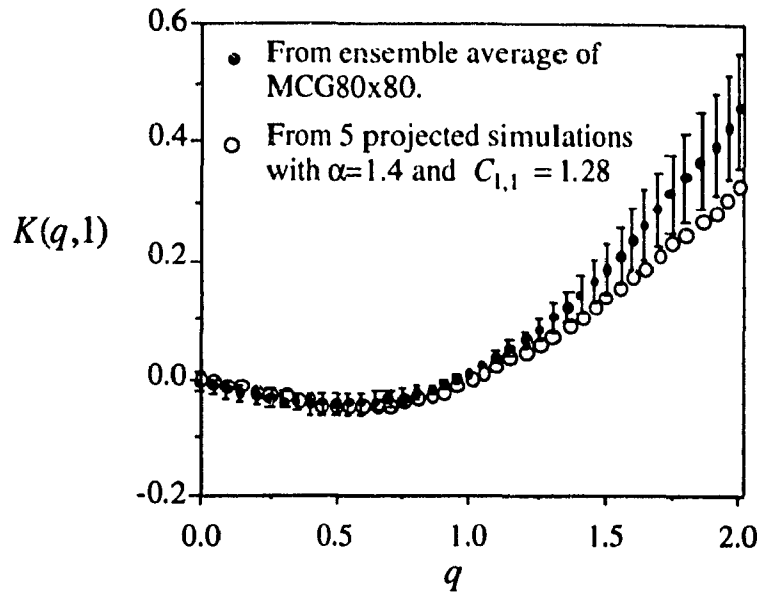


Figure 2.19. $K(q,1)$ function as estimated from the ensemble average of thirteen 6° strips (from the MCG80x80 sample) compared to the corresponding function obtained from 5 simulated multifractal fields with $\alpha=1.4$ and $C_{1,1}=1.28$ which have been projected and then thresholded up to a minimum codimension of 0.15. The agreement between the two curves is especially clear for the low q region. To preserve the clarity of the figure, errors bars are only shown for the curve corresponding to the sample MCG80x80.

2.4.3 Comments on the results.

The results shown in this chapter, together with the theoretical developments presented have provided us with a new (yet incomplete) picture for the large-scale distribution of generalized luminosities. In this picture, luminous objects in the universe would be formed by cascading processes dominated by non-linear interactions. The resulting fields (of density, luminosity, mass, etc.) would have multifractal characteristics as clearly demonstrated by the obtained estimates of the functions $c(\gamma, \eta)$ and $K(q, \eta)$ (sections 2.3.1 and 2.3.2). Due to observational limitations, not all galaxies in the universe are visible from the earth. Our research has estimated that the fractal dimension of the set of observable galaxies with limiting magnitude of 15.5 is (in 3-D) about 1.85 (sections 2.1.1 and 2.1.2) implying a codimension for the minimum observable singularity of ~ 1.15 . There is also evidence that the statistical properties of these multifractal fields would be determined by some universal parameters α and $C_{1,1}$ (~ 1.4 and ~ 1.28 respectively in 3-D). The latter quantity corresponding to the codimension of the mean luminosity of the

universe. However, as it has been stated in previous paragraphs, the values of α and $C_{1,1}$ should be accepted only as preliminary estimates due to some intrinsic statistical problems of the luminosity fields which allow only a narrow statistical range within which these measurements are valid.

In the next chapter we will add yet another important feature to this new picture of the large-scale distribution of the luminosity fields. We will detect and quantify the existence of first order multifractal phase transitions associated with self-organized critical behaviours. In this context, the next chapter will provide us with an appropriate framework to understand both the variability of the $C_{1,1}$ estimates and the observed form of the apparent luminosity distributions.

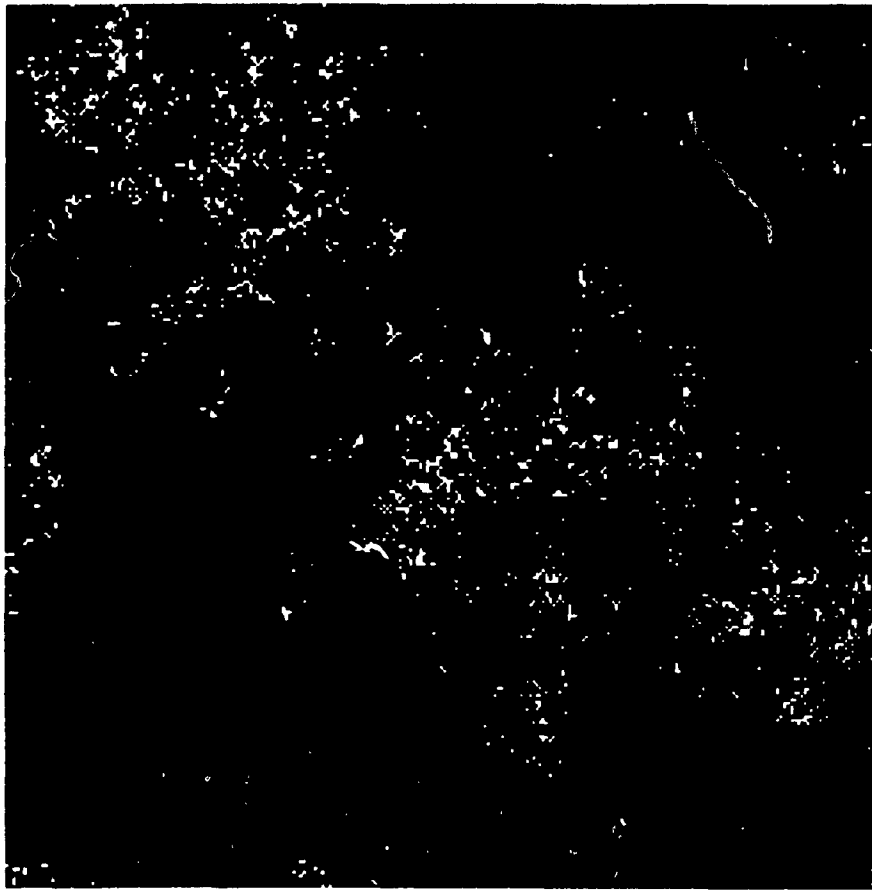


Figure 2.20. One of the five simulations of the 3-dimensional distribution of galactic luminosity used in the analysis discussed in section 2.4.2. The universal parameters are $\alpha=1.40$ and $C_{1,1}=1.28$ (see discussion in the text). In this figure events with a codimension lower than 0.15 (corresponding to "non-visible galaxies") are shown in black, whereas "visible" galaxies are shown in white. The large-scale structures observed in this figure (clusters, voids and filaments) are comparable to those observed in the sample CfA2, shown in figure 1.1a.

Chapter Three

Multifractal Phase Transitions and Self-Organized Criticality.

3.1 Motivation.

In chapter one (section 1.2) it was stated that besides multiscaling, another important signature of multifractality is the divergence of high statistical moments in the probability distribution of the observed field. In this chapter we shall study the physical origin of such divergence and its connections to first order multifractal phase transitions and self-organized criticality. We shall then search for signatures of divergence of moments in the various available generalized luminosity fields and shall attempt to define a new quantity; the dressing dimension D_{dress} , as a more appropriate qualifier of the critical behavior of these fields. As a consequence of this analysis, we shall also propose that the observed critical behavior of the luminosity fields gives us a new insight on the luminosity function $\Phi(\ell)$.

3.2 Dressed Statistics : Definition of $q_{D,\eta}$.

Multifractal fields are generically produced as a result of cascade processes (from large to smaller scales) ruled by non-linear interactions between the different scales⁴¹. As a multifractal process cascades down to very small scales, the variability and intermittence of the field increases rapidly producing regions of highly localized extreme intensity. Since this small scale limit is usually smaller than the scale of observation at which actual measurements of the field are performed, the process of observation effectively integrates or averages the field up to the scale of observation. This integrated or "dressed" field usually behaves in a manner which is statistically similar to the actual

"bare" field (ie. it has the same scaling exponents). However, in the case of the more violent and extreme singularities of the field, the integration fails to smooth out the process producing the divergence of some statistical moments. Since the presence of both scaling and divergence of moments has been understood as a signature of self organized criticality^{36,65} Schertzer et al⁶⁶ have recently shown that this type of critical behaviour is the generic outcome of multifractal processes. In particular, Schertzer and Lovejoy⁴¹ have predicted the existence of a certain critical moment $q_{D,\eta}$ (the subscript D standing for "dressing") so that for a large enough sample the moment-scaling function will diverge (ie. $K(q,\eta) \rightarrow \infty$) for all $q > q_{D,\eta}$. This divergence implies power law tails in the probability histograms of some fields; that is, for a generalized field $\ell_{\eta,\lambda}$ the probability of a point in the field of having a luminosity greater than a certain value s is given by (for very large s)

$$\Pr(\ell_{\eta,\lambda} > s) \propto s^{-q_{D,\eta}} \quad (3.1)$$

We have tested the presence of such exponents in the probability histograms of the various $\ell_{\eta,\lambda}$ fields. Figure 3.1 shows a plot[#] of $\text{Log}_{10}\{\Pr(\ell_{\eta,\lambda} > s)\}$ versus $\text{Log}_{10}\{s\}$ for the CfA2proj sample for $\eta=1, 2$ and 3 . In each case, $q_{D,\eta}$ is obtained from the value of the slope of the histogram's tail. In particular, it was estimated that $q_{D,1}=1.33 \pm 0.05$, $q_{D,2}=0.64 \pm 0.06$ and $q_{D,3}=0.36 \pm 0.04$. In this case all histograms were taken at a resolution $\lambda=128$ which is well within the scaling range of this sample (see figure 2.5). Note that these exponents do not vary in a trivial manner. Their values are determined by equation 3.3, as discussed in section 3.5

By comparing equations 3.1 and 2.6, we note that in the case of the former the right hand side shows no explicit dependence on the resolution λ of the field. This is because the exponent $q_{D,\eta}$ should be resolution independent as shown in figure 3.2 for the sample CfA2proj. It can be noticed from this figure that the value of $q_{D,1} \approx 1.35$ remains roughly constant even for very large values of λ .

[#] The probabilities have been estimated from the number of boxes in the field at resolution λ which have a generalized luminosity greater than the reference value s .

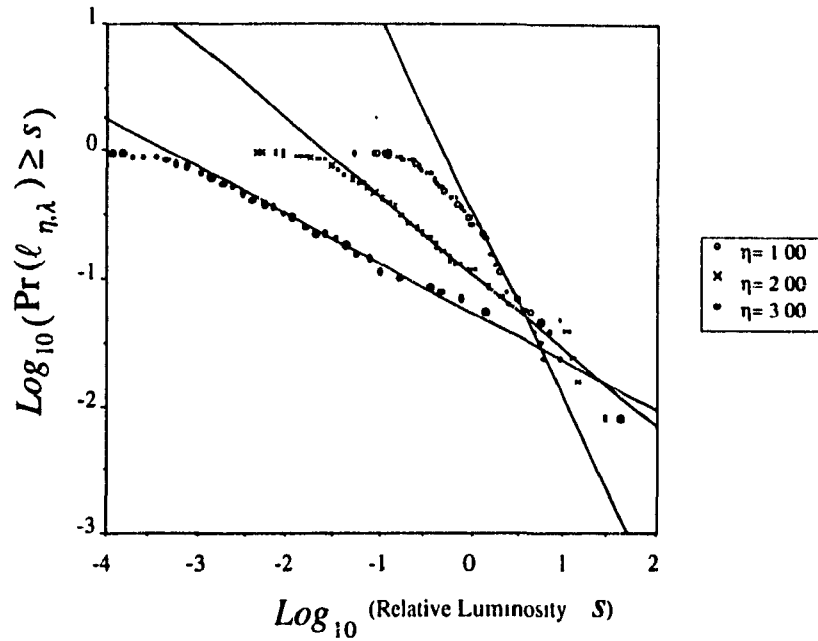


Figure 3.1. Probability histograms for three fields $\ell_{\eta,\lambda}$. The slopes of the linear regions provide estimates of the quantity $q_{D,\eta}$, which varies as a function of η . The $\ell_{\eta,\lambda}$ fields were obtained from the CfA2proj sample. $\lambda=128$ in all cases.

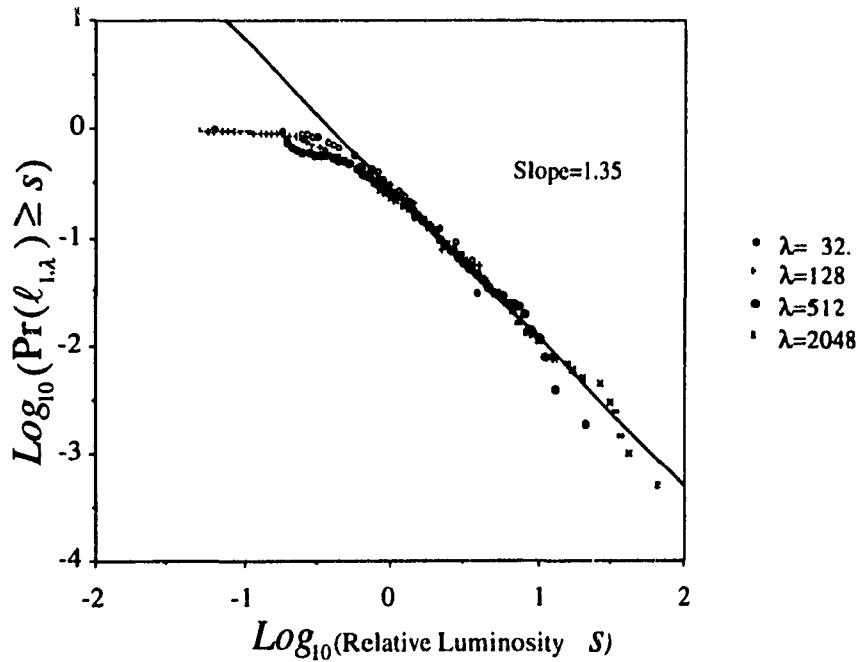


Figure 3.2. Independence of $q_{D,\eta}$ on the resolution λ as seen for the $\ell_{1,\lambda}$ fields obtained from the CfA2proj sample. For four different values of λ , the probability histograms (plotted against normalized probabilities) show a consistent estimate of $q_{D,1}=1.35$.

This independence of $q_{D,\eta}$ on the resolution λ implies that even for the raw ungridded data (that is, for the case $\lambda \rightarrow \Lambda$) $q_{D,\eta}$ should remain the same[#]. This is shown in figure 3.3. This figure also shows the sample independence of these results. Here we have plotted the probability histograms of $\ell_{1,\Lambda}$ for the samples MCG80x80, z40 and CfA2. The abscissa shows the number $N(m)$ of galaxies with an apparent magnitude greater than a reference value m plotted against apparent magnitude rather than luminosity (recall that a galaxy's magnitude is proportional to the logarithm of the luminosity, as previously shown in equation 1.12). Using equation 1.12, it can be inferred that the observed slope of 0.52 ± 0.02 implies a value of $q_{D,1} = 1.30 \pm 0.05$.

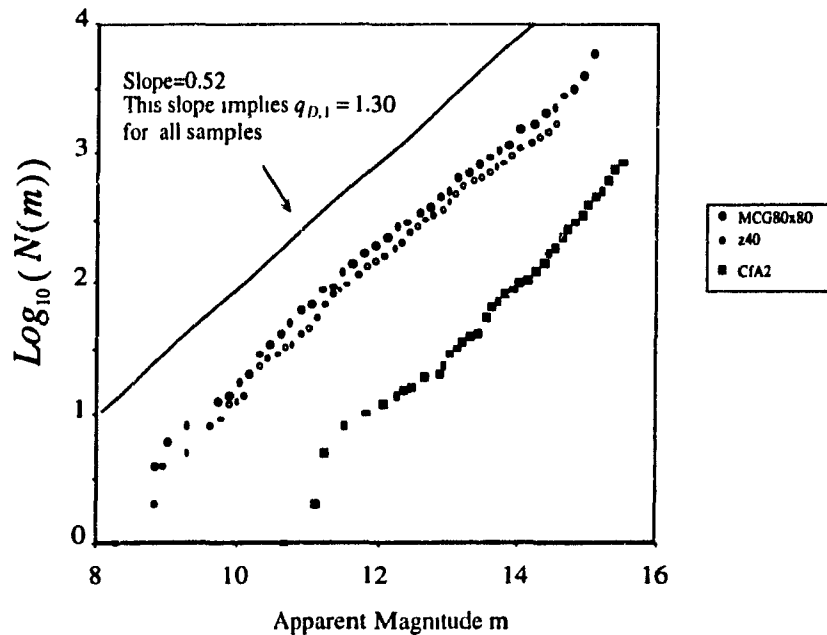


Figure 3.3. Sample independence of the estimates of $q_{D,1}$. The analysis corresponds to the apparent luminosity at highest resolution $\ell_{1,\Lambda}$ obtained from the samples MCG80x80, z40, and CfA2.

3.2.1 Estimation of the universal parameter H.

For multifractal fields (see for instance reference 60) the quantity $\Delta\ell_{1,\lambda}$, defined as the difference in luminosity between two adjacent grid boxes in a field $\ell_{1,\lambda}$, obeys the following relation (analogous to equation 2.6):

[#] This implies that the "dressing" process occurs at scales smaller than the galaxy itself, which makes sense because although in this analysis galaxies have been treated as point objects, the physics responsible for the production of luminous radiation acts mainly at intra-galactic distance scales.

$$\Pr(\Delta\ell_{1,\lambda} \geq \lambda^\gamma) \propto \lambda^{-c(\gamma+H)} \quad (3.2)$$

When the function $c(\gamma+H)$ is proportional to $(\gamma+H)$ (as in the case of power-law probability distributions), we can rewrite the right-hand-side of 3.2 as $\lambda^{-a\gamma-aH}$, where a is some proportionality constant. In the previous section we saw that when studying probability distributions, the quantity λ^γ can be replaced by s (implying resolution-independence). In such a case, (and setting a equal to $q_{D,1}$) equation 3.2 takes the following form:

$$\Pr(\Delta\ell_{1,\lambda} \geq s) \propto s^{-q_{D,1}} \lambda^{-q_{D,1}H} \quad (3.3)$$

Since the only scale-dependent term in equation 3.3 is $\lambda^{-q_{D,1}H}$, it follows that for a conservative field the probability distribution of the quantity $\Delta\ell_{1,\lambda}$ should be resolution-independent (since $H=0$ in such a case). In figure 3.4, the probability histograms of $\Delta\ell_{1,\lambda}$ (as calculated at resolutions $\lambda=64, 128$ and 512) are shown for the sample CfA2proj. The curves are observed to overlap implying that the probability distributions are independent of resolution. These results suggest that the luminosity fields are the result of a conservative and stationary process, implying $H \approx 0$.

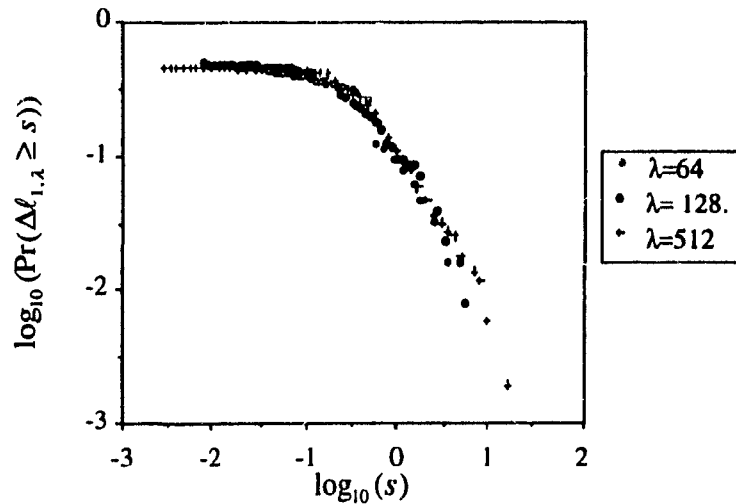


Figure 3.4. Probability histograms for the quantity $\Delta\ell_{1,\lambda}$ as estimated from the sample CfAproj at scale-ratios $\lambda=64, 128$ and 512 . The resolution independence of these curves suggests that the luminosity fields $\ell_{\gamma,\lambda}$ are the result of a conserved multifractal process, implying $H=0$.

3.3 Some Consequences of the Observed Value of $q_{D,1}$.

The observed value of $q_{D,1} = 1.33 \pm 0.05$ is relatively close to $q=1$. This implies that the estimates of $C_{1,1}$, which depend on moments of order 1, will have significant fluctuations from sample to sample (as seen in section 2.3.4 for the samples CfA2proj and MCG80x80). In physical terms, this means that the presence of rare but very extreme events in the field (which are responsible for the divergence of high statistical moments) leads to a slow convergence of the mean luminosity. Consequently, such mean, when estimated from a single sample, may actually be a poor estimate of the true mean space luminosity. This in turn explains why in section 2.3.2 (figure 2.9), the scaling of the thirteen 6° strips produced from the MCG80x80 catalogue, presented such different scaling slopes.

3.4 Implications on the Luminosity Function $\Phi(L_\lambda)$.

In section 1.1.2 we defined the luminosity function $\Phi(L_\lambda)$ as a probability density; that is, as the probability that a given galaxy possesses an absolute luminosity within the range L_λ to $L_\lambda + dL_\lambda$. It can be noticed that an integral of this function over the entire distribution of luminosities greater than L_λ is statistically equivalent to the probability defined by equation 3.1 for the case $\lambda=\Lambda$ (ie. at maximum catalogue resolution) and $\eta=1$. By denoting this integrated luminosity function as $I(L_\lambda)$ it can be seen that

$$I(L_\lambda) = \int_{L_\lambda}^{\infty} \Phi(L'_\lambda) dL'_\lambda \quad (3.4)$$

where L'_λ is just a variable of integration. In other words, for a set of galaxies located within a volume dV , the function $I(L_\lambda)$ represents a probability distribution; that is, the probability of finding at least one galaxy with an absolute luminosity greater than a certain value L_λ .

3.4.1 Experimental tests on the form of $I(L_\lambda)$.

As explained in section 1.2.2, catalogues of galactic luminosity possess a constant minimum threshold of apparent magnitude m' . In the case of the CfA2 sample, $m' = 15.5$ and figure 3.5 shows the strong distance dependence of the sample's threshold when

plotted against absolute magnitude M (see equation 1.13). In order to produce a sub-sample with constant minimum M -threshold and analyze its statistics we limited our study to galaxies closer than (or at) 100 Mpc and with an absolute magnitude $M < -19.5$.

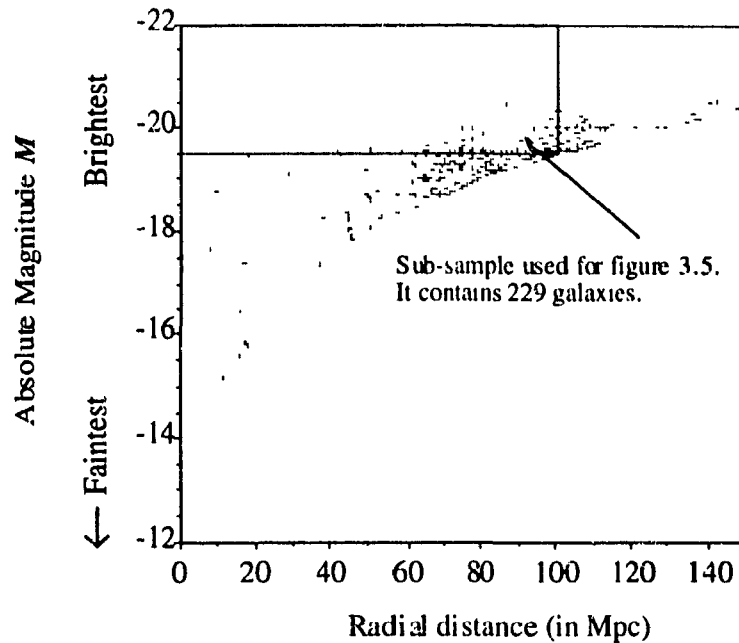


Figure 3.5. The CfA2 catalogue of absolute magnitudes M as a function of the distance from the earth (assuming a Hubble constant of $100 \text{ km s}^{-1} \text{ Mpc}^{-1}$). A sub-sample with constant threshold was created by selecting those galaxies closer than 100 Mpc and fainter than an absolute magnitude $M = -19.5$. There are 229 such galaxies. In total, there are 1091 galaxies represented in this figure.

The corresponding histogram (using $\lambda = \Lambda$) for the 229 galaxies of this sub-sample is shown on figure 3.6. Plotted on the abscissa is the number $N(M)$ of galaxies with an absolute magnitude greater than a certain reference value M . It is noticed that the histogram shows a linear behavior implying a simple $L_{\Lambda}^{-q_{01}}$ form for the luminosity function $I(L_{\Lambda})$ (recall the logarithmic dependence between luminosity and magnitudes as previously shown in equation 1.12). Figure 3.6 also shows the histogram corresponding to the 869 galaxies closer than 100 Mpc, but without any constraint on M . It is noticed that both histograms coincide exactly and show a linear behavior for the low magnitude (high luminosity) end. However, the latter histogram deviates from linearity for all galaxies with $M > -19.5$ (the limiting magnitude of the sample with constant M -threshold). Similar tests were performed using sub-samples from the z40 catalog. Results from these tests are in agreement with the ones described above. These results suggest that the 'flattening' of the luminosity curves (for low luminosities) is an artifact of the non-constant threshold of

the samples studied, rather than the consequence of a physical process. In physical terms, these results suggest that if we had knowledge of the luminosities of all unobservable galaxies (through catalogues of higher limiting apparent magnitude), then the integrated luminosity function $I(L_\Lambda)$ would retain the form $L_\Lambda^{-q_{01}}$ even for higher absolute magnitudes. This would be a definite evidence of the critical character of the galactic luminosity distribution.

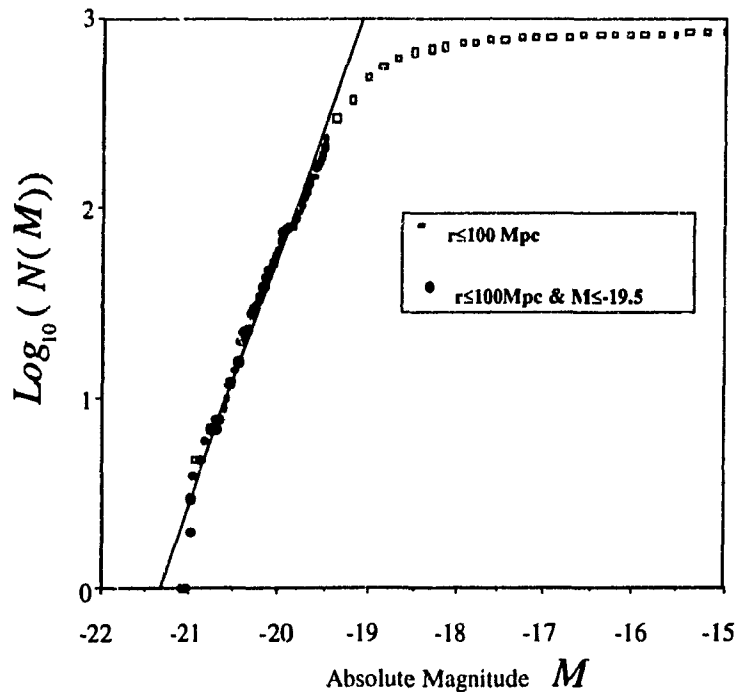


Figure 3.6. Probability histograms for the 869 galaxies shown in figure 3.5 closer than 100 Mpc, and for the 229 contained in the volume-limited sample bounded by 100 Mpc and $M \leq -19.5$. Both histograms are linear throughout the constant threshold region suggesting that the bending of the former curve arises as a result of the distance-dependent threshold of the catalogue.

As a further test of the importance of having a constant minimum threshold, the histogram for the 869 galaxies in CfA2 with $r \leq 100$ Mpc has been plotted in figure 3.7 against apparent (rather than absolute) magnitude. The abscissa shows the number $N(m)$ of galaxies with an apparent magnitude greater than a reference value m . Since in this case there exists a constant threshold throughout the sample (given by the sample's limiting apparent magnitude of 15.5) it is expected from the previous paragraph that the power-law behaviour of $I(\ell_\Lambda)$ will extend down to the fainter galaxies. Figure 3.7 shows

this histogram. It can be seen that the curve obtained agrees with the previous estimates of $q_{D,i} \approx 1.33$ and shows no departure from linearity.

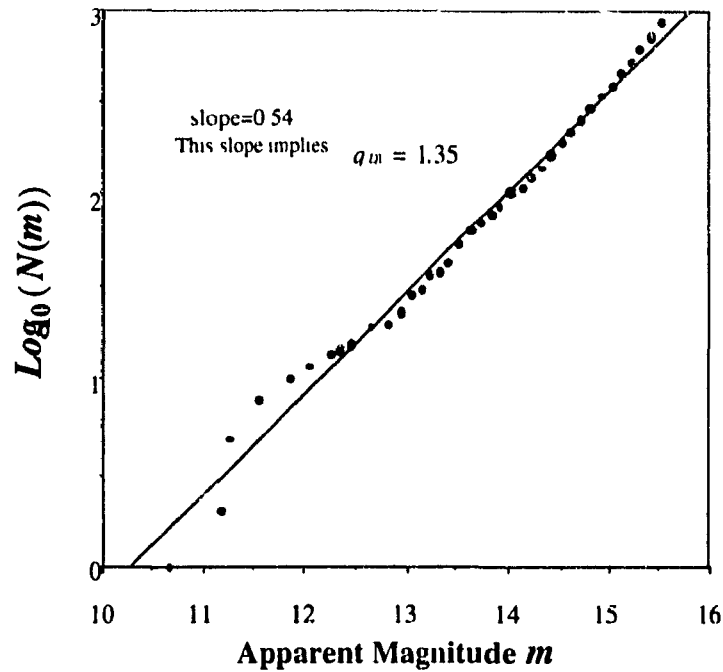


Figure 3.7 Probability histogram plotted against apparent magnitude for the 869 galaxies shown in figure 3.5 which are at a distance less than (or equal to) 100 Mpc from the earth. The linear behavior observed in this figure is consistent with the results from previous figures.

3.5 The Dressing Dimension D_{dress} .

In section 3.2 it was stated that the moment exponent function $K(q, \eta)^{\#}$ of an infinite number of realizations will diverge to infinity for all $q > q_{D,\eta}$. In the case of a finite sample size, as it is in our case, the probability histograms show a linear behavior implying a linear codimension function $c(\gamma, \eta)$ with slope $q_{D,\eta}$ (recall the linear behaviour observed in figure 2.14 for the case $\eta=1$). From equation 2.9, it follows that the corresponding dressed $K(q, \eta)$ for a limited sample will also be linear for $q > q_{D,\eta}$, implying a change on its first derivative at $q = q_{D,\eta}$. Feigenbaum⁶⁷ (among others) has shown that there is a formal analogy between multifractal dynamics and thermodynamics,

[#] All statistical functions mentioned in this section are implicitly meant to be "dressed" functions

for this reason this type of "jump" on the derivative of $K(q, \eta)$ is called a "phase transition" (of first order in this case due to the discontinuity in the first derivative). If the divergence occurs due to a dressing of moments, Schertzer *et al*⁶⁶ have shown that in such case the corresponding critical exponents $q_{D, \eta}$ obey the relation:

$$K(q_{D, \eta}, \eta) = (q_{D, \eta} - 1)D_{dress} \quad (3.5)$$

where the quantity D_{dress} is defined as the "dressing dimension" of the process. This means that the underlying cascade dynamics are spatially "dressed" (or averaged) over a space of dimension D_{dress} . The exact mechanism of such "dressing" however, is still a subject of ongoing research⁶⁴. It is expected though, that since the manner in which this "dressing" proceeds depends upon the field itself, D_{dress} may not be necessarily equal to the dimension D of the embedding space.

In appendix 2 it is shown that it is possible to estimate (under some general conditions) the form of $K(q, \eta)$ from the function $K_p(q, \eta)$ corresponding to the moment scaling function of a radially integrated (or projected) sample. In chapter two the codimension $C_{1,1}$ of the mean luminosity field was estimated as ~ 1.28 . In such case (ie. for $C_{1,1} > 1.0$), the equation that relates the projected and the unprojected functions is (see equation II.12 in appendix 2)

$$K(q_{D, \eta}, \eta) = K_p(q_{D, \eta}, \eta) + q_{D, \eta} - 1 \quad (3.6)$$

In figure 3.8 we have attempted to test equation 3.5 and estimate D_{dress} directly in 3d by plotting $K(q_{D, \eta}, \eta)$ versus $(q_{D, \eta} - 1)$ for values of η ranging between 0 and 3[#]. In this analysis, we have used 3 data sets: CfA2, CfA2proj, and MCG80x80. For the radially integrated samples CfA2proj and MCG80x80, $K(q_{D, \eta}, \eta)$ has been estimated from the corresponding values of $K_p(q_{D, \eta}, \eta)$ using equation 3.6. The result of this analysis is a roughly linear curve that passes through the origin and with a slope $D_{dress} = 1.53 \pm 0.08$. This result suggests that a good characterization of the critical behavior of the luminosity fields is not obtained from $q_{D, \eta}$ (which is η -dependent), but rather by the quantity D_{dress} which seems to be intrinsic to the multifractal cascading process, and therefore independent of η .

[#] Since equation 3.5 is defined for the function $K(q, \eta)$ as calculated over the whole space (ie. not over the fractal set), the values of $K(q_{D, \eta}, \eta)$ used on the estimate of D_{dress} have been corrected using equation 2.14 and $C_{box} = 0.15$.

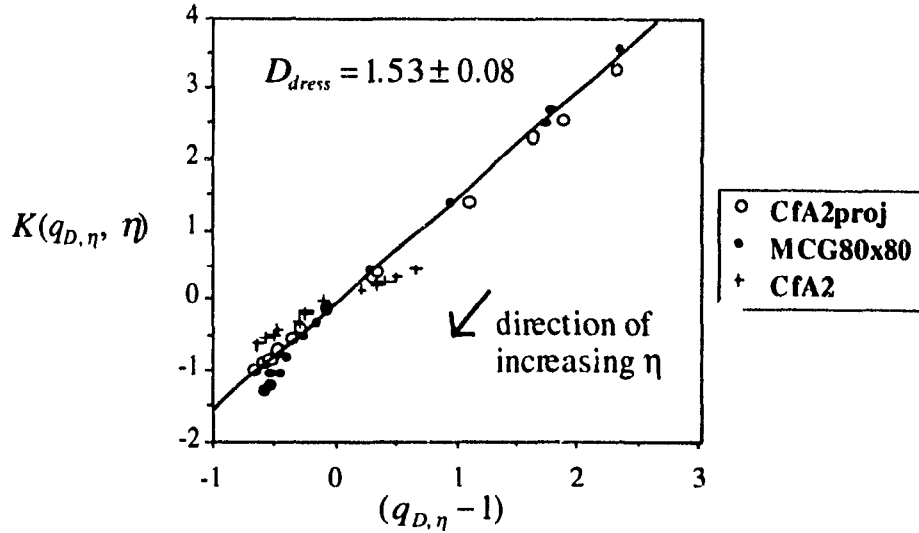


Figure 3.8. Estimate of the quantity D_{dress} using data from the samples CfA2, CfA2proj and MCG80x80. The figure shows a roughly straight line that passes through the origin in agreement with equation 3.3. From the slope of these curves we have estimated $D_{dress} = 1.53 \pm 0.08$. The values of $K(q_{D,\eta}, \eta)$ for the radially integrated samples were estimated from the corresponding values of $K_p(q_{D,\eta}, \eta)$ using equation 3.6.

3.6 Estimation of α using D_{dress} .

In section 2.4.1 the quantity α , corresponding to the multifractality index of the 3-dimensional distribution of luminosity fields was roughly estimated as 1.4. However, this estimate was statistically weak since it relied on narrow scaling regions. In this section we present a more elaborate method of estimating α . This method requires knowledge of universal multifractals and also the just acquired knowledge of dressing statistics, and in particular of the quantities $q_{D,1}$, $C_{1,1}$ and D_{dress} .

For universal multifractals (introduced in section 2.4) Schertzer *et al*⁶² have predicted that for the case $\eta=1$, the moment scaling function $K(q,1)$ obeys the general form:

$$K(q,1) = \frac{C_{1,1}}{\alpha - 1} (q^\alpha - q) \quad (3.7)$$

Replacing this form in equation 3.5, and using $q \rightarrow q_{D,1}$ we obtain the relation:

$$\frac{C_{1,1}}{\alpha - 1} (q_{D,1}^\alpha - q_{D,1}) = D_{dress} (q_{D,1} - 1) \quad (3.8)$$

Rewriting 3.8 we obtain:
$$\left(\frac{C_{1,1}}{D_{dress}(q_{D,1}-1)} \right) \left(\frac{q_{D,1}^\alpha - q_{D,1}}{\alpha - 1} \right) = 1 \quad (3.9)$$

Using the previously estimated values of $C_{1,1} = 1.28$, $q_{D,1} = 1.33$ and $D_{dress} = 1.53$ we have plotted in figure 3.9 the left hand side of equation 3.9 for $0 \leq \alpha \leq 2$ (the allowed values of α according to the theory of universal multifractals⁶²). The α corresponding to the full 3 dimensional distribution of the luminosity fields can then be read from the intersection of this curve and the value of 1 in the abscissa. Our analysis produces an estimate of $\alpha = 1.2 \pm 0.4$. The large uncertainty is due to the amplification of the error on the estimates of $C_{1,1}$, $q_{D,1}$ and D_{dress} by the non-linear form of equation 3.9. This value of α is compatible with the value of ~ 1.4 previously obtained from the sample CfA2, in section 2.4.1.

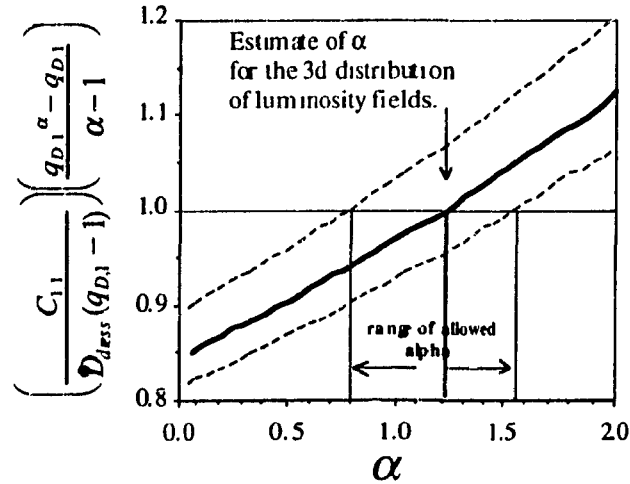


Figure 3.9. Determination of α using equation 3.5 and the universal form of $K(q,1)$ given by equation 3.7. The value of α corresponding to the multifractality index of the 3-dimensional luminosity fields can be read from the intersection of the curve and the value of 1 in the abscissa. We estimated $\alpha = 1.2 \pm 0.4$. The broken lines correspond to the extreme variations on the curve given by the uncertainties on the quantities $C_{1,1}$, $q_{D,1}$ and D_{dress} .

In this chapter we have quantified the critical behaviour of the luminosity fields by introducing the formalism of dressed statistics and verifying the presence in the data samples of its generic signatures, divergence of moments and first-order multifractal phase transitions. The understanding of these phenomena has allowed us to gain a deeper insight on the form of the luminosity function $\Phi(L)$ (section 3.4). It has also provided us with a physical justification for the slight sample dependence found in the estimates of $C_{1,1}$ (section 3.3), and finally has also supplied us with a method of estimating the multifractality index α .

Chapter Four

Conclusions.

4.1 General Comments.

In this thesis, we have presented a method that simultaneously accounts for the spatial and the luminous properties of the large-scale distribution of galaxies in the observable universe. In particular, the application of multifractal theory to the various generalized luminosity fields $\ell_{\eta,\lambda}$, has allowed us to jointly explore first the scaling predictions from analyses on the correlation function $\xi(r)$ (related to our correlation dimension D_c according to equation 1.5); and second, the so far little-understood shape of the luminosity function $\Phi(L)$ (related to the probability histograms discussed in section 3.4). Furthermore, in this thesis we have generalized the studies done by various researchers¹⁴⁻¹⁸ on the properties of the spatial galaxy density when treated as a fractal set (totally determined by a single dimension) to a more complete treatment of a multifractal density field (characterized by a full codimension function and denoted in the thesis as the case $\eta=0$). We have attempted to go even further, and have extended our analysis to the study of the properties of other important multifractal fields such as the galaxy luminosity and mass distributions ($\eta=1$ and $0.8<\eta<1.25$ respectively). Finally, we have also found evidence for universal multifractal behaviour in the generalized luminosity fields. In fact, all samples studied over the broadest possible range of scales, have been observed to have statistics compatible with $C_{1,1} \approx 1.28$, $\alpha \approx 1.2$, $H=0$, $q_{D,1} \approx 1.33$ and $D_{dres} \approx 1.53$ (see discussion in section 4.2).

One of the main technical problems encountered by our analysis has been the restricted number of galaxies contained in the available catalogues of galaxies' position and luminosity. The low number of galaxies has limited the statistical strength of our analysis, giving raise to statistical noise which in turn has increased the uncertainty on the estimates of relevant multifractal parameters. Moreover, in section 2.3.2 we showed that because of the low number of galaxies contained in the data samples, the fields $\ell_{\eta,\lambda}$ became ill-defined

as the scale-ratio λ increased to a point when the average grid-box became empty. In such cases spurious breaks on the scaling ranges are observed.

In this thesis we have pointed out two methods to overcome some of these limitations: one is simply using larger (and deeper) spatio-luminous catalogues so that the number of galaxies per box at any λ could be considerably increased. In this case it is a matter of time to wait until such catalogues (such as the APM Galaxy Survey¹³) are made public and then verify that the behavior of the scaling regions in fact improves.

The second method is to use radially integrated catalogues of relative luminosity. Since the integration of a field by just one dimension effectively increases the average number of events per box by a factor λ (as explained in section 2.3.2), it follows that this method can actually extend the range of scales within which the fields are still properly defined. One must be aware however, that this method possesses two shortcomings. Since multifractal projections are conceptually different from fractal projections (the former being a flux and the latter a projection of a set of points) the relations between projected and unprojected multifractal parameters are different from the straightforward fractal relations studied in sections 2.2.1. and 2.1.2. In particular, in appendix 2 we show that a solid understanding of the effects of projections on multifractal fields only exists for the case when $C_{1,1} > 1.0$ and $q > q_1$. The other handicap with the use of integrated (or projected) samples is that universality (in a multifractal sense) is masked by the integrating mechanism in a yet not clear manner. In particular, in appendix 2 (section II.3) we present empirical and theoretical evidence that suggests that any universal multifractal field will display a multifractality index α close to 2, independent of the α of the unprojected distribution. Consequently, in order to estimate the actual α one must resort to more indirect techniques (as the one discussed in section 3.6) which are usually accompanied by significant uncertainties on the resulting estimates of α . If the above described shortcomings are not considered fundamental or do not apply to the field under study, then the integration of fields will most certainly improve the observation of the scaling ranges and will hence allow the researcher to make (in general) more robust estimates of the statistically relevant parameters.

4.2 Multifractal Picture of the Large-Scale Distribution of Galactic Luminosity.

The results presented in this thesis, suggest that galaxies were formed as the generic outcome of cascading processes of the constituent matter existing during the early stages of the universe's development. In a multifractal context, these cascades would be ruled by

non-linear interactions between the different scales and the resulting fields of mass, density and luminosity (and consequently the distribution of galaxies) would exhibit multifractal features. The main such feature observed in our analysis has been the existence of multiscaling in the various statistical moments of the fields studied (as shown in section 2.3.1). Also, as predicted by multifractal theory, the observed fields display tremendous intermittence and variability on their intensities#. Our analysis has revealed that the mean singularity of the galactic luminosity field has a codimension $C_{1,1} \approx 1.28$.

The results at the end of chapter 2, suggest that the statistical properties governing these multifractal fields, exhibit attractive universal behaviours and are consequently determined by a finite set of parameters. In particular, our research has estimated that the multifractality index α of these fields is 1.2 ± 0.4 . The formalism presented in section 2.4, suggests that the knowledge of these two quantities: α and $C_{1,1}$, allows us to totally predict the form of the functions $K(q, \eta)$ and $c(\gamma, \eta)$ which determine the statistical properties of the galaxy distribution.

The resulting fields of mass and luminosity present some rare but extremely violent events (ie, extremely bright or massive galaxies). Because of such events, the observational "dressing" of the fields dominates the behaviour of the high statistical moments of the probability distributions inducing the existence of critical exponents related to first order multifractal phase transitions and self-organized criticality. In section 3.2 it was shown that because of these exponents, the probability histograms of the various fields yield power-law curves. In particular, the probability histogram of the galaxy luminosity field allowed us to estimate $q_{D,1} \approx 1.33$. Since for $q > q_{D,1}$ the observed statistics of the luminosity distribution depart from those of the actual one, $q_{D,1}$ effectively imposes an upper limit on the range of statistical moments within which the universal behaviour of the fields may be observed.

Our analysis has not been free from observational limitations. For instance, since not all galaxies in the universe are visible from the earth, our research has estimated that the codimension of the observable galaxies with limiting apparent magnitude of 15.5 is ~ 1.15 (section 2.1.1). Also, the use of radially integrated galaxy catalogues, has effectively increased the minimum observable singularity up to a value $\gamma_{q_1,p} \approx -0.5$, thus decreasing the range of orders of moments available for analysis. In fact, in appendix 2 we have estimated that the minimum order of moment expected to show universal behaviour is $q_1 \approx 0.6$. This value of q_1 , together with the previously discussed value of $q_{D,1}$, provide us with an observationally narrow range of orders of moments available for valid statistical

Recall for instance figure 2.3, where the absolute luminosity in the sample CfA2proj varies from galaxy to galaxy by as much as 5 orders of magnitude

analysis. In fact, our research has shown that the only orders of moment allowed for the detection of universal behaviour, are those contained within the range $0.6 < q < 1.33$. A consequence of this restricted range, is the existence of significant uncertainty on the estimates of some of the multifractal parameters previously discussed. Moreover, in section 3.3 we argued that the fact that $q_{D,1}$ is relatively close to 1, induces sample dependence on the estimates of the codimension $C_{1,1}$.

The following table summarizes the most important numerical results in this thesis.

SUMMARY OF NUMERICAL RESULTS.

QUANTITY	SYMBOL	ESTIMATED VALUE	THESIS SECTION
Codimension of mean singularity	$C_{1,1}$	1.28 ± 0.06	2.3.4
Multifractality index of 3d distribution	α	1.2 ± 0.4	2.4.1 and 3.6
Degree of non stationarity	H	~ 0	3.2.1
Minimum detectable codimension	C_{box}	1.15 ± 0.03	2.1.1 and 2.3.4
Critical exponent for first order multifractal phase transition	$q_{D,1}$	1.33 ± 0.05	3.2
Dressing dimension	D_{dress}	1.53 ± 0.08	3.5
Minimum observable singularity after projection	$\gamma_{q_1,p}$	-0.5 ± 0.1	II.1.1 (appendix 2)
Critical order of moment for projected fields	q_1	0.6 ± 0.1	II.1.1 (appendix 2)

4.3 Concluding Remarks on the Physical Implications of Multifractality.

4.3.1 The range of multiscaling.

Our analysis in chapter 2 showed that the multiscaling range of the galaxy luminosity fields extends at least up to the size of our data samples, which is in any case much greater than the value of the "correlation length" $r_0 \approx 10h^{-1}Mpc$, defined in chapter one. If this is indeed the case, it implies that either:

1. The large-scale homogeneity predicted by the Cosmological Principle is not yet reached by the samples studied in this work. In fact, other recently published catalogues, such as the "Southern Sky Redshift Survey"⁷¹ which extends $120 h^{-1}Mpc$ deep into the sky, also report the existence of large inhomogeneous structures comparable to the catalogue's size. This scenario would certainly explain the large density fluctuations observed, for instance, in the CfA2 catalogue as shown in figure 1.1a. In such a case, the clumpiness in the spatial and luminous distributions of this sample would correspond to the result of a multifractal cascade extending beyond the size of the sample, but truncated at some larger scale. According to this point of view, beyond this scaling range overall homogeneity should be observed .

2. The other possibility is that the "clustering hierarchy" observed within the scales of the catalogues (ie: individual galaxies, groups, clusters, super-clusters, etc.) will indefinitely continue up to the largest scales of the universe. This picture, first proposed by Fournier d'Albe²⁰ in 1907 was strongly revived by de Vaucouleurs⁷² in 1970 as a critic towards the uncontested homogeneous hypothesis widely popular amongst researchers of that time (and in fact of ours too). A universe with such strong clustering properties would be composed of island universes all ruled by the same multifractal statistics. Such scenario would not be compatible at this point with the standard Big Bang hypothesis. This is probably yet another reason of why this picture has not been accepted.

4.3.2 Origins of a multifractal cascade.

Independent of the question of the true extent of the multiscaling region, is the problem of finding physical processes compatible with a multifractal cascade that may lead up to the formation of galactic structures. In the context of the Big Bang hypothesis the

formation and distribution of luminous massive objects was determined by the conditions present during the first moments of the universe's life. As the universe expanded from an extremely hot fire ball, its constituent "gas" cooled decoupling energy from matter. In this context two of the most popular scenarios proposed are (see for instance references 29 and 73-76 for discussions on the subject):

1. **Hot Dark Matter:** Due probably to photon viscosity small adiabatic fluctuations in the gas density became negligible after decoupling. The remaining density fluctuations were of the size of superclusters. As the gas continued to cool down these fluctuations produced clusters and galaxies via complex gravitational and hydrodynamical non-linear interactions. As mentioned in chapter two, scaling is a property of non-linear equations and is in fact possible that if the fluctuations before decoupling were ruled by multifractal statistics, the resulting cascade may have carried with it the seeds of a multifractal structure.

2. **Cold Dark Matter:** A second scenario (which has become quite popular in the last few years) proposes that after decoupling large fluctuations were rapidly damped. In this scenario the large scale inhomogeneity of the present universe grew from small scale density fluctuations via gravitational clustering. In this case, the cascade goes from small to large scales, but its dynamics are still governed by scaling non-linear interactions. An interesting consequence of this "bottom up"⁷⁶ cascade is that scaling is transmitted from a scale to the next only after the bodies have undergone total gravitational reposition and virialization. This means that there is an important time factor for bodies which are located at large distances apart to enter the scaling regime. Consequently, the observation of homogeneity at very large scales may not be related to an overall symmetry of the universe, but rather to regions of space which have not yet been virialized and have not entered the scaling stage.

From a multifractal point of view it is important to realize that both of these scenarios are compatible with a multifractal process. Which of the two (if any) is the actual process that led to the formation of galaxies is still a cause of debate among cosmologists and by all means an open question in science. Far from solving this problem, the objective of our work in this thesis has been to shine new light onto this question and to offer a new insight; one that may facilitate the understanding of the statistical properties of the universe that surrounds us.

Appendix One

On Multifractal Notation.

The formalism and notation presented in this thesis is a "codimension-notation" formalism which has been developed from the framework of turbulent cascades⁴¹. Another formalism (a "dimension-notation" formalism) of widespread use in multifractal literature, has its origins on studies done on the theory of chaotic attractors⁷⁷. In this formalism the functions analogous to $c(\gamma)$ and $K(q)$ [#], that equivalently describe the statistical properties of the multifractal field are denoted as $f(\alpha)$ and $\tau(q)$. $f(\alpha)$ indicates the dimension of the set of points with singularity α and $\tau(q)$ describes the scaling of the q^{th} moment of the field. If we let D be the corresponding dimension of the embedding space where the multifractal cascade takes place, then both formalisms are related by

<u>Physical Quantity</u>	<u>Turbulence Formalism</u>	<u>Chaotic Attractor Formalism</u>
Order of Singularity	γ	$D - \alpha$
Codimension of the Set	$c(\gamma)$	$D - f(\alpha)$
Order of Statistical Moments	q	q
Moment Scaling Function	$K(q)$	$(q - 1)D - \tau(q)$

The advantage of the use of the turbulence notation is that all statistical functions are independent of the dimension D of the observing space. This is convenient because the multifractal cascade process that we are interested in is defined on an infinite dimensional probability space⁴¹, and hence $f(\alpha)$ and $\tau(q)$ of such process are also infinite. On the other hand $c(\gamma)$ and $K(q)$ are intrinsic to the process and remain finite.

[#] Note that the inclusion of the variable η in $K(q, \eta)$ and $c(\gamma, \eta)$ was specific to the study of the generalized luminosity fields, and most literature on the subject considers only the functions $K(q)$ and $c(\gamma)$ (with η implicitly assumed to be 1).

Appendix Two

On the Projection of Multifractals.

For multifractal fields, a projection effectively represents a flux or volume integral along one of the spatial coordinates. In this appendix, all terms: "flux", "volume integral" and "multifractal projection" will be equivalently used.

In section 2.3.2 it was concluded (from the analysis on various projections of the sample CfA2) that although angular projections may be quite complex, in the case of the multifractal luminosity fields they can be approximated by a linear cartesian volume integration along one of the coordinates. In this appendix, some preliminary results on the theory behind linear cartesian integrations of multifractal fields are presented. Our aim is not to give a complete treatment of the theory of multifractal projections, but rather to strengthen our understanding of the specific problem of the projected luminosity fields. For this reason we shall restrict the discussions in this appendix to the $C_1 > 1$ case (corresponding to the codimension of the mean singularity of the luminosity field $\ell_{1,\lambda}$).

II.1 The Effect of Projections on $K(q)$.#

Consider a multifractal field $\ell_\lambda(x, y)$ embedded in a unit square of resolution λ with coordinates along the x and y directions. Then, the 1d cartesian multifractal projection of $\ell_\lambda(x, y)$, denoted as $\ell_{p\lambda}(x)$, is defined as the integral along the y coordinate for each value x of the field:

$$\ell_{p\lambda}(x) = \int_0^1 \ell_\lambda(x, y) dy = \sum_{i=1}^{\lambda} \ell_{\lambda,i}(x, y_i) \lambda^{-1} \quad (\text{II.1})$$

where the factor λ^{-1} (coming from the quantity dy) ensures the normalization of $\ell_{p\lambda}(x)$ so that $\langle \ell_{p\lambda}(x) \rangle = 1$, and the sum is over the λ boxes of size $\lambda^{-1} \times \lambda^{-1}$ present in any column of constant value x . The integral on equation II.1 implies that the projection of a multifractal field corresponds to a "dressing" process onto a 1-dimensional space. In consequence, it is expected that the form of the statistical functions $K_p(q)$ and $c_p(\gamma)$

Note that in this appendix the index η will not be used since its application is specific to the luminosity fields, whereas the theoretical discussions that follow apply to any multifractal field.

(corresponding to the moment-scaling and codimension functions of the projected field) will be determined by the formalism of dressed statistics developed in chapter 3. In particular, we expect the existence of a critical order of moment (denoted below as q_1) above which the dressed statistics of the unprojected function $K(q)$ will be reflected by the form of the function $K_p(q)$ (see discussion below).

Consider first the case of the Trace moments $Tr(\ell_\lambda)^q$ defined as⁴¹:

$$Tr(\ell_\lambda)^q \equiv \sum_{i=1}^{\lambda^D} \left\langle \left(\frac{\ell_\lambda}{\lambda^D} \right)^q \right\rangle = \lambda^{-\tau(q)} \quad (\text{II.2a})$$

where the quantity $\tau(q)$ was previously introduced in appendix 1. Using equation 2.10 (with $\eta=1$) we find that $Tr(\ell_\lambda)^q$ is simply related to the function $K(q)$:

$$Tr(\ell_\lambda)^q = \lambda^{-Dq} \lambda^D \left\langle (\ell_\lambda)^q \right\rangle = \lambda^{K(q) - D(q-1)} \quad (\text{II.2b})$$

For the projected field, the corresponding Trace moments are found by replacing ℓ_λ by $\ell_{p\lambda}$, and D by $D-1$:

$$Tr(\ell_{p\lambda})^q \equiv \sum_{i=1}^{\lambda^{D-1}} \left\langle \left(\frac{\ell_{p\lambda}}{\lambda^{D-1}} \right)^q \right\rangle = \lambda^{K_p(q) - (D-1)(q-1)} \quad (\text{II.3})$$

Since Trace moments are unaffected by projections (since they explicitly take into account their dependence on the dimension of the observing space) equations II.2b and II.3 may be combined to obtain an explicit relation between $K(q)$ and $K_p(q)$. By equating the exponents in II.2b and II.3 we obtain that (for large enough q , as discussed below) the "projected" and "unprojected" moment scaling functions are related by :

$$K(q) = K_p(q) + q - 1 \quad (\text{II.4})$$

Recalling the definition of C_1 given by equation 2.13[#], we note that equation II.4 predicts that the corresponding "projected" codimension $C_{1,p}$ obeys the relation:

$$C_1 = \left(\frac{d}{dq} K(q) \right)_{q=1} = \left(\frac{d}{dq} K_p(q) \right)_{q=1} + 1 = C_{1,p} + 1 \quad (\text{II.5})$$

where $C_{1,p} = (dK_p(q)/dq)_{q=1}$. Equation II.5 is in agreement with equation 2.5, developed in the realm of monofractal projections.

[#] Recall that since we are assuming $\eta=1$, throughout this section the codimension $C_{1,1}$ will be denoted as C_1 .

As explained in section 3.2, the dressing mechanism which accompanies a multifractal projection implies that the probability distributions are governed by the statistics of the largest orders of moments, and consequently, lower orders are expected to be non-relevant. This implies that equations II.4 and II.5 are only valid for values of q greater than a critical value denoted as q_1 and defined as the solution of the "dressing" equation 3.5 in a 1-dimensional space:

$$K(q_1) = (q_1 - 1) = \frac{C_1}{\alpha - 1} (q_1^\alpha - q_1) \quad (\text{II.6})$$

The right hand side of equation II.6 corresponds to the form of $K(q)$ valid for universal multifractals only[#] (see section 2.4 for a discussion on universality). For the case $\alpha=2$, equation II.6 predicts that q_1 has a particularly simple form:

$$q_1 = \frac{1}{C_1} \quad \text{for } \alpha=2 \quad (\text{II.7})$$

We have tested the validity of equations II.4 and II.5 using simulated multifractal fields. Figure II.1a shows the multiscaling for the ensemble average of nine 2d fields (1024 by 1024 pixels long) all with $\alpha=2.0$ and $C_1=1.50$, implying $q_1=0.67$. Figure II.1b shows the multiscaling for the corresponding 1d projections. In both cases clear scaling is observed up to the largest scales ($\lambda=1024$).

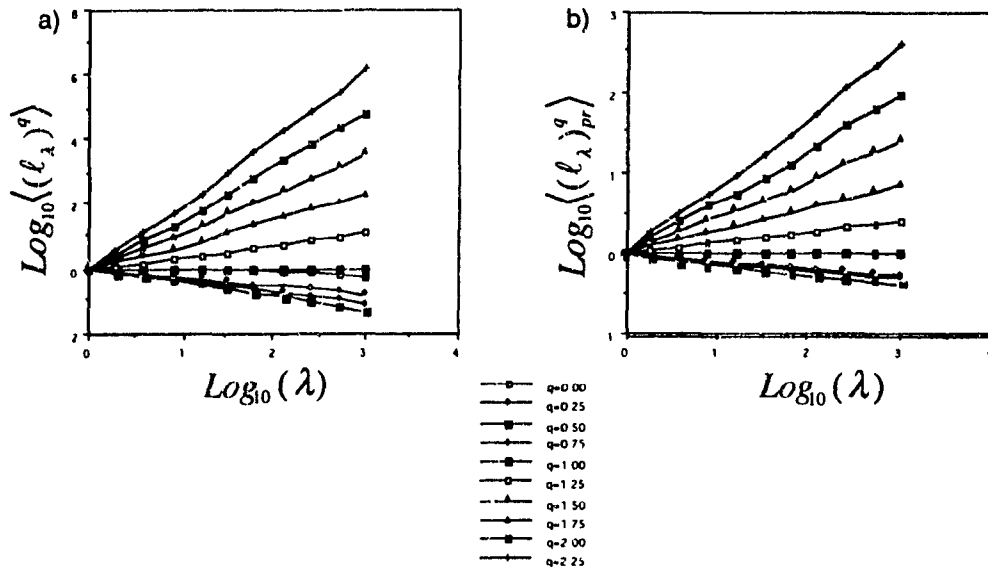


Figure II.1. Multiscaling for a) the ensemble average of nine 2d fields, and b) its corresponding 1d integration. The C_1 of the original 2d fields was 1.50. Clear scaling regions are observed for both samples.

[#] Schertzer *et al*⁶² have predicted that for a universal multifractal field $K(q) = \frac{C_1}{(\alpha - 1)} (q^\alpha - q)$

From the slopes of the curves on figures II.1a and II.1b we have estimated the corresponding $K_p(q)$ and $K(q)$ functions. These are presented in figures II.2a and II.2b. From the value of the derivatives of these curves at $q=1$ we have estimated $C_{1,p}=0.42 \pm 0.05$ and $C_1=1.50 \pm 0.06$, in agreement with equation II.5.

Figure II.2a also shows the expected form of the projected function $K_p(q)$ as predicted by equation II.4 for $q > q_1$. In figure II.2b we have attempted to infer the form of the unprojected $K(q)$ function from information obtained from the projected field. It is observed that theoretical and actual curves agree in the range $q > q_1$.

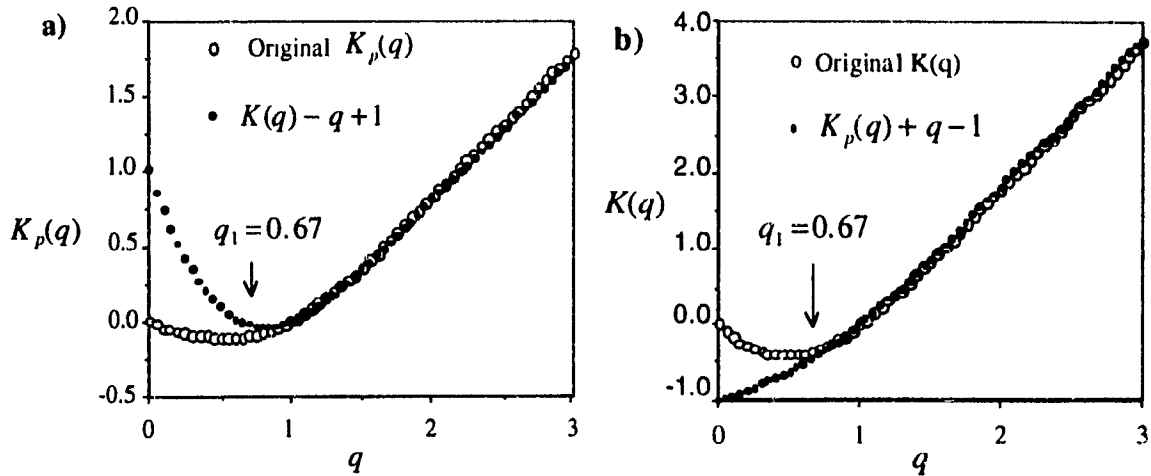


Figure II.2. Original and projected $K(q)$ functions as estimated from nine simulations all with an original $C_1=1.50$. Also plotted in figure II.2a is the predicted form of the projected function according to equation II.4. In figure II.2b we also show the form of the original $K(q)$ curve as predicted from the projected function and using equation II.4. In both cases, the agreement between theoretical and observed curves is clear for $q > q_1 = 0.67$.

II.1.1 The case of the galactic luminosity field $\ell_{1,\lambda}$.

For the case $\alpha \neq 2$ (as it is for the case of the luminosity field $\ell_{1,\lambda}$) equation II.6 predicts that:

$$q_1(a+1) - aq_1^\alpha = 1 \quad \text{where } a \equiv \frac{C_1}{\alpha - 1} \quad (\text{II.8})$$

A trivial solution (ie. independent of α and C_1) of II.8 is $q_1=1$. A physically more interesting result may be found by plotting the left-hand-side of II.8 as a function of q_1

and reading off the value of q_1 where the curve reaches 1. Using the values obtained in chapters 2 and 3 ($C_1=1.28$ and $\alpha=1.2$) we have used the above described procedure to estimate the value of q_1 corresponding to the apparent luminosity field $\ell_{1,\lambda}$. The abscissa in figure II.3 shows the left-hand-side of equation II.8. This curve is observed to reach 1 at $q_1=0.6\pm 0.1$. This value imposes a lower bound on the values of q expected to display multifractal properties related to those of the real 3-dimensional distribution. In particular universality is not expected to be observed for $q < q_1$ (as already stated in section 2.4.1).

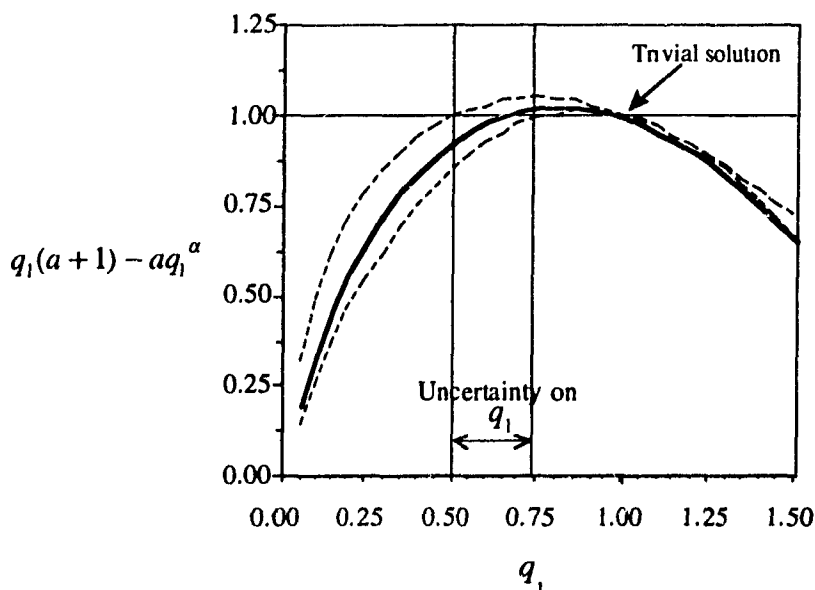


Figure II.3. Estimation of q_1 for the field $\ell_{1,\lambda}$. The abscissa displays the left-hand-side of equation II.8. From the value of q where the curve becomes equal to 1, we have estimated $q_1=0.6\pm 0.1$. The broken lines correspond to the extreme variations of the curve given by the uncertainty on the quantity $a \equiv C_1 / (\alpha - 1)$

According to equation 2.12 there is a certain singularity (denoted as γ_{q_1}) corresponding to the order of moment q_1 . γ_{q_1} is given by:

$$\gamma_{q_1} = \left(\frac{d}{dq} K(q) \right)_{q=q_1} \quad (\text{II.9})$$

Using the universal form shown in equation II.6 and the already estimated values of C_1 , α , and q_1 we have estimated that $\gamma_{q_1} \approx 0.5$. Since equation II.4 implies that $K_p(q) = K(q) - 1$ then the corresponding projected quantity $\gamma_{q_1,p}$ is given by:

$$\gamma_{q_1,p} = \left(\frac{d}{dq} K_p(q) \right)_{q=q_1}$$

$$\gamma_{q_1,p} = \gamma_{q_1} - 1 \quad (\text{II.10})$$

implying that for the projected field $\ell_{1,\lambda}$ the codimension function $c(\gamma, l)$ should show scaling only for $\gamma > \gamma_{q_1,p} \approx -0.5$. This value is in agreement with the lowest observed singularity exhibiting non-linear behaviour in figure 2.13.

II.2 Generalization to the $\eta \neq 1$ Case.

Lavallée⁶⁴ has pointed out that any multifractal field (ie. not necessarily a universal multifractal) obeys the relation:

$$K(q, \eta) = K(q\eta) - qK(\eta) \quad (\text{II.11})$$

From equation II.4 we know that $K(x) = K_p(x) + x - 1$ for any $x > x_1$. Consequently, we re-write II.11 as:

$$K(q, \eta) = K_p(q\eta) + q\eta - 1 - qK_p(\eta) - q\eta + q$$

$$K(q, \eta) = K_p(q, \eta) + q - 1 \quad , \text{ for } q > q_1 \quad (\text{II.12})$$

where $K_p(q, \eta) = K_p(q\eta) - qK_p(\eta)$. In section 3.4 equation II.12 was used to predict the unprojected counterparts of the values $K(q_{D,1}, \eta)$. Recalling that $q_{D,1} \approx 1.33$, it follows that the use of equation II.12 was justified on the ground that $C_{1,1} > 1$ and $q_{D,1} > q_1$ for the field $\ell_{1,\lambda}$.

Since $K(q, \eta)$ is a function of two variables, we expect that there exists a critical value of η (denoted as η_1) above which equation II.12 is valid. η_1 may be defined as the solution of the "dressing" relation II.6, but with the variable q held constant:

$$K(q, \eta_1) = (q - 1) \quad (\text{II.13})$$

Using the universal form of $K(q, \eta)$ (given by equation 2.16) we estimate η_1 as:

$$\eta_1 = \left(\frac{(\alpha - 1)(q - 1)}{C_{1,1}(q^\alpha - q)} \right)^{\frac{1}{\alpha}} \quad (\text{II.14})$$

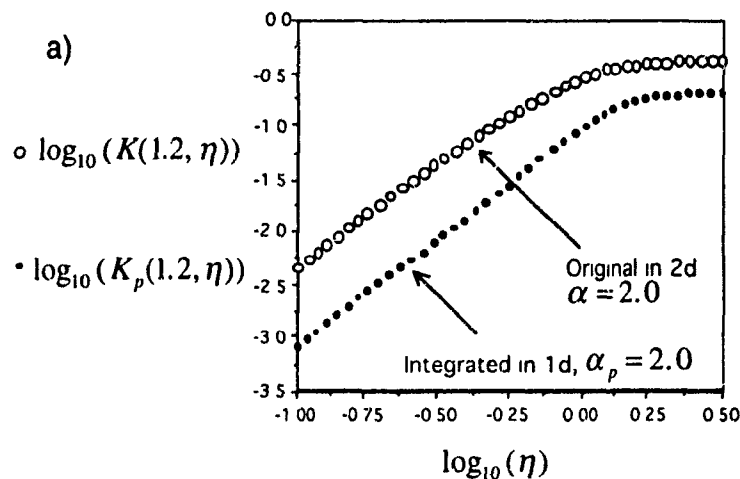
Using the observed values of α and $C_{1,1}$ for $\ell_{1,\lambda}$ and $q=1.2$ we obtain $\eta_1(1.2)\approx 0.74$ and consequently $\log_{10}(\eta_1(1.2))\approx -0.13$. This value is in agreement with the minimum value of η observed to have displayed universal behaviour in figure 2.18.

II.3 Comments on the Application of the DTM Technique to Integrated Fields.

We now show some numerical evidence that suggests that when performing a DTM analysis (see section 2.4.1) on an integrated field, the observed value of α (as estimated from the slope of the linear region in a $\log_{10} K_p(q, \eta)$ versus $\log_{10}(\eta)$ graph) generally approaches the value of 2, independent of the α of the unprojected distribution. Figure II.4a shows the results from a DTM analysis on five 2-dimensional simulations all having $\alpha=2.0$ and $C_{1,1}=1.50$, and a maximum resolution $\Lambda=512$. Also shown is the result of the DTM performed on the corresponding integrated samples. Both curves are fairly linear and parallel over a wide range of η 's, implying that the "projected" α (denoted as α_p) is also equal to 2.0. In this analysis we have used $q=1.20 > q_1=0.67$ (as given by equation II.7).

Figure II.4b shows the results of a DTM analysis performed on a different set of five simulations. This time $\alpha=1.30$ and $C_{1,1}=1.50$. Also shown are the results from the analysis on the integrated fields. Although both curves display clear linear behaviours, they are no longer parallel (as in the previous case). Moreover, α_p is observed to be equal to 2.04.

Similar analyses were performed on simulations having other values of α and $C_{1,1}$. The results from those analyses are in agreement with the ones described here.



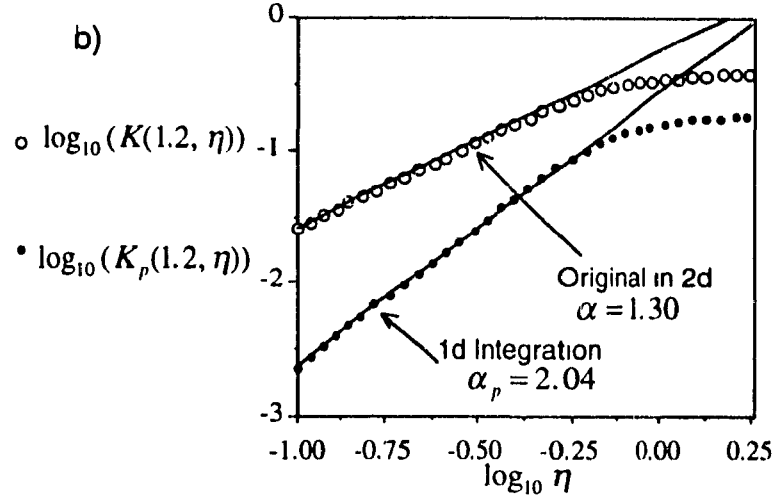


Figure II.4. DTM analysis for two sets of five 2d universal multifractal fields and their corresponding projections. a) $\alpha=2.0$ and $C_1=1.50$ and b) $\alpha=1.30$ and $C_1=1.50$. It is argued that this figure gives numerical evidence suggesting that the value of α deduced from projected fields (and using a DTM technique) is close to 2.0 even for the cases when the unprojected fields display an α very different from 2.0. Similar analyses performed on other simulated fields confirmed these results for the case $\alpha>1.0$, $C_1>1$ and $q>q_1$.

The behaviour shown in figure II.4 may be theoretically interpreted as the signature of the dressing mechanism which accompanies the integration of the fields. If we assume that the projection of the fields, in a yet unclear manner, makes $K_p(q, \eta)$ analytic at $\eta=0$, then in the region of low η 's (where the DTM analysis possesses its strongest statistical validity) we can expand $K_p(q, \eta)$ in a Maclaurin series#. Let us start by recalling equation II.11 for the projected field:

$$K_p(q, \eta) = K_p(q\eta) - qK_p(\eta) \quad (\text{II.15})$$

We then expand about the origin each of the terms on the right-hand-side of II.15. Finally, by retaining only values up to second order we obtain the following result:

$$K_p(q, \eta \rightarrow 0) \approx \eta^2 \frac{1}{2} \frac{d^2 K_p(0)}{dq^2} (q^2 - q) + K_p(0)(1 - q) \quad (\text{II.16})$$

Notice that this is not allowed in the case of ordinary universal multifractal fields since such fields are not analytic at the origin⁶².

Since $K_p(0)=0$ for any conservative field, equation II.16 indicates that $K_p(q,\eta)$ will always behave as a quadratic function of η near the origin. Thus, if the assumption of analyticity near the origin is true, then the fact that the α observed in projected fields approximates the value of 2 should be interpreted simply as a strong signature of a multifractal projection.

Bibliography.

1. Peebles, P.J.E. 1980. *The Large Scale Structure of the Universe*. Princeton Univ Press, Princeton.
2. Peebles, P.J.E. and Hauser, M. G.. 1974. *Astrophys J. Suppl* **28**. 19.
3. Peebles, P.J.E. 1975. *Astrophys. J.* **196**. 647
4. Groth, E.J. and Peebles, P.J.E. 1977. *Astrophys. J.* **217**. 385.
5. Davis, M. and Peebles, P.J.E. 1983 *Astrophys J.* **267**. 465.
6. Balian, R. and Schaeffer, R. 1988. *Astrophys. J.* **335**. L43.
7. Martinez, V.J. 1991. In *Applying Fractals to Astronomy*. Eds A. Heck and J.M. Perdgang. Springer-Verlag Publ 135.
8. Coleman, P.H. and Pietronero, L. 1992 *Phys Rep* **213**. 312.
9. Mandelbrot, B.B. 1975. *Les Objects Fractals* Flammarion. Paris.
10. Grassberger, P and Procaccia, I. 1983. *Phys. Rev. Lett* **50**. 346.
11. Einasto, J., Klypin, A.A., Saar, E., Shandarin, S.F. 1984 *M.N.R.A.S.* **206**. 529.
12. Einasto, J., Klypin, A.A., Saar, E. 1986 *M.N.R.A.S.* **219**. 457.
13. Maddox, S.J., Efsthathiou, G., Sutherland, W J., Loveday, J. 1990. *M.N.R.A.S. Short Comm.* **242.43**.
14. Gott, J.R., Weinberg, D.H., Melott, A L. 1987 *Astroph. J.* **245**. 1.
15. Castagnoli, C. and Provenzale, A. 1990. *Vistas in Astronomy.* **33**. 323.
16. Calzetti, D., Giavalisco, M , Ruffini, R , Taraglio, S., Bahcall, N A 1991. *Astron.Astrophys.* **245.1**
17. Luo, X. and Schramm, D N. 1992 *Science.* **256**. 513.
18. Borgani, S., Murante, G., Provenzale, A., Valdarini, R. 1993, *Phys. Rev. E.* **47**. 3879.
19. Martinez, V J , Jones, B J.T., Dominguez-Tenreiro, R , van den Weygaert, R. 1990 *Astrophys. J.* **357**. 50.
20. Fournier d'Albe, E E. 1907. *Two New Worlds*. London: Longmans Green.
21. Charlier, C.V.L. 1922. *Ark. Mat. Astron. Fys.* **16**. No 16.
22. Pietronero, L. 1987. *Physica A.* **144**. 257
23. Calzetti, D., Giavalisco M., Ruffini, R., Wiedenmann, G 1991. *Astron. Astrophys.* **251**. 385.
24. Dogterom, M and Pietronero, L 1991. *Physica A.* **171**. 239.
25. Huchra, J.P , Davis, M , Latham, D , Tonry, J. 1983 *Astrophys. J. Suppl.* **52**. 89.
26. Huchra, J.P., Geller, M , de Lapparent, V., Corwin, H. 1990. *Astrophys. J. Letters* **72** 433.
27. de Lapparent, V., Geller, M.J., Huchra, J P. 1986. *Astrophys J* **302**. L1.
28. Kirshner, R.P., Oemler, A , Schectman, S.A 1981. *Astrophys. J. Letters.* **248**. L57.
29. Zel'dovich, Ya B., Einasto J , Shandarin, S.F. 1982. *Nature.* **300**. 407.

30. Zwicky, F. 1957. *Morphological Astronomy*. Springer-Verlag, Berlin.
31. Abell, G.O. 1965. *Ann.Rev Astr and Ap.* 3 1.
32. Kiang, T D. 1961 *M.N.R.A.S.* . 122. 263.
33. Schechter, P. 1976. *Astrophys. J* 203 297
34. Bahcall, N A. 1977. *Ann. Rev. Astrophys.* 15. 505.
35. Turner, E.L. and Gott, R. 1976 *Astrophys. J.* 209. 6
36. Bak, P., Tang, C., Wiesenfeld, K. 1987. *Phys Rev. Lett* 59. 381.
37. Dominguez-Tenreiro, R. and Martinez, V.J. 1989. *Astrophys. J.* 389. L9.
38. Wen, Z., Deng, Z.-G, Liu, Y.-Z, Xia, X.-Y. 1989. *Astron. Astrophys.* 219. 1.
39. Schertzer, D. and Lovejoy, S. 1991. In *Non-Linear Variability in Geophysics*. Eds. D. Schertzer and S. Lovejoy. Kluwer Academic. Holland. 41.
40. Lovejoy, S. and Schertzer, D. 1985. *Water Resour. Res.* 21. 1233.
41. Schertzer, D. and Lovejoy, S. 1987 *J. Geo. Res.* 92. 9693.
42. Hooge, C. 1993. *Master's of Science Thesis*. McGill University. Canada.
43. Jones, B.J.T., Martinez, V.J., Saar, E., Einasto, J. 1988. *Astrophys. J.* 332. L1.
44. Atmanspacher, H., Scheingraber, H., Wiedenmann, G. 1989. *Phys. Rev. A* 40. 3954.
45. Wiedenmann, G., Atmanspacher, H., Scheingraber, H. 1990. *Can. J. Phys* 68. 827.
46. Martinez, V.J. 1990. *Vistas in Astronomy.* 33 337.
47. Wiedenmann, G. and Atmanspacher, H. 1990. *Astron. Astrophys.* 229. 283.
48. Coleman, P.H. and Pietronero, L. 1992 *Physica A* 185. 45.
49. Falconer, K. 1990 *Fractal Geometry. Mathematical Foundations and Applications*. John Wiley & Sons Publ. Chapters 6 and 8.
50. Börner, G. and Mo, H.J. 1990. *Astron. Astrophys.* 227. 324.
51. Smith, E. and Jacobs, K. 1973. *Introductory Astronomy and Astrophysics*. W.B. Saunders Publishers.
52. Geller, M.J. and Huchra, J.P. 1983. *Astrophys. J. Suppl.* 52. 61.
53. Zwicky, F., Herzog, P., Wild, M, Karpowicz, M., Kowal, C.T. 1961-68. *Catalogue of Galaxies and Clusters of Galaxies* Six vols.
54. Kogoshvili, 1986. *Merged Catalogue of Galaxies*. Also available from NASA's Astronomical Data Center *Selected Astronomical Catalogs*. Vol I.
55. Fischer, N., Lewis, T, Embleton, B.J. 1987. *Statistical Analysis of Spherical Data*. Cambridge Univ Press. 38.
56. Lovejoy, S and Schertzer, D. 1992. *Multifractals in Geophysics*. Course notes from AGU-CGU-MSA spring meeting. Montréal.
57. Parisi, G. and Frisch, U. 1985. In *Turbulence and predictability in geophysical fluid dynamics and climate dynamics*. Ed by M. Ghil, R. Benzi, G. Parisi. Nort-Holland Publishers.

58. Pecknold, S., Lovejoy, S., Schertzer, D., Hooge, C., Malouin, J.F. 1993. In *Cellular Automata: Prospects in Astrophysical Applications*. Ed by J.M. Perdgang and A. Lajeune. World Scientific, Singapore. 228
59. Schmitt, F., Lavallée, D., Schertzer, D., Lovejoy, S. 1992. *Phys. Rev. Lett.* **68**. 305.
60. Tessier, Y., Lovejoy S., Schertzer, D. 1993 *J of App. Meteor.* Vol 32 **2**. 223.
61. Lavallée, D., Lovejoy, S., Schertzer, D. 1991. In *Fractals in Geography*. Eds L. de Cola and N. Lam. Prentice and Hall Publishers
62. Schertzer, D. Lovejoy, S. Lavallée, D. Schmitt, F. 1991. In *Nonlinear Dynamical Structures*. Eds R.Z. Sagdeev, U. Frisch, S. Moiseev and N. Erokhin. World Scientific, Singapore.
63. Ratti, S.P, Salvadori, G., Gianni, G., Lovejoy, S., Schertzer, D. 1991. *Proceedings of the 21st Int'l Symposium on Multiparticle Dynamics*. Wuhan
64. Lavallée, D. 1991. *Ph D Thesis*. McGill University. Canada.
65. Bak, P., Tang, C., Wiesenfeld, K 1988. *Phys. Rev. Lett. A* **38**. 364.
66. Schertzer, D., Lovejoy, S., Lavallée, D. 1993. In *Cellular Automata: Prospects in Astrophysical Applications*. Ed by J.M. Perdgang and A. Lajeune. World Scientific, Singapore. 216.
67. Feigenbaum, J.F. 1987. *J. of Stat. Phys.* **46**. 5-6.
68. Schertzer, D., and Lovejoy, S. 1985. *P.C.H Journal*. **6**. 623.
69. Carter, B., and Henriksen, R.N. 1991. *J. of Math. Phys.* **32**. 2580.
70. Limber, D. N. 1954. *Astrophys. J.* **119**. 655.
71. Da Costa, LN., Pellegrini, PS., Sargent, LW., Tonry, J., Davis, M., Meiksin, A., Latham, DW., Menzies, JW, Coulson, IA. 1988. *Astrophys J*, **327**, 544.
72. de Vaucouleurs G. 1970. *Science*. **167**. 1203.
73. Bond, J.R., Efstathiou, G., Smith, J. 1981. *Phys. Rev. Lett.* **45**. 1980.
74. Blumenthal, G.R., Faber, S.M., Primack J.R., Rees, M.J. 1988. In *the Early Universe: Reprints*. Ed by E.W. Kolb and M.S. Turner. Frontiers in Physics. Addison & Wesley Publ. 617.
75. Buryak, O.E., Demiansky, M., Doroshkevich, A.G 1992. *Astrophys. J.* **393** . 464.
76. Provenzale, A. 1991 In *Applying Fractals in Astronomy*. Ed by A. Heck and J.M. Perdgang. Springer-Verlag Publishers. 99.
77. Halsey, T.C., Jensen, M.H., Kadanoff, L.P., Procaccia, I. 1986. *Phys. Rev. A* **33**. 1141.